論文 / 著書情報
Article / Book Information

題目(和文)	
Title(English)	Study on High Speed VCSEDs Based on Lateral Resonator Integration for Optical Interconnects
著者(和文)	DalirHamed
Author(English)	Hamed Dalir
出典(和文)	学位:博士(学術), 学位授与機関:東京工業大学, 報告番号:甲第9578号, 授与年月日:2014年3月26日, 学位の種別:課程博士, 審査員:小山　二三夫,淺田　雅洋,梶川　浩太郎,植之原　裕行,宮本　智之,大橋　弘美
Citation(English)	Degree:Doctor (Academic), Conferring organization: Tokyo Institute of Technology, Report number:甲第9578号, Conferred date:2014/3/26, Degree Type:Course doctor, Examiner:,,,,,
学位種別(和文)	博士論文
Type(English)	Doctoral Thesis

Study on High Speed VCSELs Based on Lateral Resonator Integration for Optical Interconnects

by

Hamed Dalir

March 2014

Dissertation submitted in partial fulfilment for the degree of

Doctor of Philosophy

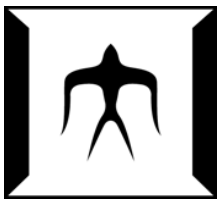

Department of Electronics and Applied Physics

Interdisciplinary Graduates School of Science and Engineering

Tokyo Institute of Technology

Advisor: Prof. Fumio Koyama

This project is dedicated to "Japan Society for the Promotion of Science" (JSPS), where has never failed to give us financial and moral support, for giving all our need during the time we developed our system and for teaching us that even the largest task can be accomplished if it is done one step at a time.

Table of Contents

1 Chapter 1: Introduction

1.1 Overview of Optical Interconnect Technology and the Role of VCSELs

Half-century ago, when Gordon Moore, the cofounder of Intel, in 1965, wrote an article on Electronics Magazine entitled “Cramming more components onto integrated circuits”[1], at that time, Moore's basic statement was: “The complexity for minimum component costs has increased at a rate of roughly a factor of two per year”. Assuredly over the meantime this rate can be expected to not increase. But for the longer term, the expansion rate would be a bit more for sure. So that, Industry people embarked on reduction of transistor size in order to integrate much more transistors on a chip. In Fig. 1-1 the increasing demand of transistors on the chip can be seen, which over one million transistors used in 2007. However, Most of Moore’s law is based upon shrinking the dimensions of the transistors on the chip, while the laws of physics do not allow transistor technology to be qualified.

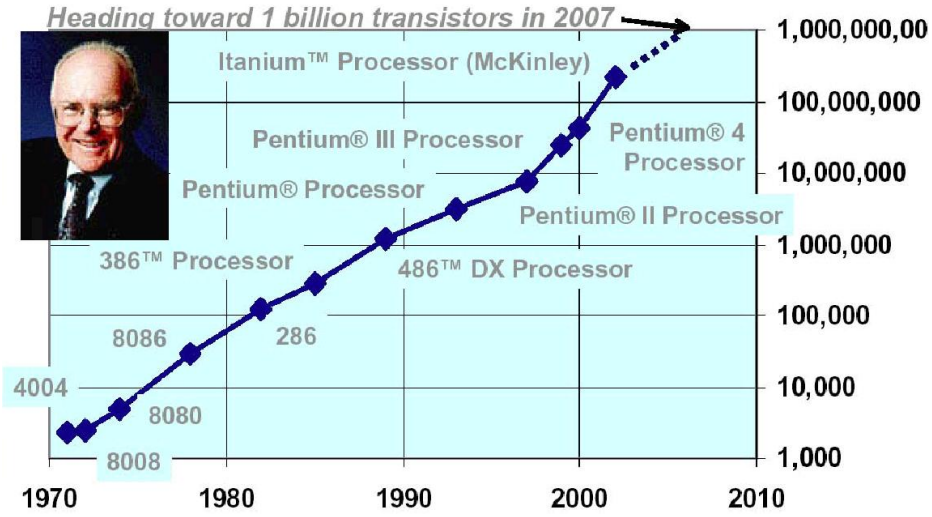

Fig. 1-1 Illustrates the drastic increase of transistors as a function of years.

For further improving the capacity of microprocessors, currently being used copper-based interconnects are becoming the constriction due to their physical limitations [2]. Electrical Board-level Interconnects have a lot of drawbacks. Such as: signal integrity problems, transmission-line effects, high rising and falling time with a large delay time, extensive channel loss for long distance, skin effect, frequency-dependent dielectric loss , manufacturing variations, geometrical issues, reflection loss (Echo effect), dense connections, self-coupling and so on.

Moreover, as frequency rises, signal loss, distortion, and cross-talk become worse in electrical interconnects. In order to keep up with the development of microprocessors, spick-and-span technology for interconnections is desired. Optics is a viable alternative compared with copper interconnects due to its short signal delay, high bandwidth, low power dissipation and freedom from electromagnetic interference [3]. Fig. 1-2 shows a schematic of board-level interconnect in telecommunication.

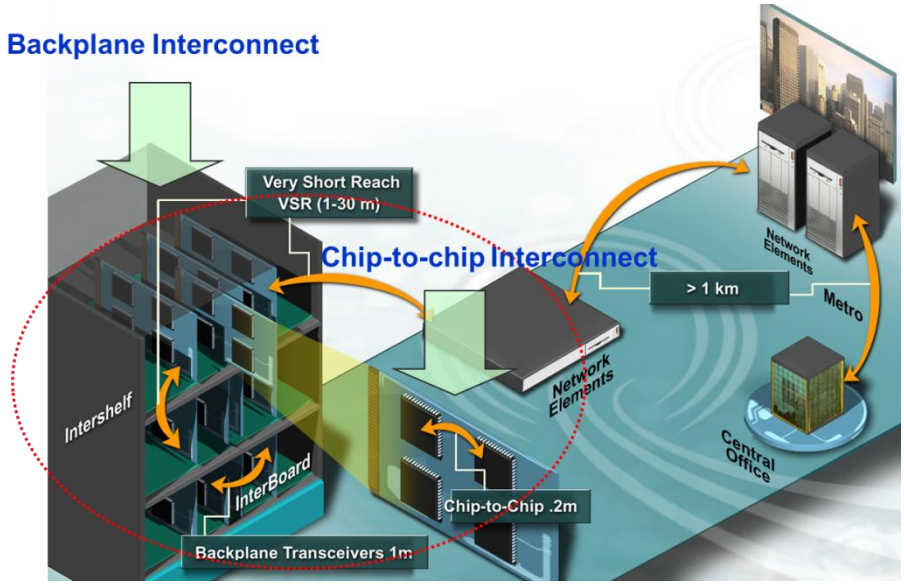

Fig. 1-2 Schematic of board-level interconnect in telecommunication

According to International Technology Roadmap of Semiconductor (ITRS-2003) [4], in near future, off-chip and on-ship frequency will rise exponentially and optical interconnect needs to be boost his capacity and speed (see Fig. 1-3).

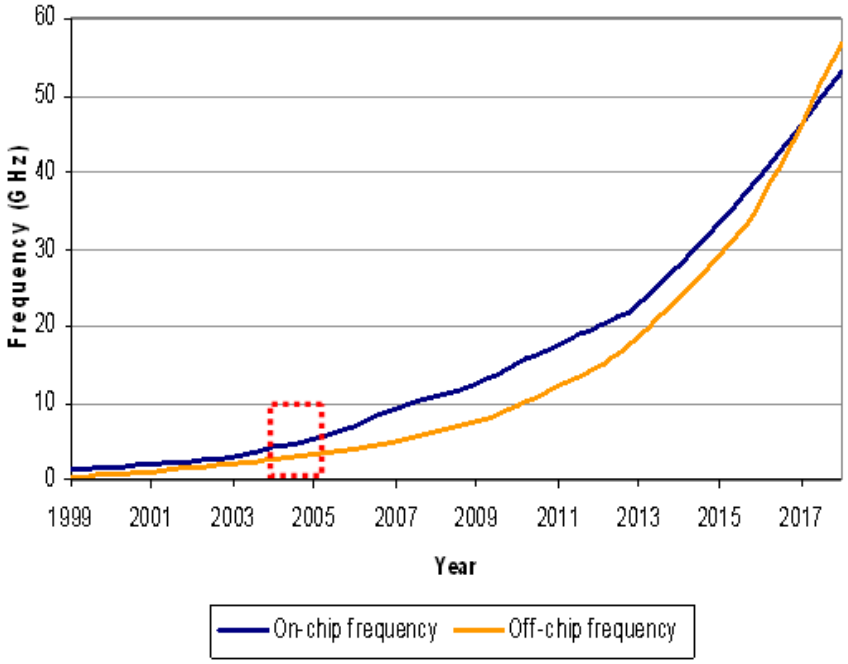

Fig. 1-3 ITRS-2003 map for the demand of increasing capacity for on-chip and off-chip frequency.

On the other hand, several groups reported results that a factor of two of the ultimate capacity of existing optical fibre technology is required. Thus without radical innovation in the current physical network infrastructure, we face what has been widely referred to as a "capacity crunch" that could severely constrain future Internet growth, as well as having social and political ramifications. Capacity crunch or pick data means the situation that the demand is larger than the provided interconnects. Fig. 1-4 anticipated that the capacity crunch will happen in 2020[5].

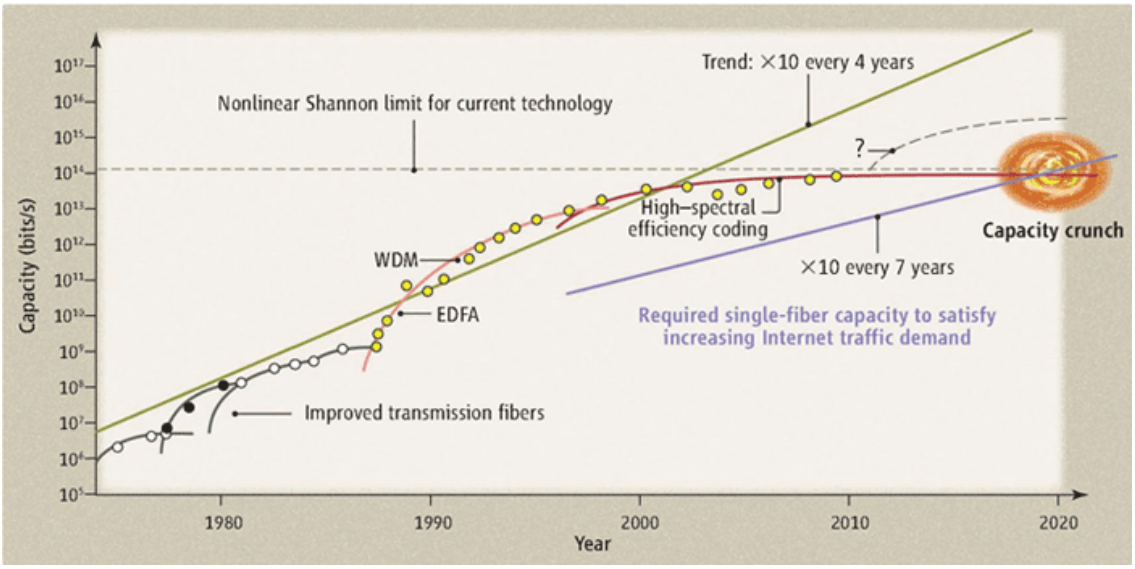

Fig. 1-4 Anticipated capacity crunch situation in the current optical interconnect.

The Vertical Cavity Surface Emitting Lasers (VCSELs) have been grown highly in popularity and their capability has been appended. Unfavourable conventional edge-emitting devices, VCSELs are made with a short resonant cavity, which supports a single longitudinal mode. Light is emitted perpendicularly to the plane of crystal growth, approbating the creation of two-dimensional transmitter arrays for high bandwidth-density applications. VCSELs have small footprints, dissipate less power, are cost effective and also they can be simply fabricated into arrays. Thus VCSELs have been heavily engaged in high-bandwidth communications and are exclusively glamorous candidates for use in optical interconnects in data centres and supercomputers [6,7]. VCSEL was first proposed and fabricated by K. Iga and his colleagues at the Tokyo Institute of Technology, Japan in the late 1970s (see fig.1-5(a)). They indicated that in order to realize low threshold current, VCSELs should have (1) extremely small cavity volume, (2) high optical gain, and (3) mirrors with extremely high reflectivity (>95%) [8]. Several years later, implementation of an electrically pumped GaAs/AlGaAs VCSEL pulsing at room temperature was reported by F. Koyama at

the Tokyo Institute of Technology, Japan in 1989,(fig.1-5(b)) [9]. Despite to all efforts on the VCSELs, limitation of 3-dB bandwidth is the remained challenge for our era.

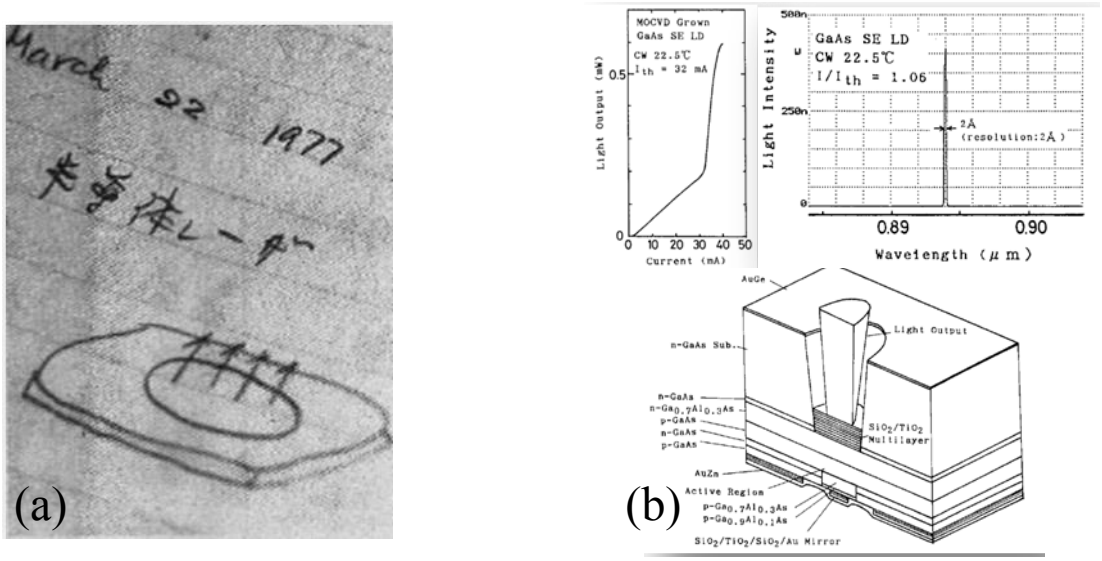

Fig. 1-5. (a) Concept of VCSEL demonstration by Iga, and (b), First electrically pumped GaAs/AlGaAs VCSEL pulsing at room temperature by Koyama.

1.2 Limit of Directly Modulated VCSELs

To notice the limits of the modulation characteristics, a rate equation analysis is necessary part. Interact of stimulated emission between photon and carrier reservoir is the simplest way for the direct modulation of VCSEL.

$$\frac{dN}{dt} = \frac{\eta_i}{qV} I - \frac{N}{\tau} - v_g g N_p \tag{1-1}$$

$$\frac{dN_p}{dt} = \Gamma v_g g N_p - \frac{N_p}{\tau_p} + \Gamma R'_{sp} \tag{1-2}$$

where N and N_p is carrier and photon density, respectively. η_i is the internal efficiency, I is the current injection, q is the electronics charge, V is the volume of active region, τ is the carrier lifetime, v_g is the group velocity, g is the modal gain, Γ is the optical confinement factor, R'_{sp} is the spontaneous emission into the defined mode, and τ_p is the photon lifetime.

Here, $R'_{sp} << \nu_g g N_p$, thus the last term in photon density can be ignored. The modal gain can be defined by the following formula:

$$g(N, N_p) = \frac{g_0}{1+\varepsilon N_p} \ln\left(\frac{N+N_s}{N_{tr}+\varepsilon N_p}\right) \quad (1\text{-}3)$$

Once we have the rate equation; small signal analysis can be realized by small sinusoidal modulation of currents as following:

$$I(t) = I_0 + \Delta I(t) \quad (1\text{-}4)$$

$$N(t) = N_0 + \Delta N(t) \quad (1\text{-}5)$$

$$N_p(t) = N_{p0} + \Delta N_p(t) \quad (1\text{-}6)$$

Where N_0 and N_{p0} are the steady state solution of carrier and photon densities. In order to find the steady state solution, at first we need to set the rate equations equal to zero.

$$\frac{\eta_i}{qV} I - \frac{N_0}{\tau} - \nu_g g N_{p0} = 0 \quad (1\text{-}7)$$

$$\Gamma \nu_g g N_{p0} - \frac{N_{p0}}{\tau_p} + \Gamma R'_{sp} = 0 \quad (1\text{-}8)$$

From the above equation we can find:

$$\Gamma \nu_g g - \frac{1}{\tau_p} + \Gamma R'_{sp} = 0 \quad (1\text{-}9)$$

While, $R'_{sp} << \nu_g g N_p$, we can rewrite the relation as follow:

$$\Gamma \nu_g g - \frac{1}{\tau_p} = 0 \quad (1\text{-}10)$$

By replacing of eq. 1-3 in 1-10 once we can drive:

$$\Gamma \nu_g \frac{g_0}{1+\varepsilon N_p} \ln\left(\frac{N_0+N_s}{N_{tr}+\varepsilon N_{p0}}\right) - \frac{1}{\tau_p} = 0 \quad (1\text{-}11)$$

Carrier density at the steady state condition can be realized by the eq. 1-11, replacing to eq.1-7, steady state amount for photon-density can be obtained.

$$N_{p0} = \frac{1}{\nu_g g}\left(\frac{\eta_i}{qV} - \frac{N_0}{\tau}\right) = \frac{1}{\nu_g g}\left(\frac{\eta_i}{qV} - (AN_0 + B{N_0}^2 + C{N_0}^3)\right) \quad (1\text{-}12)$$

Now, the VCSEL is modulated by the superimposition of the injected current at steady state, and sinusoidal current as shown in eq. 1-4. It can be define same way for the carrier and photon density as written in eq. 1-5 and 1-6, by substitution of them in eq.1-1 and 1-2, we have:

$$\Delta N^{\cdot} = \frac{\eta_i}{qV}\Delta I - \left(\frac{g_0 N_{p0}}{1+\varepsilon N_{p0}} + A + 2.BN_0 + 3.C{N_0}^2\right)\Delta N + g_0 \frac{N_0 - N_{tr}}{(1+\varepsilon N_{p0})^2}\Delta N_p \quad (1\text{-}13)$$

$$\Delta N_p^{\cdot} = \left(2\Gamma\beta BN_0 + V\frac{g_0 N_{p0}}{1+\varepsilon N_{p0}}\right)\Delta N + \left(V g_0 \frac{N_0 - N_{tr}}{(1+\varepsilon N_{p0})^2} - \frac{1}{\tau_p}\right)\Delta N_p \quad (1\text{-}14)$$

The eq. 1-13 and 1-14 can be expressed as follows:

$$\begin{bmatrix}\Delta N^{\cdot} \\ \Delta N_p^{\cdot}\end{bmatrix} = [M]\begin{bmatrix}\Delta N^{\cdot} \\ \Delta N_p^{\cdot}\end{bmatrix} + \frac{\eta_i}{qV}\begin{bmatrix}\Delta \mathrm{I} \\ 0\end{bmatrix} \quad (1\text{-}15)$$

M is a matrix like:

$$[M] = \left[\begin{bmatrix}-\gamma_{NN} & -\gamma_{NS} \\ \gamma_{SN} & -\gamma_{SS}\end{bmatrix}\right] \quad (1\text{-}16)$$

where:

$$\gamma_{NN} = \frac{g_0 N_{p0}}{1+\varepsilon N_{p0}} + A + 2.BN_0 + 3.C{N_0}^2 \quad (1\text{-}17)$$

$$\gamma_{NS} = A + 2.BN_0 + 3.C{N_0}^2 + \frac{g_0 N_{p0}}{1+\varepsilon N_{p0}} \quad (1\text{-}18)$$

$$\gamma_{SN} = 2\Gamma\beta BN_0 + V\frac{g_0 N_{p0}}{1+\varepsilon N_{p0}} \quad (1\text{-}19)$$

$$\gamma_{SS} = \frac{1}{\tau_p} - V g_0 \frac{N_0 - N_{tr}}{(1+\varepsilon N_{p0})^2} \quad (1\text{-}20)$$

Then we have:

$$\begin{bmatrix}\gamma_{NN+j\omega} & \gamma_{NS} \\ -\gamma_{SN} & \gamma_{SS}+j\omega\end{bmatrix}.\begin{bmatrix}\Delta N \\ \Delta N_p\end{bmatrix} = \frac{\eta_i}{qV}\begin{bmatrix}\Delta \mathrm{I} \\ 0\end{bmatrix} \quad (1\text{-}21)$$

Via using the Cramer rule we obtain:

$$N_m = \frac{\eta_i I_m}{q\Delta}\begin{bmatrix}1 & \gamma_{NS} \\ 0 & \gamma_{SS}+j\omega\end{bmatrix} \quad (1\text{-}22)$$

$$N_{pm} = \frac{\eta_i I_m}{q\Delta}\begin{bmatrix}\gamma_{NN+j\omega} & 1 \\ -\gamma_{SN} & 0\end{bmatrix} \quad (1\text{-}23)$$

where Δ is the matrix determinant like:

$$\Delta = {\omega_R}^2 - \omega^2 + j\omega\gamma_R \quad (1\text{-}24)$$

Where ω_R is the relaxation oscillation frequency and can be obtained as follow:

$$\omega_R{}^2 = \frac{g_0 N_{p0}}{\tau_p} \tag{1-25}$$

$$f_R = \frac{\omega_R}{2\pi} = \sqrt{\frac{g_0 N_{p0}}{\tau_p}} = \sqrt{\frac{g_0 \eta_i}{qV}(I - I_{th})} \tag{1-26}$$

From the eq. (1-25) and (1-26) we can say that by increase of the photon density we can enlarge the relaxation oscillation frequency.

Also γ_R is defined as a damping factor as follow:

$$\gamma_R = K f_R{}^2 + A + 2.BN_0 + 3.CN_0{}^2 \tag{1-27}$$

and,

$$K = 4\pi^2 \tau_p [1 - \frac{\partial N}{N_p}] \tag{1-28}$$

From eq. 1-27 and 1-28 we see that an increase of the relaxation oscillation frequency causes increase of the damping factor too.

Finally we can define the 3-dB down cut off frequency as following:

$$\omega_{3dB}{}^2 = \omega_R{}^2 [1 - 0.5\left(\frac{\gamma_R}{\omega_R}\right)^2 + \sqrt{(\omega_R{}^2 [1 - 0.5\left(\frac{\gamma_R}{\omega_R}\right)^2)^4 + \omega_R{}^4}\,] \tag{1-29}$$

In eq. 1-29 we can see that increase of photon density which is eventually lead to increase of both damping and relaxation, does not increase the 3-dB cut off. This means that the bandwidth of conventional VCSEL will finally collapse to the saturation level. Besides this the amount of photon in the cavity cannot increase linearly, thus the bandwidth of conventional VCSEL will be limited not only to the parasitics but also to the relaxation oscillation frequency and photon density.

1.3 Recent Progress on Ultra-fast Modulation of VCSELs

In VCSELs, the uppermost rate of direct modulation is restricted by intrinsic limitation of relaxation oscillation frequency. As a general rule of thumb, a directly modulated laser can support a bit rate of up to 1.55 times of its relaxation resonant frequency. Recently a new relationship between 3-dB bandwidth and relaxation oscillation frequency was achieved via using Gain-Lever Effect in Quantum-Dot Lasers [10], which can be used in the same way for the VCSEL. To increase the speed of VCSELs, various methods have

been proposed including injection-locking [11,12], coupled cavity [13] and modulator-integration [14]. Previously, our group have been working on the optical external feedback to enhance the modulation bandwidth of VCSELs [15]. While the optical feedback scheme has been successfully employed for increasing the speed of DFB/DBR lasers [16,17]. However, we found that integration of VCSEL is a key issue to solve all problems. There have been various reports on the vertical integration and their functionalities. However cost of the vertical coupled cavity VCSEL was much larger than the conventional VCSEL, so that it did not use in practical application world widely. We realized that by laterally integration of VCSEL with another VCSEL while the plump structure is as same as conventional 980 nm VCSEL, we can keep the advantages of the new functionalities based on same price as conventional VCSEL.

1.4 State-of-the-art of 980 nm VCSELs

The wavelength of 980 nm has various merits in comparison to the 850 nm. The main advantages are deeper barriers, suppressing escape of non-equilibrium carriers and thus enhancing temperature stability of the gain, also in order to improve the differential gain it is relatively easier to use strained materials compare to 850 nm, the transparency of GaAs at 980 nm, enabling light emission through the bottom mirror and the substrate, and lower operating voltages, which is very significant for the low voltage CMOS drivers. In aspect of the advantages mentioned above it becomes important for VCSEL-based data-com applications, leading to research and development of high speed and also high temperature stable 980 nm VCSELs and integrated devices. In 2007, the maximum bandwidth of 980 nm VCSELs was reported by the group of Prof. Coldren from the UCSB to 35 Gbps [18,19]. They have used oxide aperture with tapering the shape where the oxidation layers was quiet deeper than the conventional one, by optimization of the doping profiles, they achieved maximum bandwidth of larger than 20 GHz. This is currently one of the world-

wide fastest 980 nm VCSELs. Although such high speed at room temperature was attained, at higher temperatures the maximum speed was initially limited to 20 Gbps at 85°C, demonstrated by Bimberg's group at the Technical University of Berlin in 2006 [20,21]. One year later Agilent researchers have demonstrated 980 nm VCSELs operating at 25 Gbps at 70°C [22].

1.5 Scope of the Doctoral Dissertation

In this Dissertation, in the chapter 2, a novel method to boost the modulation speed of 980 nm VCSELs will be considered, which is based on the self-feedback by employing photon-photon resonance (PPR) effect. Theoretical results indicate that the 3-dB bandwidth of single mode coupled cavity VCSEL can be expanded by 60% in comparison to that of directly modulated conventional VCSEL [23]. Also we have shown good agreements between the theory and fabricated results by carefully designing of our structure using film mode matching method. In the experiment we got 3-dB bandwidth of over 29 GHz which was primary limited by the photo-detector [24]. This device is currently fastest 980 nm VCSEL. In addition to them some further calculation regarding to the future trend is highlighted. Finally we have shown by engineering the aperture shape of the coupled cavity, phase can be fixed at out-of phase, which the enhancement is obtaining in different currents, also elevated temperature results indicate that the phase is locked at out-of phase. This device concept will be compatible with existing manufacturing processes and can be easily manufactured in large volume, making it attractive for optical interconnects. In the next chapter, we have shown the potential application of VCSEL for radio over fibre application based on PPR effect [25], while the conventional VCSEL cannot be used for this matter, by beating of transverse mode we made our device well matched for this application. In the following chapter, we have shown that through intensity manipulation of transverse field, high speed modulation bandwidth free from relaxation oscillation fre-

quency can be obtained [26]. In the chapter 6, we showed the smallest ever reported an integrated electro-absorption modulator with VCSEL. Experimental results indicate the lowest driving voltage <400 mV_{pp} [27]. For further increase in link capacities, multiplexing technologies will be needed in future. To meet this demand, degrees of freedom for multiplexing technology are time, wavelength, complex, constellation, polarization, space and mode, such as wavelength division multiplexing (WDM), space division multiplexing (SDM), and mode division multiplexing (MDM) and so on. It is noted that a multi-mode waveguide potentially exhibits larger transmission capacity than a single-mode waveguide. An interesting approach is to multiplex spatial modes in a multi-mode waveguide, carrying multi-channel signals. Key issues of mode division multiplexing for optical interconnects are compact and robust mode multiplexing technology, low wavelength dependence, low polarization dependence and so on. There have been several studies on spatial mode multiplexing/demultiplexing. The concept of multiple-input-multiple-output transmission used in wireless communications has been applied to multi-mode fibre channels, which is called optical MIMO [28]. Also, there have been reports on spatial mode DEMUX using MMI coupler [29]; fibre coupler and HCG hollow waveguide filter [30], and so on. We still need challenges for compact and robust MUX/DEMUX optical devices. Our target is to realize a compact and scalable multiplexer /demultiplexer device based on a tapered hollow waveguide for high-capacity optical interconnects.

Important criteria's are low wavelength dependence, no noticeable polarization dependence, low insertion loss, low crosstalk and compactness. Thus with take caring of these criteria, in the chapter seven a novel spatial-mode multiplexer/demultiplexer based on a tapered hollow waveguide with bragg reflectors will be proposed. Clear demultiplexing for different spatial modes will be shown. In addition, low wavelength sensitivity and polarization independence were predicted. Also, high efficiency of vertical radiation could

be expected from 70% for higher order modes to 96% for the fundamental mode. This device concept would be useful for spatial-mode multiplexing interconnects and integration with surface-normal optical devices such as VCSEL and so on. In the following of this chapter, in order to further increase the capacity and speed a novel method to ambulate 90 degree of light based on tapered hollow waveguide is proposed. The modelling shows that this device can act as a low wavelength dependency. Also at the same time low polarization dependency can be obtained, where the power efficiency is relatively high.

1.6 References

1) Gordon E. Moore, “Cramming More Components onto. Integrated Circuits,” Electronics, vol. 38, no. 8, pp. 114–117, 1965.

2) D. A. B. Miller, “Physical Reasons for Optical Interconnection,” Int’l J. Optoelectronics 11, 155-168, 1997.

3) D. A. B. Miller, “Rationale and Challenges for Optical Interconnects to Electronic Chips,” Proc. IEEE 88, 728-749, 2000.

4) http://public.itrs.net/Files/2003ITRS/Home2003.html

5) D. J. Richardson, “Filling the Light Pipe”, Applied Physics, Vol. 330 no. 6002 pp. 327-328, 2010.

6) T. Anan, N. Suzuki, K. Yashiki, K. Fukatsu, H. Hatakeyama, T. Akagawa, K. Tokutome, and M. Tsuji, “High-speed 1.1-μm range InGaAs VCSELs,” presented at the OFC, San Diego, CA, Paper OThS5, 2008.

7) Y.-C. Chang, C.S. Wang and L.A. Coldren, “Small-dimension power-efficient high-speed vertical-cavity surface-emitting lasers,” Electron Letter , vol. 43, no. 7, 2007.

8) K. Iga, “Surface emitting laser–its birth and generation of new optoelectronics field,”IEEE J Select. Topics Quantum Electron, Vol. 6, no. 6, pp. 1201–1215, 2000.

9) F. Koyama, S. Kinoshita, and K. Iga, “Room temperature continuous wave vertical cavity surface emitting laser and high-power 2D laser arrays,” in Tech. Digest, Conf. Lasers and Electro-Optics, paper FC1, pp. 380–381, 1989.

10) Y. Li, N. A. Naderi, V. Kovanis and L. F. Lester, “Enhancing the 3-dB Bandwidth via the Gain-Lever Effect in Quantum-Dot Lasers,”IEEE Photonics Journal, Volume 2, Number 3, Jun. 2010.

11) X. Zhao, D. Parekh, E. K. Lau, H. K. Sung, M. C. Wu, W. Hofmann, M. C. Amann, and C. Chang-Hasnain, "Novel cascaded injection-locked 1.55-mu m VCSELs with 66 GHz modulation bandwidth," Optics Express, vol. 15, no. 22, pp. 14810-14816, Oct. 2007.

12) SeungHun Lee, Devang Parekh, Takahiko Shindo, Weijian Yang, Peng Guo, Daisuke Takahashi, Nobuhiko Nishiyama, Connie J. Chang-Hasnain and Shigehisa Arai“Bandwidth enhancement of injection-locked distributed reflector lasers with wirelike active regions,” Vol. 18, No. 16 / OPTICS EXPRESS 16370, Aug. 2010.

13) C. Chen and K. D. Choquette “Push-Pull Modulation of Coupled-Cavity VCSELs,” Optical Fiber Communication Conference (OFC) San Diego, California, VCSEL-Based Devices (OTuK), Mar. 2009.

14) A. Paraskevopoulos et.al, “Ultra-High-Bandwidth (>35GHz) Electrooptically- Modulated VCSEL,” OFC2006, PDP22, Anaheim, California Mar. 2006.

15) T. Ohta, T. Uchida, M. Arai, T. Kondo and F. Koyama, "Enhanced modulation bandwidth of surface-emitting laser with external optical feedback", Opto-Electronics and Communications Conference/International Conference on Optical Internet, No. 15E1-4, 2004.

16) G. Morthier, R. Schard, O. Kjebon, “Extended modulation bandwidth of DBR and external

cavity lasers by utilizing a cavity resonance for equalization,"IEEE Journal of Quantum Electronics, Vol.36, No.12, pp.1468-1475, 2000.

17) U. Troppenz, J. Kreissl, W. Rehbein, C. Bornholdt, T. Gaertner, M. Radziunas, A. Glitzky, U. Bandelow, M. Wolfrum, 40 Gb/s directly modulated InGaAsP passive feedback DFB laser, in: Proceedings of the 32nd European Conference on Optical Communication ECOC, Post deadline session, pp. Th4.5.5/1-2, 2006.

18) Y. C. Chang, C. S. Wang, L. A. Coldren "High-efficiency high-speed VCSELs with 35 Gbit/s error-free operations". IEEE Electron Lett, vol. 43, no.19, 1022–1023, 2007.

19) Y. C. Chang "Engineering vertical-cavity surface-emitting lasers for high-speed operation". Thesis, University of California Santa Barbara, Dec. 2008.

20) F. Hopfer, A. Mutig, G. Fiol, M. Kuntz, V. A. Shchukin, D. Bimberg, S. S. Mikhrin, I. Krestnikov, D. Livshits, Kovsh AR, Bornholdt C "20 Gb/s 85_C error free operation of VCSEL based on submonolayer deposition of quantum dots". IEEE-LEOS 20th international semiconductor laser conference (ISLC), Kohala Coast, HI, USA, Sep. 2006.

21) F. Hopfer, A. Mutig, G. Fiol, M. Kuntz,V. A. Shchukin,V.A. Haisler,T. Warming, E. Stock,S. S. Mikhrin, I. Krestnikov, D. Livshits, A. Kovsh, C. Bornholdt, A. Lenz, H. Eisele, M. Dähne, N. Ledentsov, D. Bimberg "20 Gb/s 85_C error-free operation of VCSELs based on sub monolayer deposition of quantum dots". IEEE J Sel. Top Quant. Electron, vol.13, no 5, 2007.

22) Lin C-K, Tandon A, Djordjev K, Corzine SW, Tan MRT " High-speed 985 nm bottom emitting VCSEL arrays for chip-to-chip parallel optical interconnects". IEEE J Sel Top Quant Electron 13, 5, 1332–1339, 2007.

23) H. Dalir and F. Koyama, "Bandwidth enhancement of single-mode VCSEL with lateral optical feedback of slow light", IEICE Electron. Express, vol. 8, no. 13, pp.1075-1081, 2011.

24) H. Dalir and F. Koyama, "29GHz directly modulated 980nm vertical-cavity surface emitting lasers with bow-tie shape transverse coupled cavity", Appl. Phys. Lett., vol. 103, no. 091109, 2013.

25) H. Dalir, A. Matsutani, M. Ahmed, A. Bakry, F. Koyama, "High Frequency Modulation of Transverse-Coupled-Cavity VCSELs for Radio over Fiber Applications," IEEE Photonics Technology Letter", accepted, 2013.

26) H. Dalir and F. Koyama, "Push-Pull Modulation of Spatial Intensity Distribution of Transverse Coupled Cavity VCSEL", JJAP-Regular, submitted.

27) H. Dalir, Y. Takahashi, F. Koyama "Compact low driving voltage (<400mVpp) electro-absorption modulator laterally integrated with VCSEL", Electronics Letters, accepted 2013.

28) H. R. Stuart, "Dispersive Multiplexing in Multimode Optical Fiber", Science, vol. 289, Issue. 5477, pp. 281-283, 2000.

29) J. Leuthold , R. Hess,J. Eckner, P. A Besse, H. Melchior "Spatial mode filters realized with multimode interference couplers". Opt. Lett.,vol 21, pp. 836-839, 1996.

30) A. Imamura, W. Yang, J. Ferrara, Y. Hashidume, X. Gu, F. Koyama and C. J. Chang-Hasnain, OECC, Kaohsiung, Taiwan, 6E1-4, 2011.

2 Chapter: Transverse Coupled Cavity VCSEL for Bandwidth Enhancement

2.1 Rate Equation Model and Steady-State Solutions

In this chapter a novel method to raise the modulation bandwidth of vertical-cavity surface-emitting lasers (VCSEL) is proposed. The results show that the modulation bandwidth can be boosted by employing the lateral optical feedback of slow-light waveguide [1].

Fig. 2-1 shows the schematic of our proposed VCSEL structure with lateral optical feedback. Optical lateral confinement is formed using wide and narrow oxide layers, which leads to a leaky traveling wave in the lateral direction by reducing the width of a narrow oxide, the end reflector, which can be either an oxide layer or an etched facet, makes the lateral optical feedback into the VCSEL. It is noted that the group velocity of lateral traveling light in a Bragg reflector waveguide can be slow down [2], thus we are able to form ultra-compact an external optical feedback resonator. A typical optimal length of a lateral slow light waveguide is merely L_S = 8 μm to get the bandwidth enhancement up to 40 Gbps operations, which will be described later. The modelling was carried out for the bandwidth enhancement by using the Lang-Kobayashi rate equation [3]. The photon density and the carrier density are represented by $S(t)$ and $N(t)$, respectively.

$$\frac{dN}{dt} = \frac{\eta_i}{qV} I - \frac{N}{\tau_s} - v_g g N_p \tag{2-1}$$

$$\frac{dN_p}{dt} = \frac{1}{2}(1-\alpha)(\Gamma v_g g - \frac{1}{\tau_{ph}})N_p + \Gamma R'_{sp} + 2K_C \cos(\Theta)\sqrt{N_p(t) - N_p(t-\tau)} \tag{2-2}$$

$$\frac{d\Psi}{dt} = \frac{1}{2}\alpha \frac{dG}{dN}\Delta N - K_C \sin(\Theta)\sqrt{\frac{N_p(t-\tau)}{N_p(t)}} \tag{2-3}$$

where $G(t)$ is the modal gain including nonlinear gain, $\tau_{ph}$is the photon lifetime, $\tau_s$is the carrier lifetime, Γ is the confinement factor, θ is the relative phase of lateral feedback

light, *J(t)* is the injected current density, *d* is the active region thickness, K_C is its coupling feedback coefficient and τ is the delay time for optical feedback [4]. In this modelling, the frequency chirping effect was ignored, and the phase θ is time-independent. From equations (1) and (2), one can derive the following small-signal intensity modulation response.

$$H(\omega)=\frac{\Gamma\frac{dG}{dN}S_0\left(\frac{1}{\tau_{ph}}+2K_C.\cos(\theta)\right)}{\Gamma\frac{dG}{dN}S_0\left(\frac{1}{\tau_{ph}}+2K_C.\cos(\theta)\right)+\left(j\omega+\frac{1}{\tau_s}+\Gamma\frac{dG}{dN}S_0\right)\times\left(j\omega+K_C.\cos(\theta)\times(1-e^{-i\omega\tau})+\varepsilon S_0\left(\frac{1}{\tau_{ph}}+2K_C.\cos(\theta)\right)\right)} \quad (2\text{-}4)$$

where ε is the nonlinear gain coefficient and $\frac{dG}{dN}$ is the differential gain. The result is the same as refs. [1] and [4]. In this device light is confined from top and bottom mirrors, so the light guides zigzag in a lateral direction. Light coupled from a VCSEL to a Bragg reflector waveguide through a narrow oxide, ambulates perpendicularly in the lateral direction which is causes slowing light. The group velocity v_g is reduced by a factor of more than 20 for a single mode VCSELs. Thus, if we use such a slow light waveguide for optical feedback we are able to reduce the length of the feedback waveguide, which is given by:

$$L_S=\frac{\tau\times v_g}{2} \quad (2\text{-}5)$$

The modulation response is dependent on the delay time τ, the coupling feedback coefficient K_C and the phase given by:

$$\theta=2\beta L_s+\theta_R \quad (2\text{-}6)$$

where β is the propagation constant of the slow light waveguide and θ_R is the reflection phase shift at the end reflector. The coupling feedback coefficient K_C can be obtained from the field distribution in a slow light waveguide coupled from a VCSEL. Fig. 2-1(b) and (c) show the calculated intensity distribution of a laterally coupled VCSEL and slow light waveguide by using a mode-matching method (FIMMWAVE, Photon Design Co.). By varying the vertical position of the narrow oxide layer, coupling strength can be changed while mainly we can change it by altering the width of oxide layer. Its coupling coefficient K_C could be estimated as shown in the fig. caption. In the modeling, a slow light waveguide was assumed to be transparent, however, in real situations, injection current is needed to compensate the absorption loss of the waveguide.

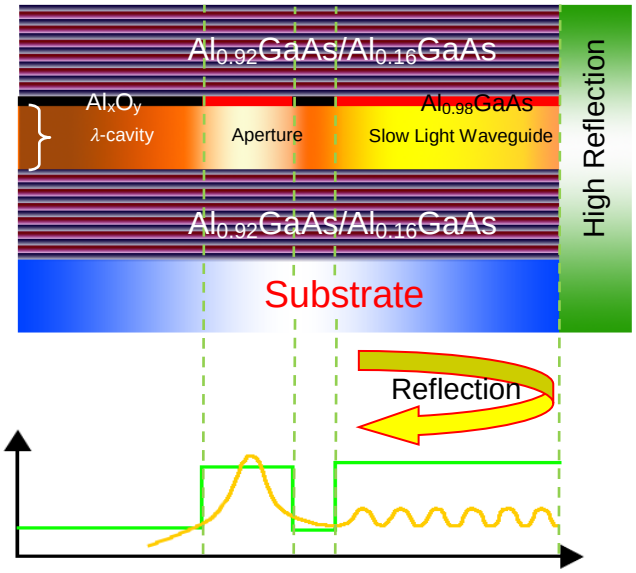

(a)

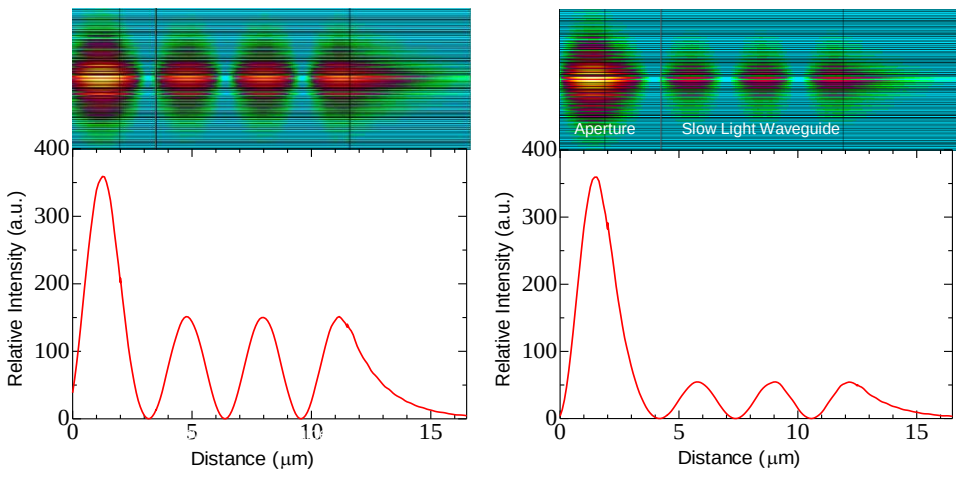

(b) (c)

Fig. 2-1. (a) Schematic structure of VCSEL with lateral optical feedback of slow light, (b), and (c) Calculated intensity distribution of VCSEL with coupled slow light waveguide for different trench bottom layer and coupling coefficient; (b) 1.5 μm-oxide-layer: $K_C = 2.3\times10^{11}\ sec^{-1}$ and (c) 2.5 μm-oxide-layer: $K_C = 0.7\times10^{11}\ sec^{-1}$.

The manipulation of the speed of light has been appealing much interest in these days. Especially, slow light seen in semiconductor amplifiers and micro-resonators has been studied for optical buffer memories, optical delay lines and etc. Also, the slow group velocity of light drastically reduces the size of various optical devices. An important issue of slowing light devices is how to couple with slow light in a Bragg reflector waveguide. In the current device light is confined from top and bottom with 40 pairs of $Al_{0.92}GaAs/Al_{0.16}GaAs$, so the light travels zigzag with the angle of Φ in lateral direction. Near the cut of condition Φ will close to 90 (fig.2-2), therefore light ambulates perpendicular in lateral movement which is leads to slowing light. The slow-down factor is over 20 in the wavelength range of 987 – 990 nm. Thus, if we use such a slow light waveguide for optical feedback we are able to reduce the length of the feedback waveguide. The slowdown factor is f written by the following equation (2-7), where n is the refractive index of the cavity; n_g is the group index, and v_g is the group velocity.

$$f = \frac{c}{n\ v_g} = \frac{n_g}{n} \qquad (2\text{-}7)$$

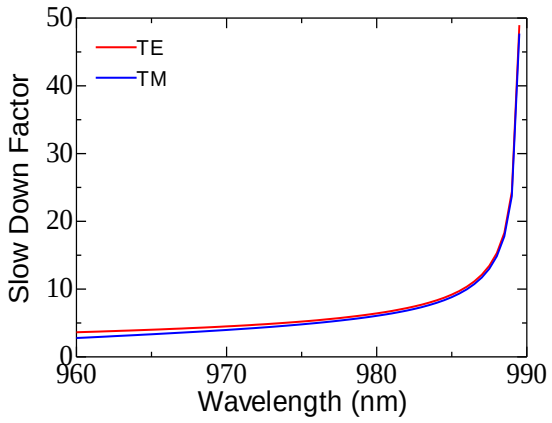

Fig.2-2 Calculated slow down factor as a function of wavelength.

2.2 Small-Signal Frequency Response

The calculated small signal response is shown in Fig. 2-3 for conventional VCSEL and laterally-coupled VCSEL. We assumed material parameters for conventional 980 nm VCSELs. The oxide aperture is assumed as 2×2 μm^2. The bias current fixed at 2 mA. The important parameters are the coupling coefficient K_C and the delay time τ. By optimizing the structure parameters in lateral coupling, we see 60% improvement in the 3-dB modulation bandwidth. If the relaxation oscillation frequency is 25 GHz without optical feedback, the modulation bandwidth can reach at 40 GHz. Fig. 2-4 shows the calculated 3-dB bandwidth versus delay time for different coupling coefficients. It is noted that the phase and the delay time are not independent parameters related by eqs. (2-4) and (2-5). We found that there is no bandwidth enhancement with in-phase coupling ($\frac{\pi}{2} < \theta < \frac{\pi}{2}$) while we see the bandwidth enhancement with out-of-phase coupling. The maximum 3-dB bandwidth is obtained for $K_C = 2.3 \times 10^{11}\,\text{sec}^{-1}$ and $\tau = 3.6ps$.

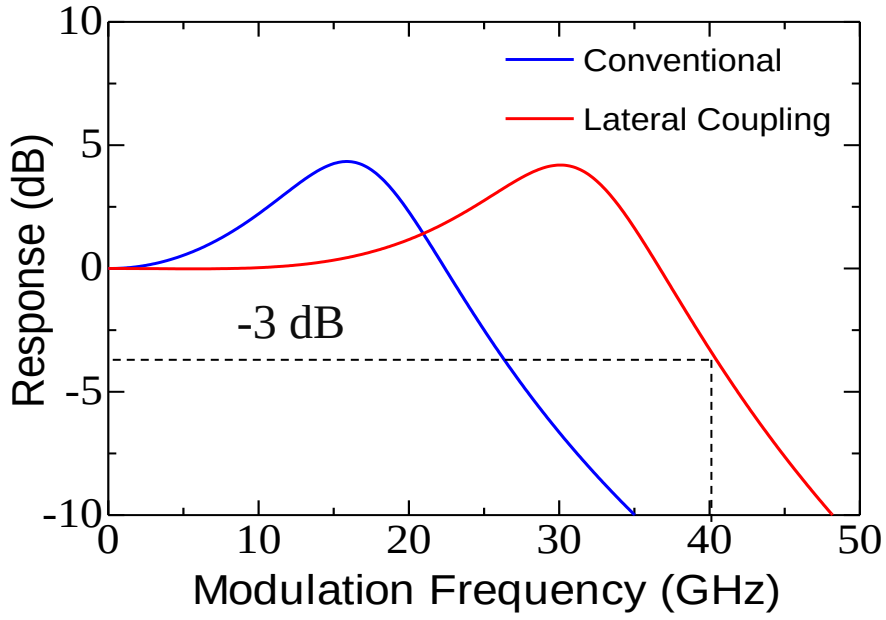

Fig. 2-3 Small-signal modulation response of 980 nm conventional VCSEL and VCSEL with lateral coupling scheme.

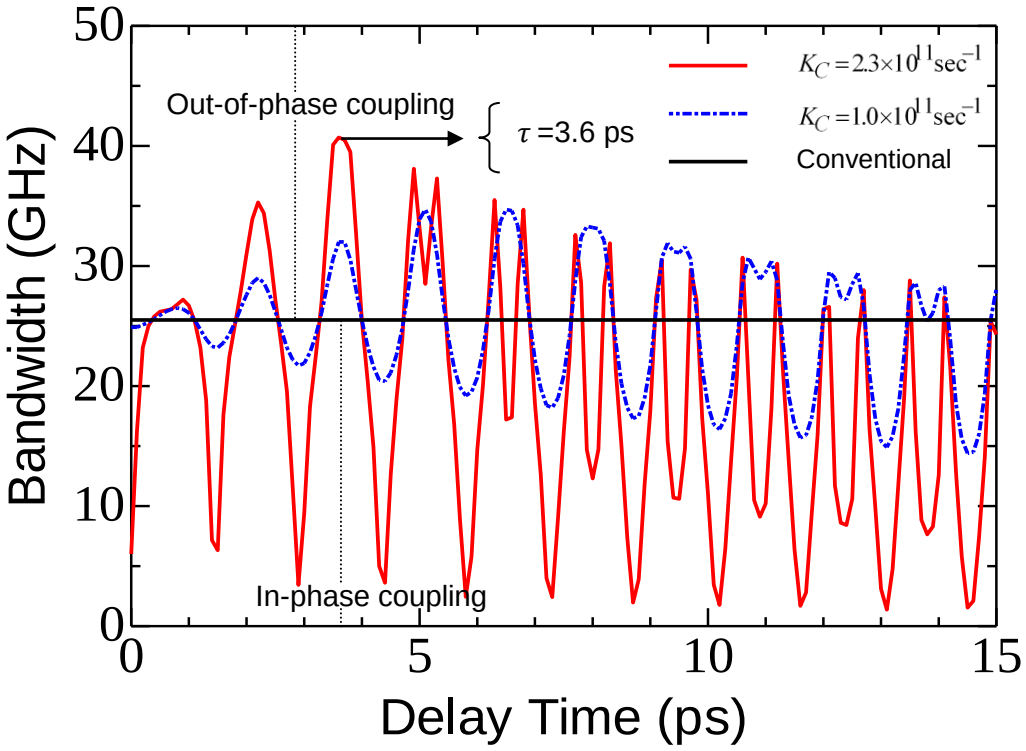

Fig.2-4 Calculated 3-dB modulation bandwidth versus delay time with different coupling coefficients K_C scheme.

2.3 Large-Signal Frequency Response

The simulation of NRZ quasi-random large signal modulation with eqs (2-1) and (2-2) was carried out. Fig. 2-5(a) and (b) show the calculated eye patterns of conventional VCSEL and laterally coupled VCSEL at optimal condition, respectively. A 40 Gbps pseudo random bit sequence (PRBS) with a 2^{11}-1 word length was assumed. The swing of the modulation current was considered to be from 1.25 to 2.75 mA for both cases, which results us an extinction ratio of over 5 dB for lateral-optical-feedback VCSEL. This lateral-optical-feedback VCSEL shows clear eye opening even for 40 Gbps. A pattern-effect can be significantly avoided with help of lateral-optical feedback.

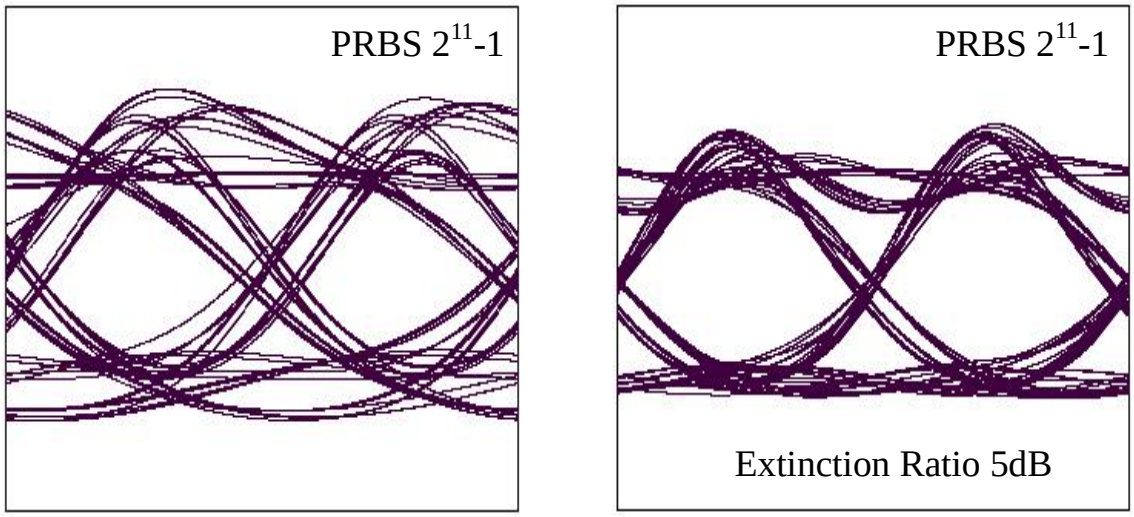

(a) (b)

Fig. 2-5 Large-signal modulation response of 980 nm conventional VCSEL and VCSEL with lateral coupling scheme;(a) eye pattern of conventional VCSEL, (b) laterally coupled VCSEL with $K_C = 2.3 \times 10^{11} \sec^{-1}$ and $\tau = 3.63 ps$.

2.4 Device Structure

Figures 2-6 shows the schematic cross-section of the fabricated transverse coupled cavity (TCC) VCSEL. The vertical structure is the same as conventional 980 nm InGaAs/GaAs VCSEL. The bottom mirror consists of a 41-period Si-doped $Al_{0.92}GaAs$/ $Al_{0.16}GaAs$ DBR on a 500 nm thick silicon-doped GaAs buffer layer. The active region has three $In_{0.2}GaAs$/GaAs quantum wells embedded in one-λ thick $Al_{0.3}Ga_{0.7}As$ separate confinement hetero-structure layer. 300 Å thick $Al_{0.98}GaAs$ is inserted in order to form lateral oxide confinement [5]. The top mirror consists of a 26-period carbon-doped $Al_{0.92}GaAs$/ $Al_{0.16}GaAs$ DBR, followed by a highly doped p-contact layer. .

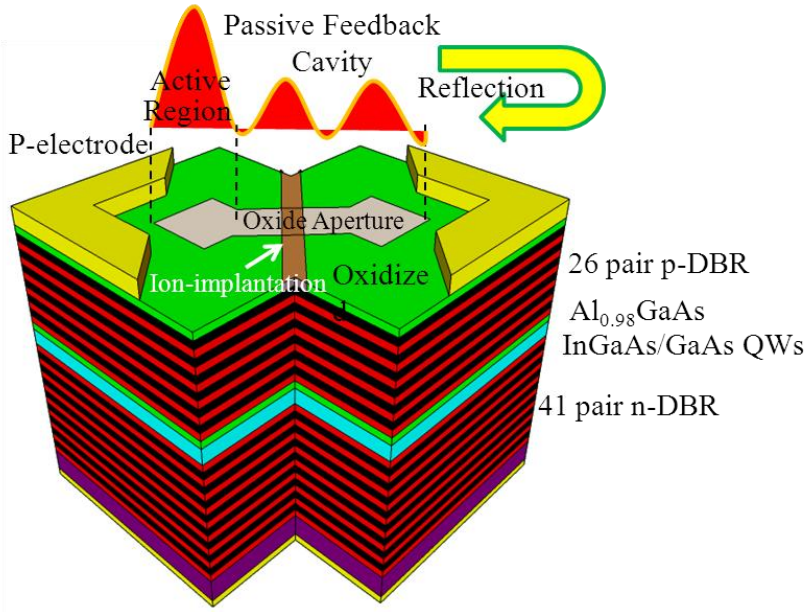

Fig. 2-6 The Schematic Structure of the transverse coupled cavity VCSEL.

Fig. 2-7 (a) shows the mechanism of PPR on TCC VCSEL. When the transverse fields travel from the laser cavity to feedback cavity the end interface of the feedback cavity functioning as a perfect mirror in the lateral direction, as a result the lateral optical coupling into the VCSEL is obtained. Fig. 2-7(b) depicts the extended modulation bandwidth obtained by applying PPR effect. Typically 3-dB bandwidth has linked to the carrier-photon resonance (CPR), largely because the CPR has inherent physical limitations. However, the direct modulation bandwidth can be substantially improved by employing the PPR effect.

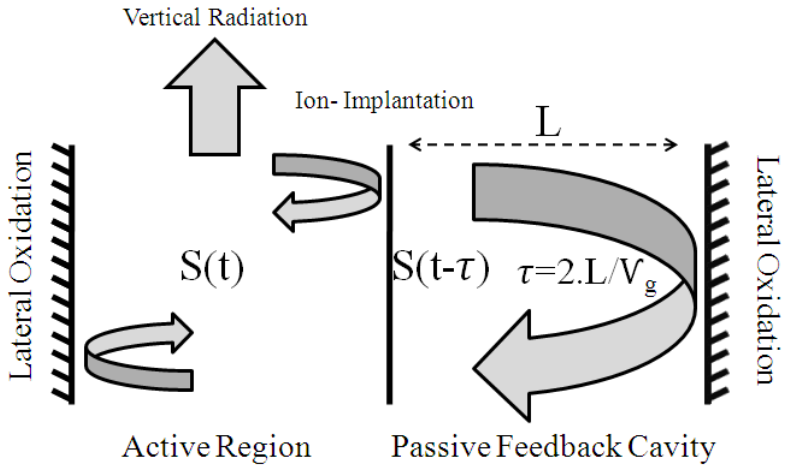

(a)

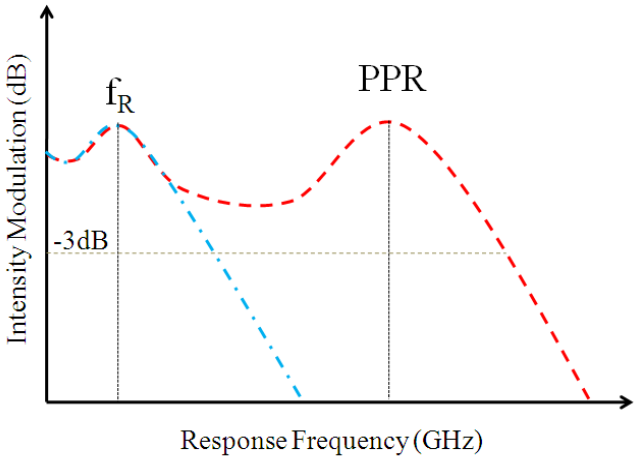

(b)

Fig. 2-7(a) Mechanism of exploiting PPR based on TCC VCSEL (b) extended modulation bandwidth obtained by applying PPR effect.

2.5 Origin of PPR Effect on the Bandwidth Enhancement

The origin of the improvement of modulation bandwidth by PPR effect can be simply explained by the frequency shift to the transverse laser mode induced by strong optical feedback. 3-dB cut off frequency can be expanded by the interference between the original optical frequency in absent of feedback and the ambulated frequency after the feedback is occurred. The difference between two frequencies corresponds to the boosted 3-dB cut off frequency. By a weak optical feedback in the laser cavity the carrier density will increases when the cavity phase is in out-of phase. This increase of carrier density induces the change of the optical frequency of the laser oscillation and results in red-shift of the relaxation oscillation frequency, while reduction in carrier density leads to the blue shift of laser.

From eq.2-3, once we can define the detuning parameter as follow:

$$\Delta\omega = \frac{1}{2}\alpha\frac{dG}{dN}\Delta N - K_C \sin(\Theta)\sqrt{\frac{N_p(t-\tau)}{N_p(t)}} \quad (2\text{-}8)$$

This second term of the above relation is zero for the VCSEL in the absence of feedback.

The resonance angular frequency made by the interference of self-feedback can be given:

$$\Delta\omega_{feedback} = K_C \sin(\Theta)\sqrt{\frac{N_p(t-\tau)}{N_p(t)}} \quad (2\text{-}9)$$

Boosted oscillation frequency in the presence of weak optical feedback can be given by:

$$\omega_{boosted}{}^2 = \omega_R{}^2 + \Delta\omega_{feedback}{}^2 \quad (2\text{-}10)$$

In addition to this, using eq. 2-3, we can plot the gain as a function of phase, while the line-width enhancement factor is a key issue [6]. In Fig 2-8 upper and lower value of modal gain is located at out-phase in-phase condition, respectively. In Fig. 2-9 the ratio change of photon lifetime in the presence of feedback over the photon life time of solitary laser is considered. In Figs. 2-8 and 2-9 the parameter were used for strong and weak optical feed-back is same as Fig.2-4.

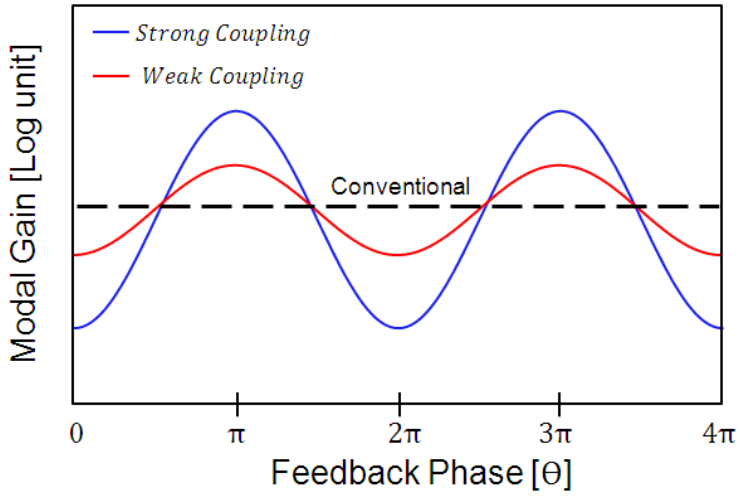

Fig. 2-8 Calculated modal gain for VCSEL with/without optical feedback.

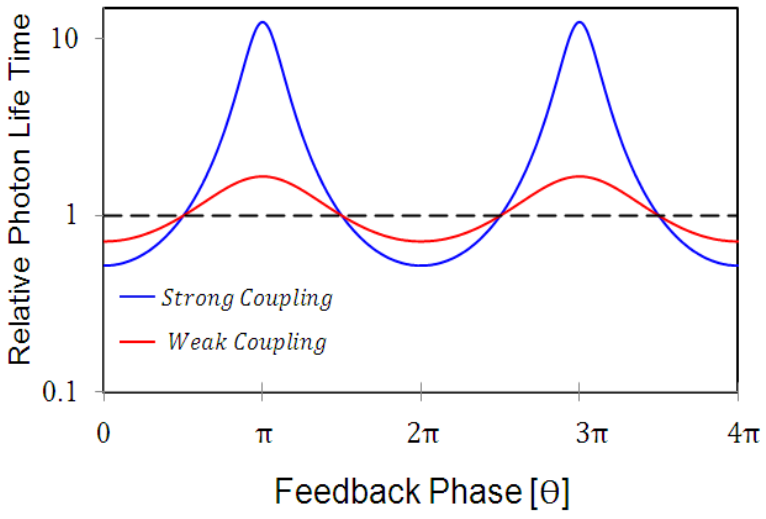

Fig. 2-9 Calculated relative photon-life time for VCSEL with/without optical feedback.

Assuming the phase of the feedback cavity in the vicinity of pie, we can reduce the effective photon life time, at the same time modal gain will enlarge. In addition to them relaxation oscillation frequency will have some red shift, as a result modulation bandwidth will be enhanced.

2.6 Three Dimensional Modelling

Fig. 2-10 illustrates the calculated intensity distribution of bow-tie shape coupled cavities by using a three dimensional film-mode-matching method (FIMMWAVE, Photon Design Corp.). 25-pairs of $Al_{0.92}GaAs$/ $Al_{0.16}GaAs$ for the top-mirror reflectivity and 40-pairs of $Al_{0.92}GaAs$/ $Al_{0.16}GaAs$ for the bottom DBR are assumed for the modelling. The layer structure is designed to have a cut-off wavelength of 983 nm, which is corresponding to the resonant wavelength for plane wave in the vertical direction. The oxide aperture size for each cavity is 4 μ m×2 μ m. In the modelling an air and perfect matching layer (PML) were set at the surface of the top DBR and the bottom interface of the structure side, respectively. From the left side of the model a slow light Eigen-mode of the Bragg reflector waveguide is excited. Increasing the width of the joint section of the bow-tie shape oxide aperture decreases the coupling efficiency between the two cavities. Coupling efficiency was figured out from the calculated intensity distribution in the following steps.

$$\beta = \iint I_{in} \times dxdz \tag{2-11}$$

and,

$$\alpha = v_g \times \int I_{out} \times dx \tag{2-12}$$

where β is the confined energy in the left VCSEL cavity,α is the coupled power per unit time to the right VCSEL, I_{in} is the intensity in the left VCSEL cavity, I_{out} is the flux traveling to the right VCSEL cavity. $v_g=c/n_g$ is the group velocity of the slow-light mode with a group index of n_g. The group index is typically around 100 for the slow light waveguide.

Then it can be defined the radiation loss per unit time from the left VCSEL cavity by dividing eq.2-11 by eq.2-12:

$$\frac{1}{\tau_{\text{out}}} = \frac{v_g \times \int I_{out} \times dx}{\iint I_{in} \times dxdz} \tag{2-13}$$

Assumption is that the internal absorption loss in a VCSEL cavity is 20 cm^{-1}. The coupling efficiency can be given by the following equation:

$$\eta = \frac{\frac{1}{\tau_{\text{out}}}}{\frac{1}{\tau_{\text{in}}} + \frac{1}{\tau_{\text{out}}}(1+\phi)} \tag{2-14}$$

where ϕ is the relative scattering loss in the bow-tie section and $1/\tau_{in}$ is the absorption loss per unit time. The definition of the coupling efficiency is the same as the slope efficiency of top emitting VCSELs, namely the slope of the laser's top emitting output power versus drive current. Fig. 2-11 shows the calculated coupling efficiency and scattering loss as a function of bow-tie connection length. By optimizing the structure parameters in lateral coupling, we see 92% of coupling efficiency and scattering loss of 0.2 % when the bow-tie connection length is around 0.5 μm. Increasing the length of the bow-tie connection to 2 μm, the coupling efficiency is decreased to 45% and radiation loss is increased to 1.7 %. A radiation loss of 1.7 % per one round trip in the cavity is corresponding to 0.6 cm^{-1} of average loss per unit length. Thus, the scattering loss at the bow-tie joint section is much smaller than the internal absorption loss.

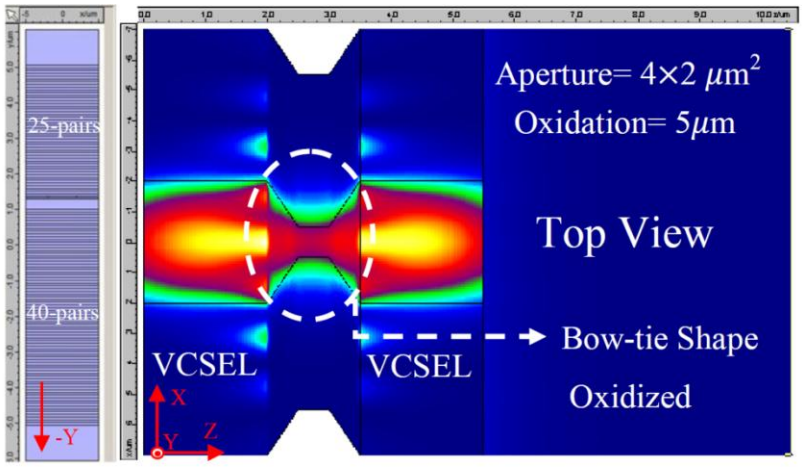

Fig. 2-10 Calculated top view field distribution of TCC VCSEL and slow light wave guide by using a three dimensional mode-matching method.

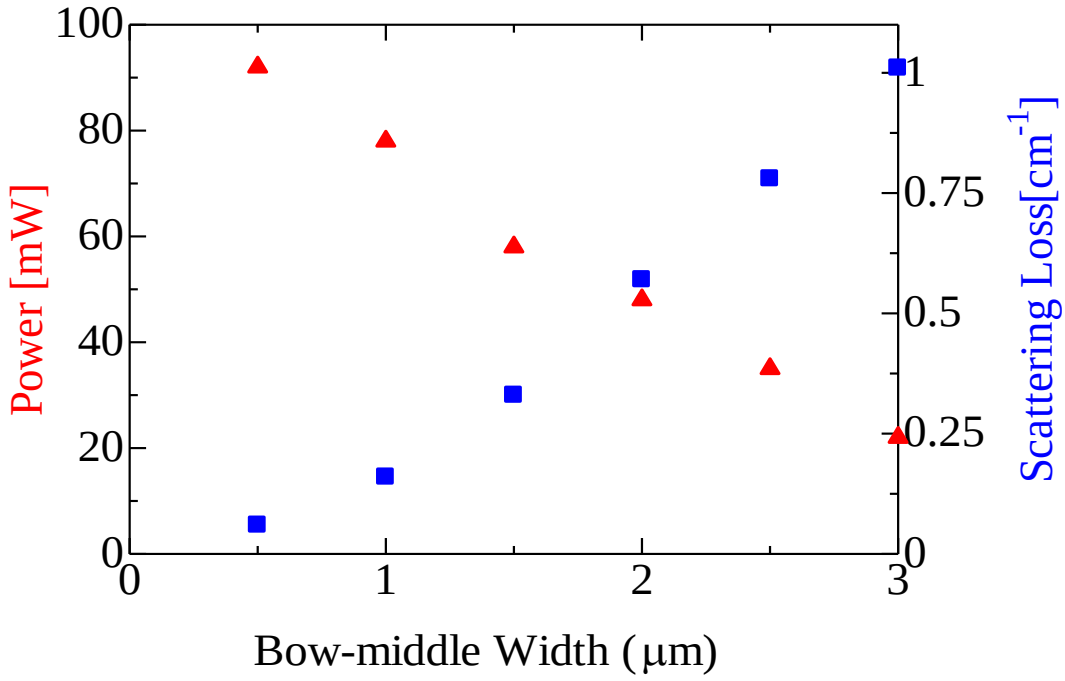

Fig. 2-11 Calculated coupling efficiency and scattering loss as a function of bow-middle width, and red insets, is the radiation loss per cm.

2.7 Fabrication Process

The device is made on a wafer grown by metal organic chemical vapour deposition (MOCVD). The active region includes three 980 nm GaInAs/GaAs quantum wells (3QWs). In order to form transverse coupled cavity structures, bow-tie shaped mesas were formed by dry-etching process and followed by wet-oxidation process. Two square apertures of 8.5 μm × 8.5 μm are jointly connected to form bow-tie shaped oxide apertures while the joint region is less than few microns, which leads to a leaky travelling wave in the lateral direction. One of the square oxide apertures is operated as a VCSEL while the other side functions as a feedback cavity. The end interface of the feedback cavity functioning as a perfect mirror in the lateral direction makes the lateral optical coupling into the VCSEL. Bow-tie shaped mesas are planarized using polymer (ALX-2010, Asahi Glass). The proton implantation with six-step different acceleration voltages from 60 to 350 kV doses of 10^{15} cm^{-2} was performed at the centre of the joint connection of the coupled cavities. According to the measured depth profile, the protons penetrated almost the entire top DBR, the total thickness of which was 4 μm. An electrical isolation over 1 MΩ corresponding to a leakage below 2 μA was attained under forward bias conditions of the two cavities. P-type (Au/Zn/Au) and n-type (AuGe/Ni/Au) electrodes are formed on both sides of the wafer.

The fabrication process flow is shown briefly in the following:

1) Wafer structure

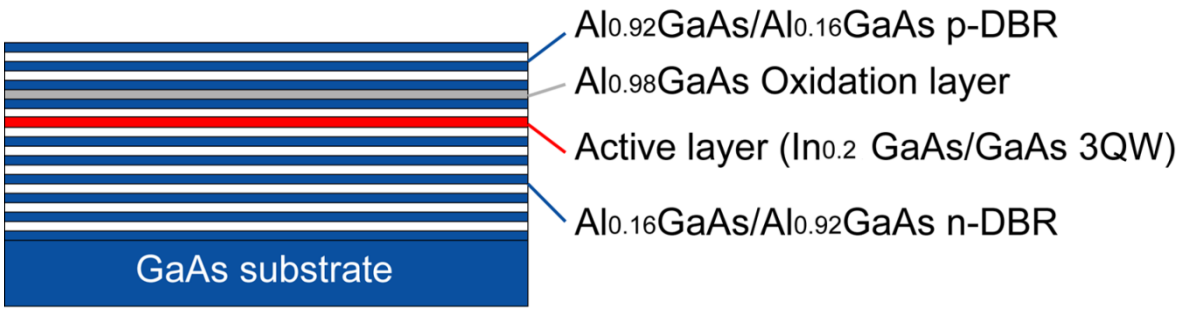

2) SiO_2 sputtering

Sputtering time should be 2hrs, corresponding to 470-490 nm thickness (Violet blue to pink colour)

3) Resist coating

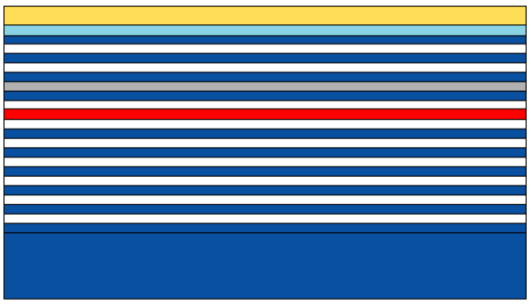

	1st spin-Time	2nd Spin-Time	Prebake-Time
OAP	500 rpm 5 sec	4000 rpm 30 sec	100°C 90 sec
AZ 5200NJ Twice	500 rpm 5 sec	1500 rpm 30 sec	100°C 90 sec

4) Exposure and Development (preparing for proton implementation)

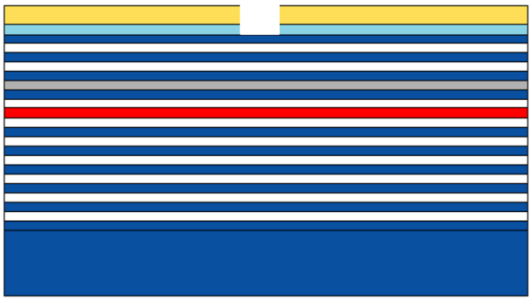

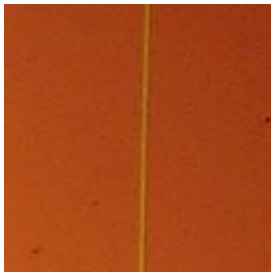

Exposure 12 sec
AZ Developer 50 sec
BHF 30 sec

5) Resist removal

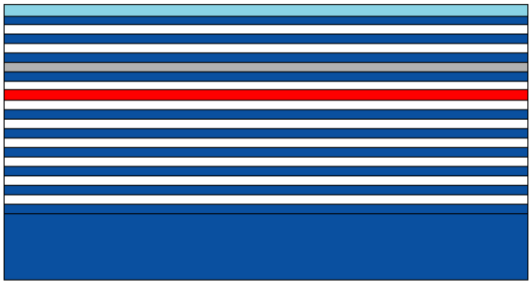

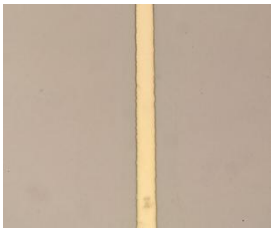

Plasma Aching 2-3 hrs.

6) Resist coating

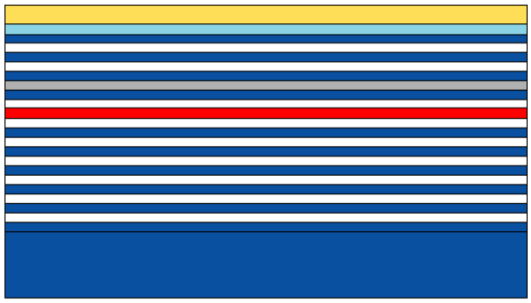

	1st spin-Time	2nd Spin-Time	Prebake-Time
OAP	500 rpm 5 sec	4000 rpm 30 sec	100°C 90 sec
AZ 5200NJ	500 rpm 5 sec	3000 rpm 30 sec	100°C 90 sec

7) Exposure and Development

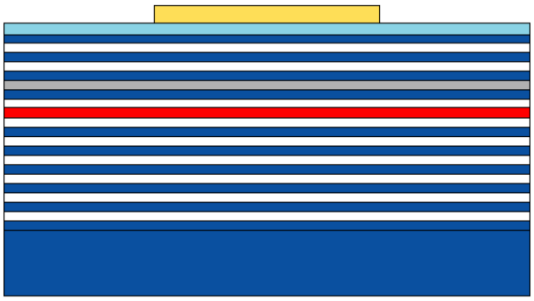

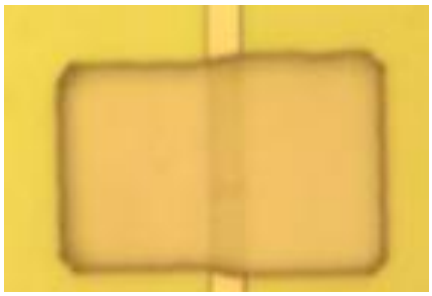

Exposure 6 sec
AZ Developer 40 sec

8) SiO_2 etching

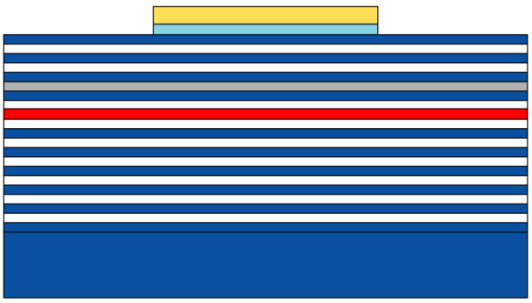

BHF 30 sec

9) ICP and Resist Removal

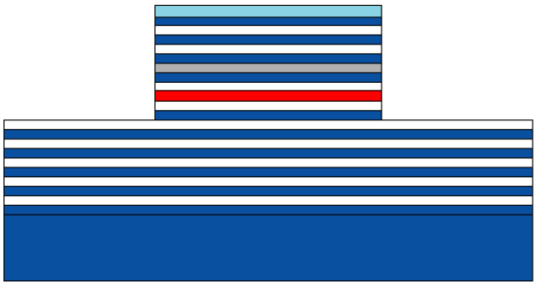

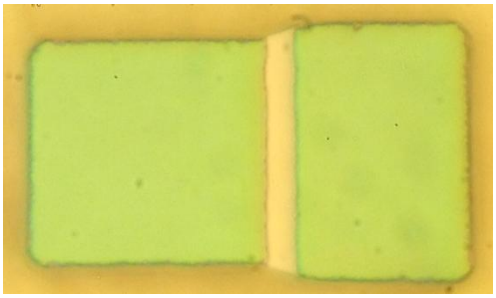

10) Oxidation

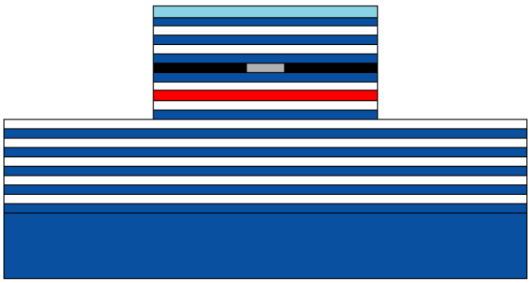

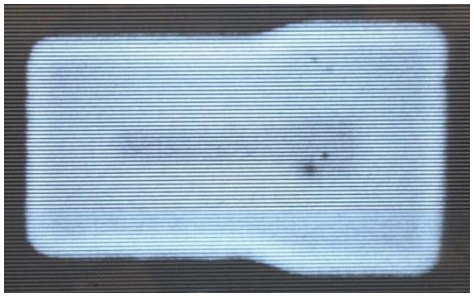

11) Resist coating

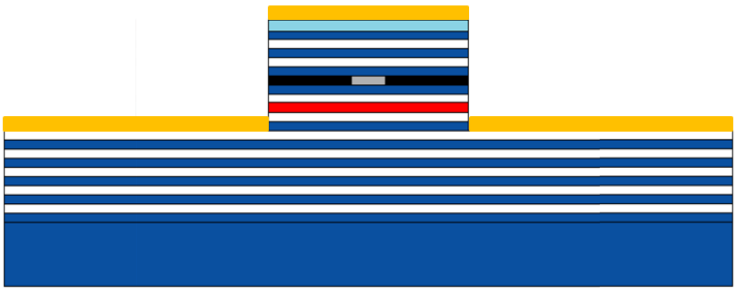

	1st spin-Time	2nd Spin-Time	Prebake-Time
OAP	500 rpm 5 sec	4000 rpm 30 sec	100°C 90 sec
AZ 5200NJ Twice	500 rpm 5 sec	1500 rpm 30 sec	100°C 90 sec

12) Exposure and Development (N-electrode)

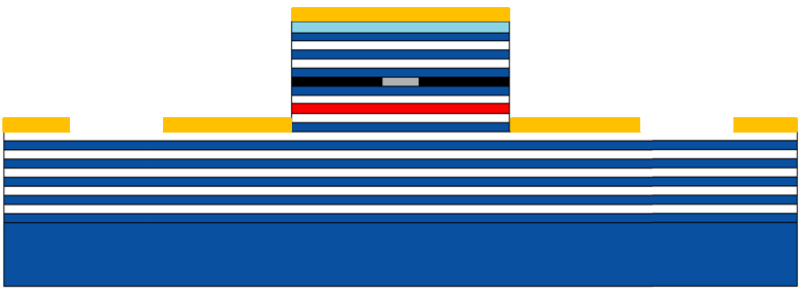

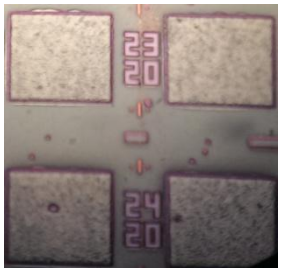

13) ICP etching (N-electrode)

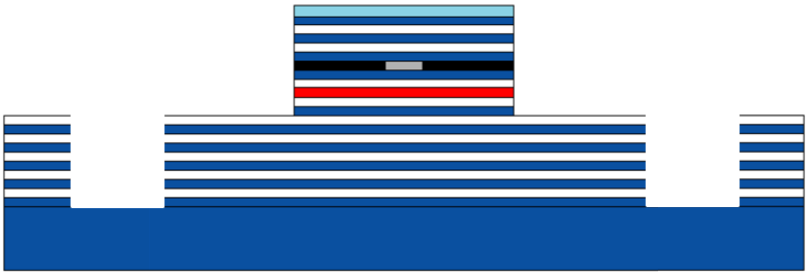

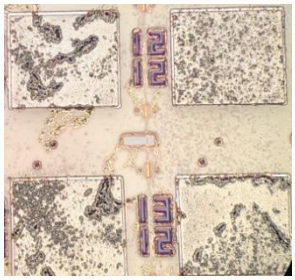

14) Electrode evaporation (N-electrode)

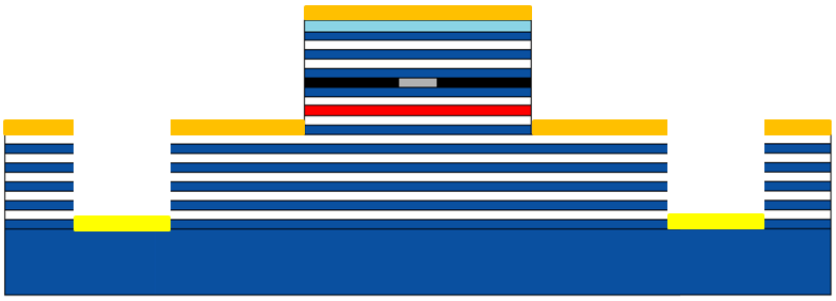

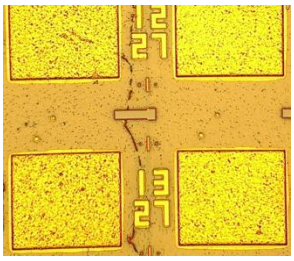

15) Polymer coating

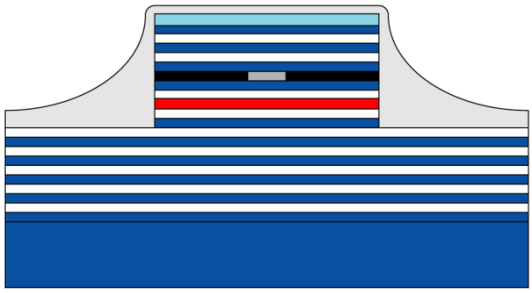

	1st spin-Time	2nd Spin-Time	Prebake-Time
AP	500 rpm 5 sec	4000 rpm 30 sec	100°C 90 sec
Al 2010 Twice	500 rpm 5 sec	5000 rpm 30 sec	60°C 90 sec

16) Exposure and Development

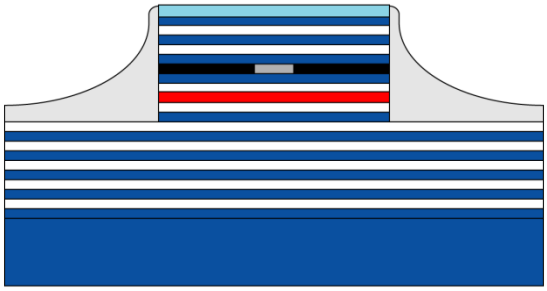

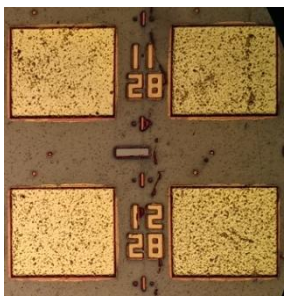

17) Cure

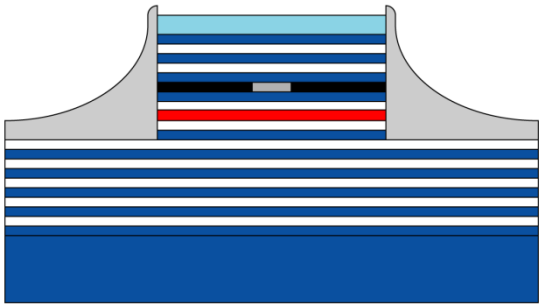

30 min-300°C

18) SiO_2 removal

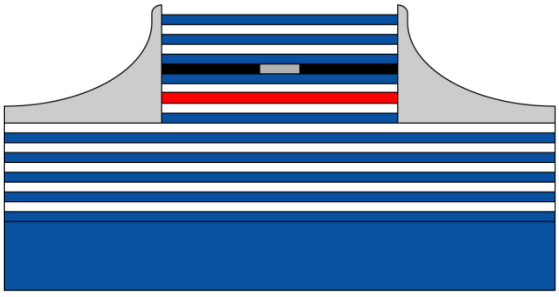

BHF 30 sec

19) Resist coating

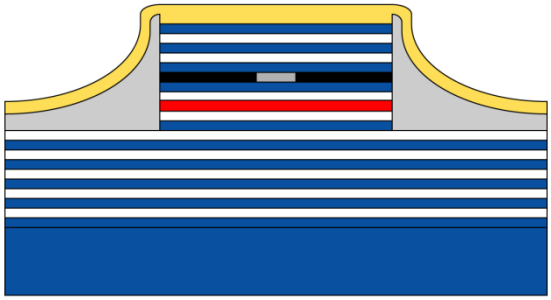

	1st spin-Time	2nd Spin-Time	Prebake-Time
PMGI	500 rpm 5 sec	4000 rpm 30 sec	150°C 90 sec
AZ 5200NJ	500 rpm 5 sec	1500 rpm 30 sec	100°C 90 sec

20) Exposure and Development (P-electrodes)

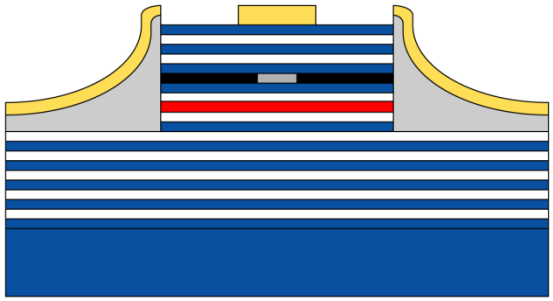

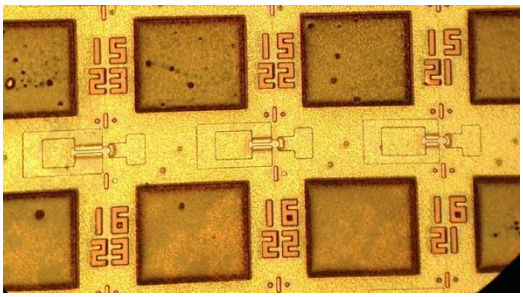

21) Evaporation (P-electrodes)

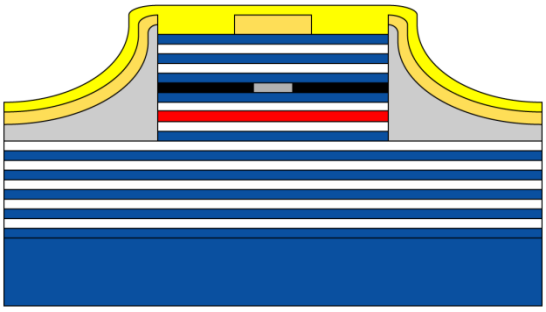

Au/Zn/Au
20 nm/40 nm/200 nm

22) Lift off and Annealing

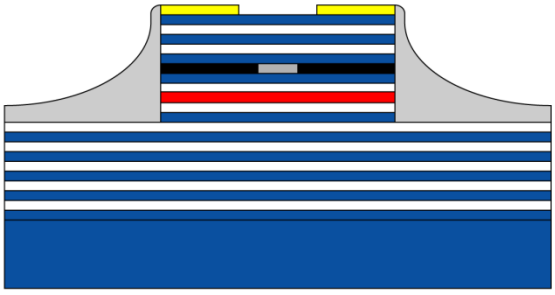

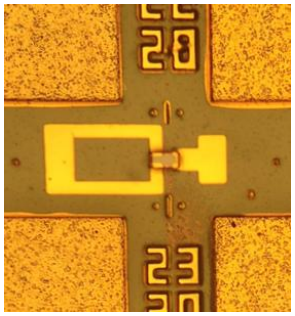

23) Evaporation (N-electrodes) and Annealing

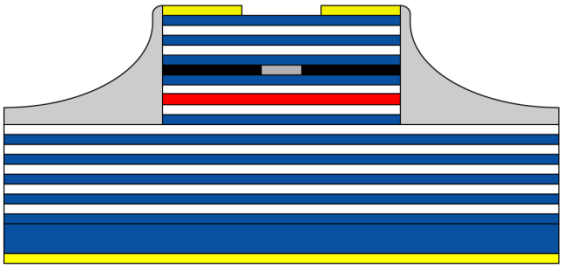

AuGe/Au
100 nm/100 nm

2.8 Measurement Set-up

The measurement setup for modulation characteristics of small signal and large signal is shown in Fig. 2-12. One side cavity of a TCC VCSEL is directly modulated by superimposing a RF signal while the other side is open circuited or connected to a DC supplier for quasi-single and multi-mode aperture devices, respectively. Output light is captured by a photo-detector (PD) with a bandwidth of 25 GHz through a multi-mode fibre. The small signal modulation response is measured by using a network analyser with a bandwidth of 40 GHz. Also large signal results from the back-to-back, via multiplexing of 4 × 12.5 Gbps channels is achieved which potentially can reach up to 50 Gbps. The black and red parts in the Fig. 2-12 show the measurement set up of small signal and large signal, respectively.

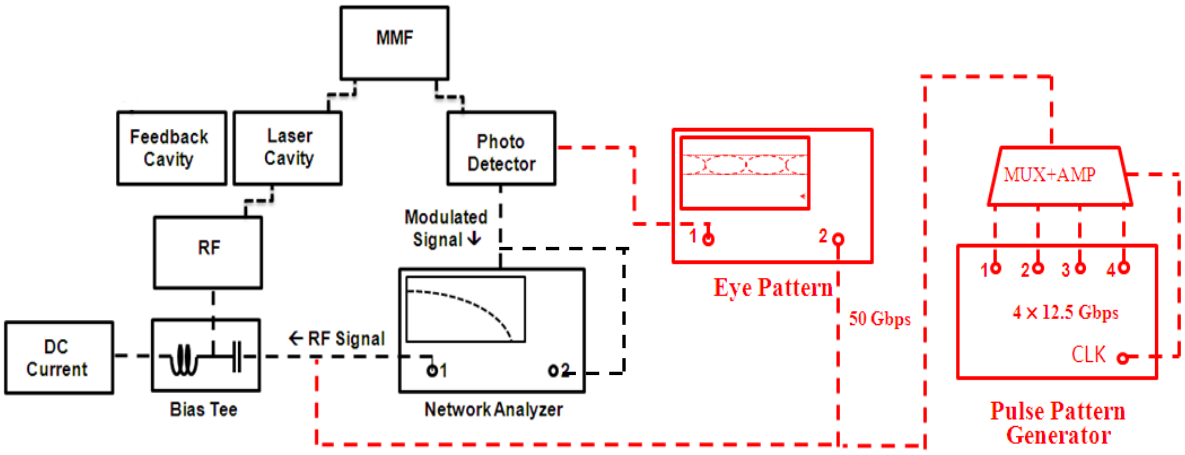

Fig. 2-12 Measurement setup for dynamic modulation characteristics of quasi single mode VCSEL.

2.9 Static Characteristics

Static results of TCC VCSEL has been carried out for two different aperture sizes. Fig. 2-13 (a) and (b) show the oxidation aperture for multi-mode and quasi-single mode VCSEL respectively.

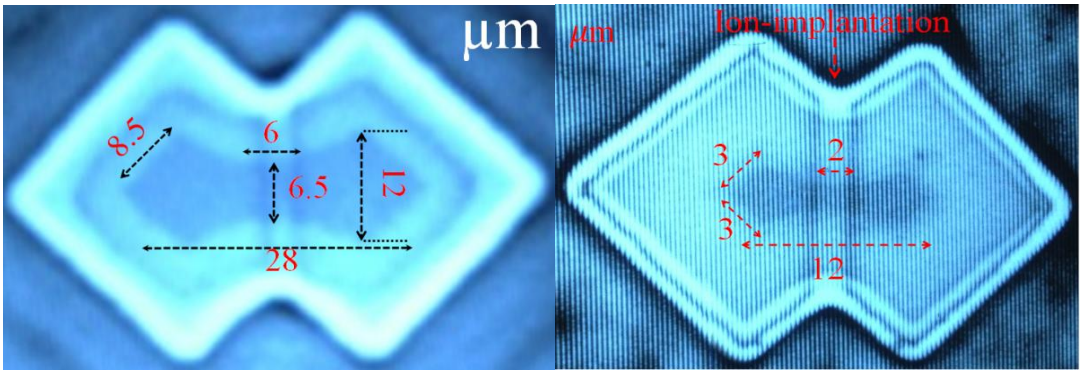

(a) (b)

Fig. 2-13 (a) Multi-mode and (b) quasi-single mode TCC VCSEL.

2.9.1 Multi-mode TCC VCSEL

Fig.2-14 shows the measured L-I curves of multi-mode TCC VCSEL for different feedback currents while the laser current is varied from 0-10 mA. Threshold currents are as low as 0.7 mA. Applying a reverse voltage of 1 V in the feedback cavity provides a smooth L/I curve, showing that the ripple is due to the transverse optical feedback. A multi-mode fibre (MMF) and optics were used so that the output from each cavity is collected independently. We measured the spatially resolved lasing spectrum spectra of the two cavities as shown in Fig. 2-15. The result shows that two cavities are coherently coupled and hence show the same lasing wavelength of the dominant modes of each cavity. We also measured the near-field pattern (NFP) of the fabricated device. Figure 2-16 shows the measured NFP of a TCC VCSEL while a VCSEL cavity was pumped by a fixed current of 6 mA and no injection current was delivered to the feedback cavity at open circuit. Thanks to the ion implant, the differential resistance of over 10 MΩ is achieved leading to reduce the leakage current between the top p-type electrodes to be below 1 μA. Figure 2-16 clearly shows the transverse optical coupling between the two cavities.

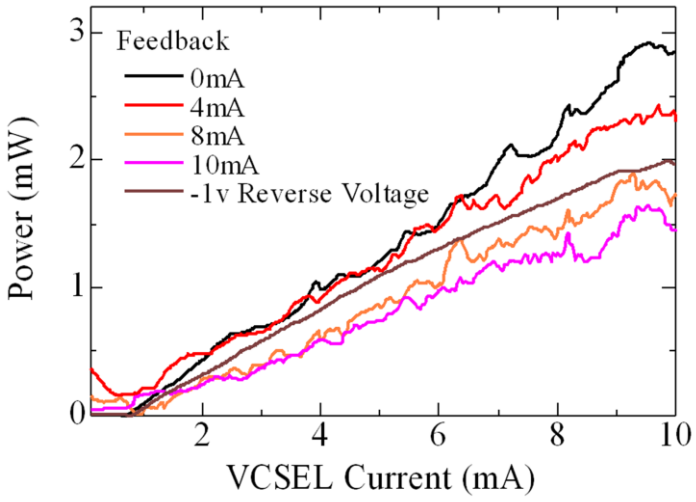

Fig. 2-14 L/I characteristics with different currents in the feedback cavity.

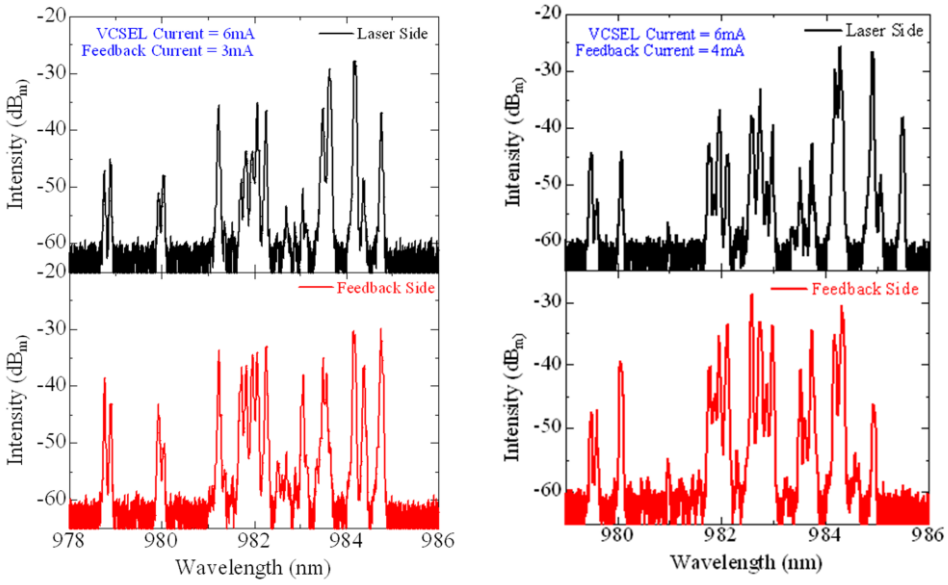

(a) (b)

Fig. 2-15 Lasing spectra for the feedback cavity and the laser cavity for (a) 3 mA and (b) 4 mA currents of feedback cavity, respectively with the fixed 6 mA of laser side.

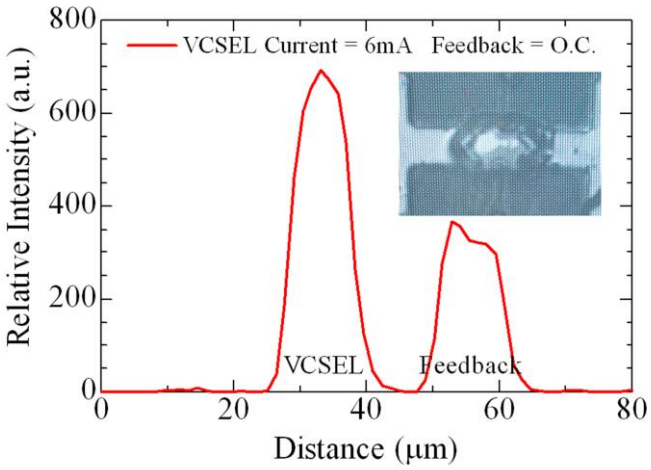

Fig. 2-16 Measured NFP of TCC VCSEL with a fixed current of 6mA in a VCSEL side and no injection current to the feedback cavity at open circuit.

2.9.2 Quasi Single-mode TCC VCSEL

Fig. 2-17 shows the measured L/I characteristics of VCSELs with and without optical feedback fabricated by the same epi-wafer. A "conventional VCSEL" without optical feedback has a neck width of the bow-tie joint region is too short, resulting in no-feedback effect. The observed ripples would be the evidence to prove the fact that lateral optical feedback takes place even without current injection on the feedback cavity. We measured the spatially resolved lasing spectrum emitted from the laser cavity through a multi-mode fibre. A quasi-single-mode operation with side mode suppression ratio of 23 dB was obtained at a bias current of 6 mA as shown in Fig. 2-18.

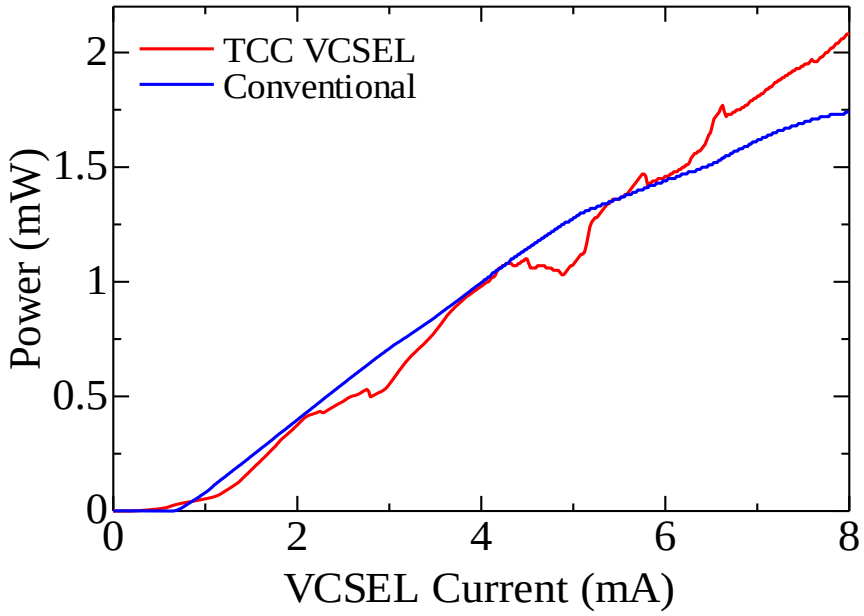

Fig. 2-17 L/I characteristics for TCC –QSM VCSEL and conventional VCSE without optical feedback.

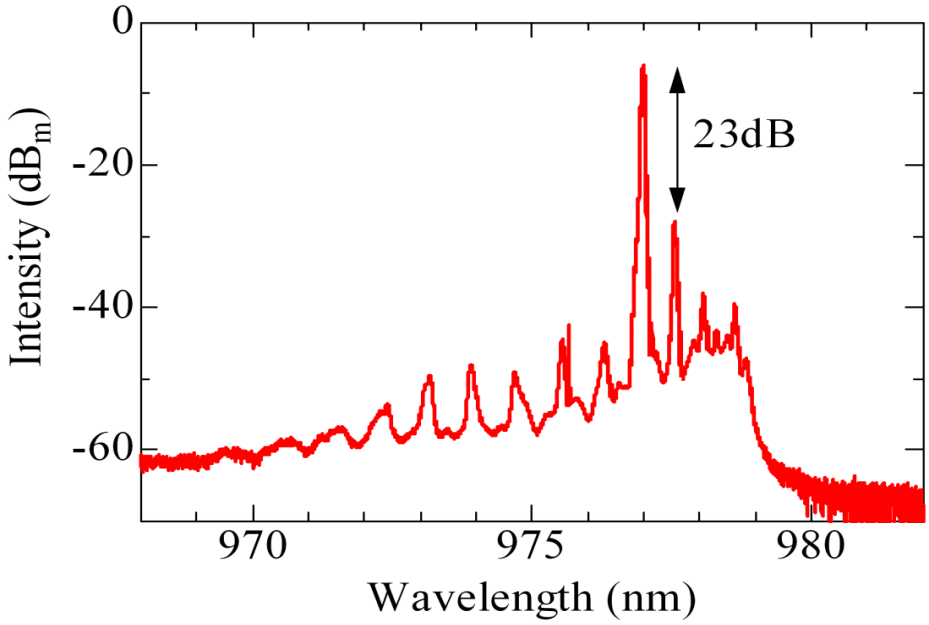

Fig. 2-18 Lasing spectrum of the laser side for TCC VCSEL at 6mA.

2.10 Dynamic Results

Small signal and eye pattern results were attained for the multi-mode and quasi-single mode 980 nm TCC-VCSEL with aperture size as described in Fig. 2-13 (a) and (b), respectively. Measurement of quasi-single mode was done as shown in Fig. 2-12, while in order to control the phase of feedback for multi-mode case a DC supply was required to be connected to the feedback cavity side. In addition, The DC supplier acts as loss compensator in the large size of feedback cavity.

2.10.1 Multi-mode TCC VCSEL

Fig. 2-19 illustrates the measured small signal response of a multi-mode TCC VCSEL with and without transverse feedback at a fixed injection current of 10 mA into a VCSEL cavity. By applying a reverse bias voltage of 1 V, we could avoid the optical feedback effect as shown in Fig. 2-14. It is shown that the injection current in the feedback cavity enables us to control the phase and the amplitude for feedback light. By applying a reverse bias voltage in the feedback cavity, the 3-dB bandwidth was clearly decreased to 9 GHz, which is in the same level of a conventional VCSEL. We could see a noticeable bandwidth enhancement by more than a factor of three to the compare with the VCSEL without optical feedback. The control of the feedback phase and amplitude enables to go beyond 25 GHz. The result shows that the bandwidth is increased to go beyond 29 GHz of the limitation of the photo detector we used. This bandwidth is currently world's fastest 980 nm VCSEL. The basic physics behind would be similar to the bandwidth enhancement due to photon-photon resonances in edge emitting lasers [7,8]. It is noted that the multi-mode operation with photon-photon resonances enables us to tailor the modulation transfer function so that a flat frequency response can be extended far beyond the relaxation oscillation frequency. An advantage of our scheme is that tailoring the transfer function could also compensate the limitation of the parasitic capacitance.

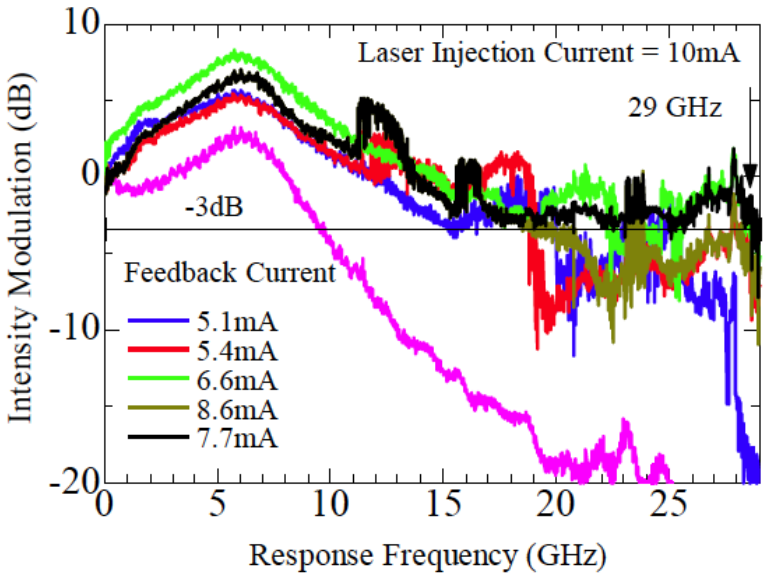

Fig. 2-19 Measured small-signal modulation response of 980 nm transverse coupled cavity VCSEL.

A 36 Gbps non-return-to-zero large signal modulation with a pseudo random bit sequence of 2^{31}-1 was carried out as shown in Fig. 2-20. Injection currents into a laser and a feedback cavity are 6 and 2 mA, respectively. An extinction ration is over 4 dB. Our TCC VCSEL shows clear eye opening even for 36 Gbps while the eye was completely closed without feedback. We could see a large bandwidth enhancement over a factor of 3 thanks to the multi-mode photon-photon resonance effect, while the device structure and the operating conditions have not been fully optimized yet.

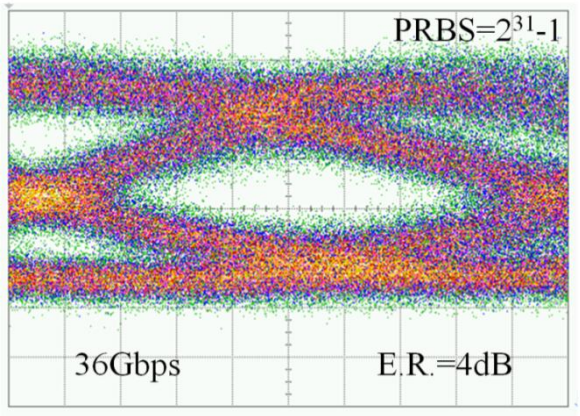

Fig. 2-20 Measured 36 Gbps eye pattern for TCC-VCSEL with a 2^{31}-1 word length. Injection currents into a laser and a feedback cavity are 6 mA and 2 mA, respectively.

However, using this device in practical application needs a lot of effort to control the phase. To overcome this obstacle, we have designed smaller aperture of feedback cavity to get the out-of phase condition automatically, which leads to bandwidth extension in all ranges.

2.10.2 Quasi Single-mode TCC VCSEL

Figure 2-21 shows the measured small signal response of a TCC-QSM VCSEL with and without optical feedback at a fixed bias current of 6 mA into a VCSEL cavity. The 3-dB bandwidth without optical feedback is around 9 GHz, which is limited in a standard 980 nm VCSEL epi-wafer design we used. We can see a noticeable extension of 3-dB bandwidth by a factor of 3 in comparison with a VCSEL without optical feedback. The dashed line shows the calculated modulation response of conventional VCSELs by using a standard rate equation analysis. It is noted that the quasi-single-mode operation with photon-photon resonances enables us to tailor the modulation transfer function so that a flat frequency response can be extended far beyond the relaxation oscillation frequency. An advantage of our scheme is that tailoring the transfer function could also compensate the limitation of the parasitic capacitance. Even without injection current in a feedback cavity functioning as a passive resonator, the transverse optical feedback makes large contribution to the bandwidth enhancement as observed in the multi-mode TCC VCSEL. We are able to avoid the precise control of phase tuning current in the multi-mode coupled cavity, which also avoids extra power consumption and difficulty in stability in multi-mode coupled cavities.

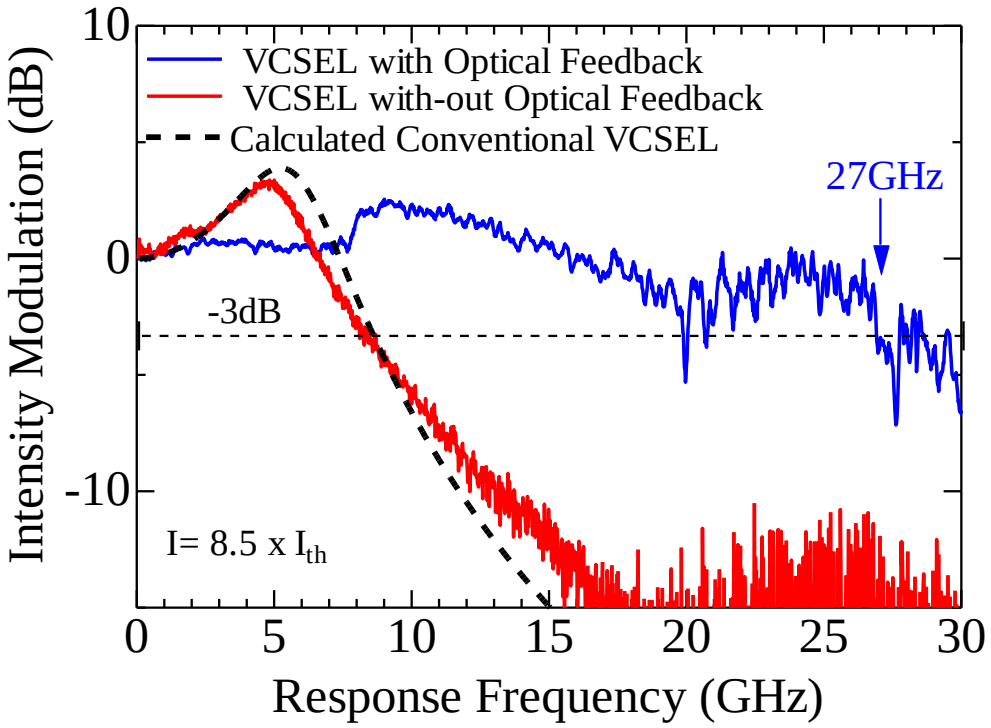

Fig. 2-21 Measured small-signal modulation response of transverse coupled cavity VCSEL with and without optical feedback

We also carried out large signal modulation. Figure 2-22(a) shows 25 Gbps non-return-to-zero (NRZ) eye patterns for VCSELs with and without optical feedback while a pseudo random bit sequence (PRBS) with a word length of 2^{31}-1 was used. Bias currents into a VCSEL cavity were fixed at 5.5 mA for the both cases, while the feedback cavity is un-pumped. The voltage swing was fixed at 400 mV_{pp}. An extinction ratio was 5 dB. Figure 2-19(b) shows 30 Gbps NRZ large signal modulation results with and without feedback with PRBS of 2^{31}-1. Bias current was increased to 6 mA, resulting in an extinction ratio of 3.5 dB. The bit rate could be increased up to 36 Gbps as shown in Fig.2-22(c) with an increased bias current up to 10 mA. An extinction ratio was 4 dB. Our TCC VCSEL showed clear eye opening even for 36 Gbps while the eye pattern was completely closed without feedback. The proposed scheme enables us to upgrade 10 Gbps VCSELs to 36 Gbps VCSELs by simply introducing a bow-tie shape aperture in a standard 980 nm VCSEL epi-wafer.

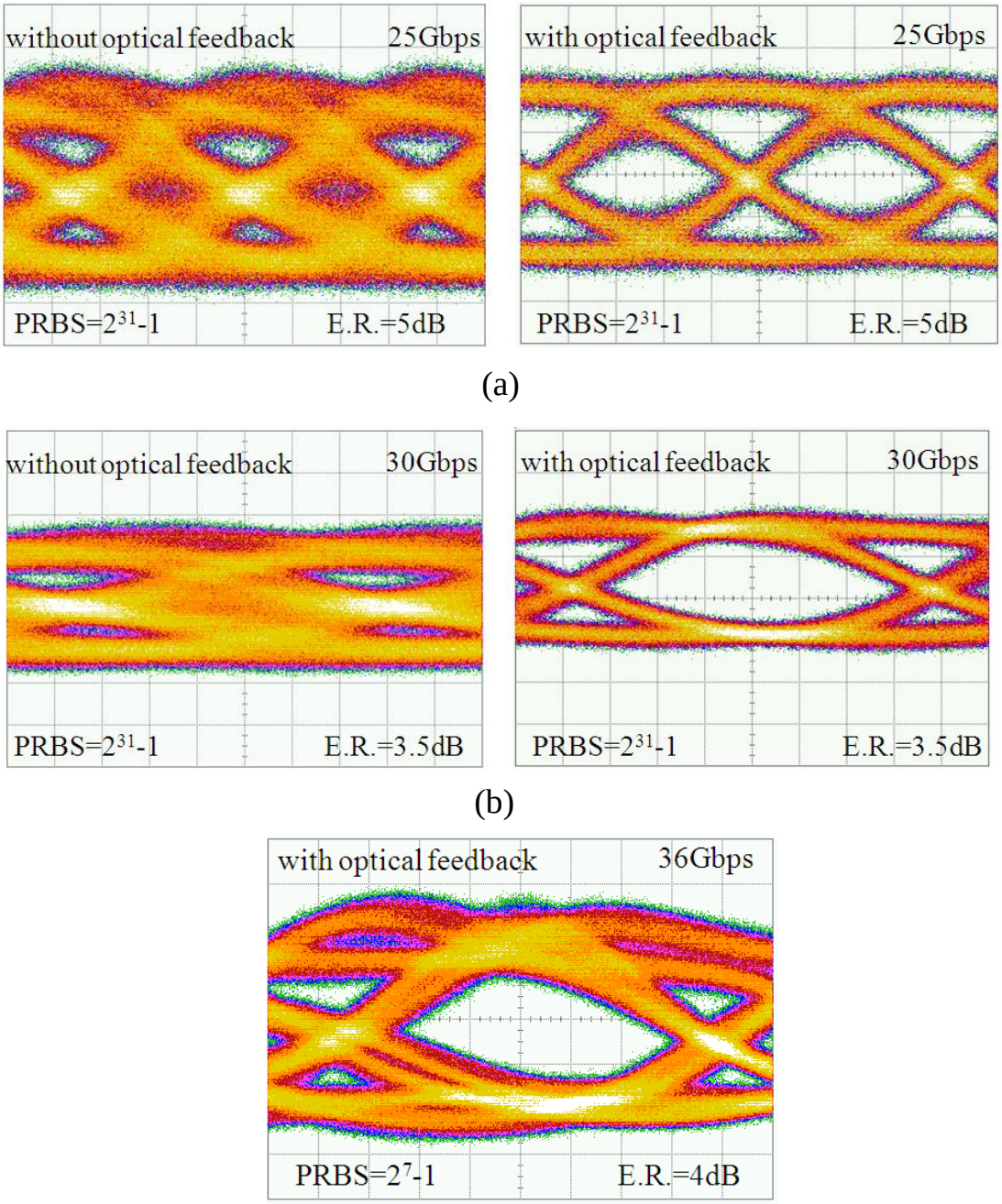

Fig. 2-22 Measured eye patterns for VCSEL with and without feedback, (a) 25 Gbps with an extinction ratio of 5 dB, PRBS of 2^{31}-1 and bias current of 5.5 mA for the both cases, (b) 30 Gbps with an extinction ratio of 3.5 dB and PRBS of 2^{31}-1 and bias current of 6 mA, and (c) 36 Gbps with word length of 2^{7}-1, an extinction ratio of 4 dB and a bias current injected of 10 mA.

2.11 Band of Hope

We carried out the modelling based on Lang-Kobayashi's equations including optical feedback [3]. Figure 2-23 shows the calculated 3-dB modulation bandwidth as a function of the coupling strength of two cavities for different delay time in the optical feedback. The result for a conventional VCSEL without optical feedback is also shown for comparison. We assumed material parameters for conventional 980 nm VCSELs. The oxide aperture is assumed as 3×3 μm. The 3-dB bandwidth of conventional VCSELs is 10 GHz, which is very similar to our measured VCSEL without optical feedback. For a VCSEL with optical feedback, the important parameters are the coupling strength between the two cavities and the delay time of optical feedback. Given a coupling strength of 2×10^{11} s^{-1} and delay time of 5 ps, the modelling shows a 3-dB bandwidth of around 25 GHz, which is close to the present QSM device experiment. The coupling strength per unit time was experimentally estimated from the measured photo-current when the feedback cavity was used as a photo-diode. The delay time of optical feedback is counted from the group index and the length of the feedback cavity. The details will be reported elsewhere. By making cavities smaller and increasing the coupling strength, we expect the modulation bandwidth beyond 40 GHz. Also, the optimization of a base epi-wafer structure, reducing the parasitic capacitance and the series resistance could also be a great help for further increase in modulation bandwidths. The negative sign of the horizontal axis is corresponding to the out-of-phase of optical feedback. In order to obtain the bandwidth enhancement, the feedback light should be out-of-phase. An interesting observation is that such out-of-phase coupling can be obtained without any phase tuning current in the feedback cavity in our present experiment. This finding would be due to scattering loss in the joint section of the bow-tie shape aperture, which will be our future interesting subject.

Figures 2-24 (a) and (b) show the calculated eye patterns of conventional VCSEL and TCC VCSEL at 40 Gbps and 50 Gbps, respectively. While the pseudo-random bit sequence is 2^7-1 word length. Both the bias current and the swing of the modulation current are assumed to be 1 mA, which gives us an extinction ratio of 6 dB for a VCSEL with feedback. A coupling strength of $2\times10^{11}s^{-1}$ and delay time of 5 ps were assumed for the TCC VCSEL. Our TCC VCSEL shows clear eye opening for 40 Gbps while the eye is completely closed for the conventional VCSEL. Also we can still see an eye opening for 50 Gbps. Pattern-effects can be significantly reduced thanks to optical feedback. The difference between here and section 2-2, 2-3 is comes from difference of the photon-life time, while here this value is 1 ps two times smaller than the section 2-2 and 2-3. Keeping almost same value for the coupling as before, this will lead to eventually increase the relative loss inside the cavities and also increases the PPR frequency. Over all 3times larger bandwidth can be expected from the modelling same as experimental data.

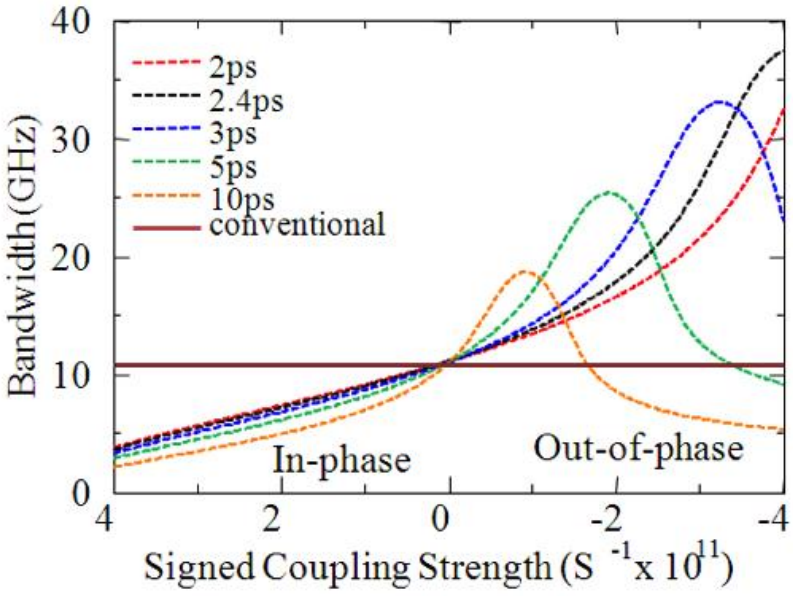

Fig. 2-23 Calculated small signal response as a function of the coupling strength of two cavities for different delay time in the optical feedback.

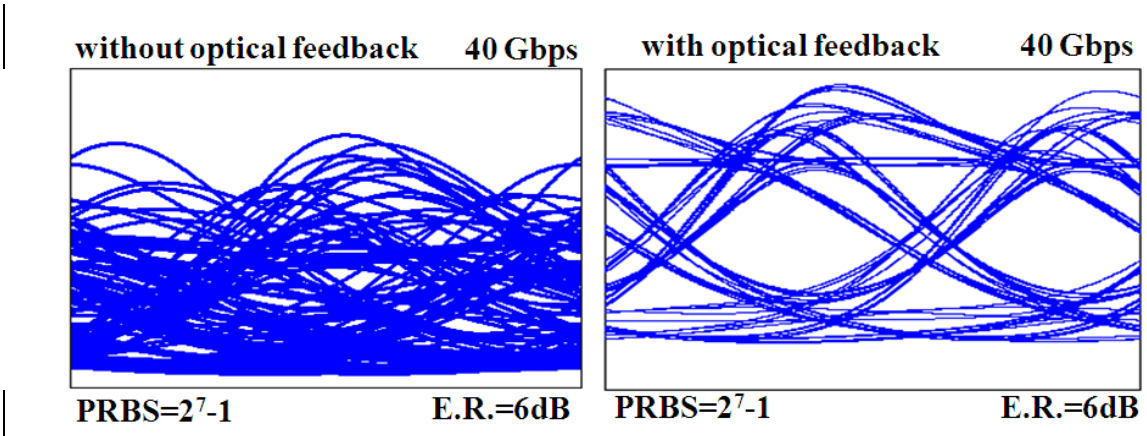

(a)

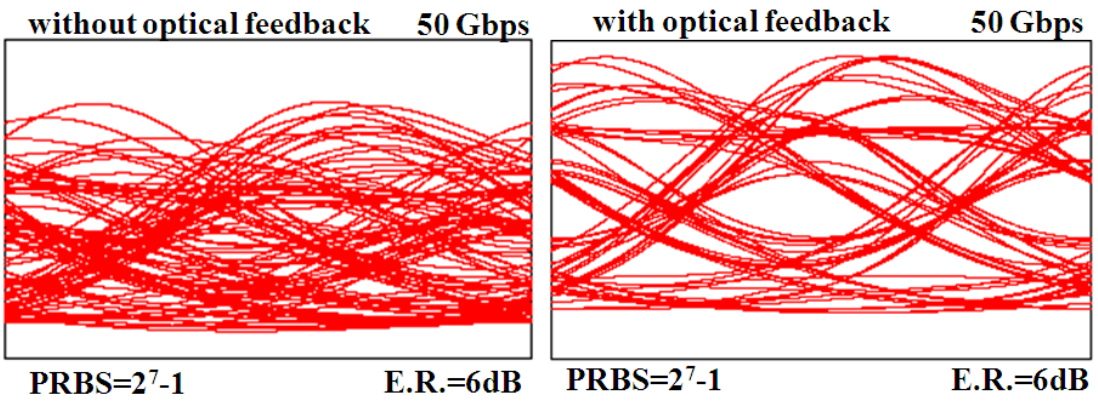

(b)

Fig. 2-24 Calculated eye patterns for VCSELs with and without feedback,(a) For 40 Gbps and (b) 50 Gbps with an extinction ratio of 6 dB and PRBS of 2^7-1, while a bias current of 1 mA is assumed for the both cases.

2.12 Temperature and Current Dependence

In Fig 2-25 (a) and (b), we measured the eye pattern results of QSM-TCC VCSEL at 20 Gbps and 25 Gbps with PRBS of 2^{31}-1, and the extinction ratio is < 5 dB, respectively. While temperature was elevated from 0° C to 70° C, we could see clear eye opening all over the range. These results clearly prove that our proposed device can be used for industrial purposes.

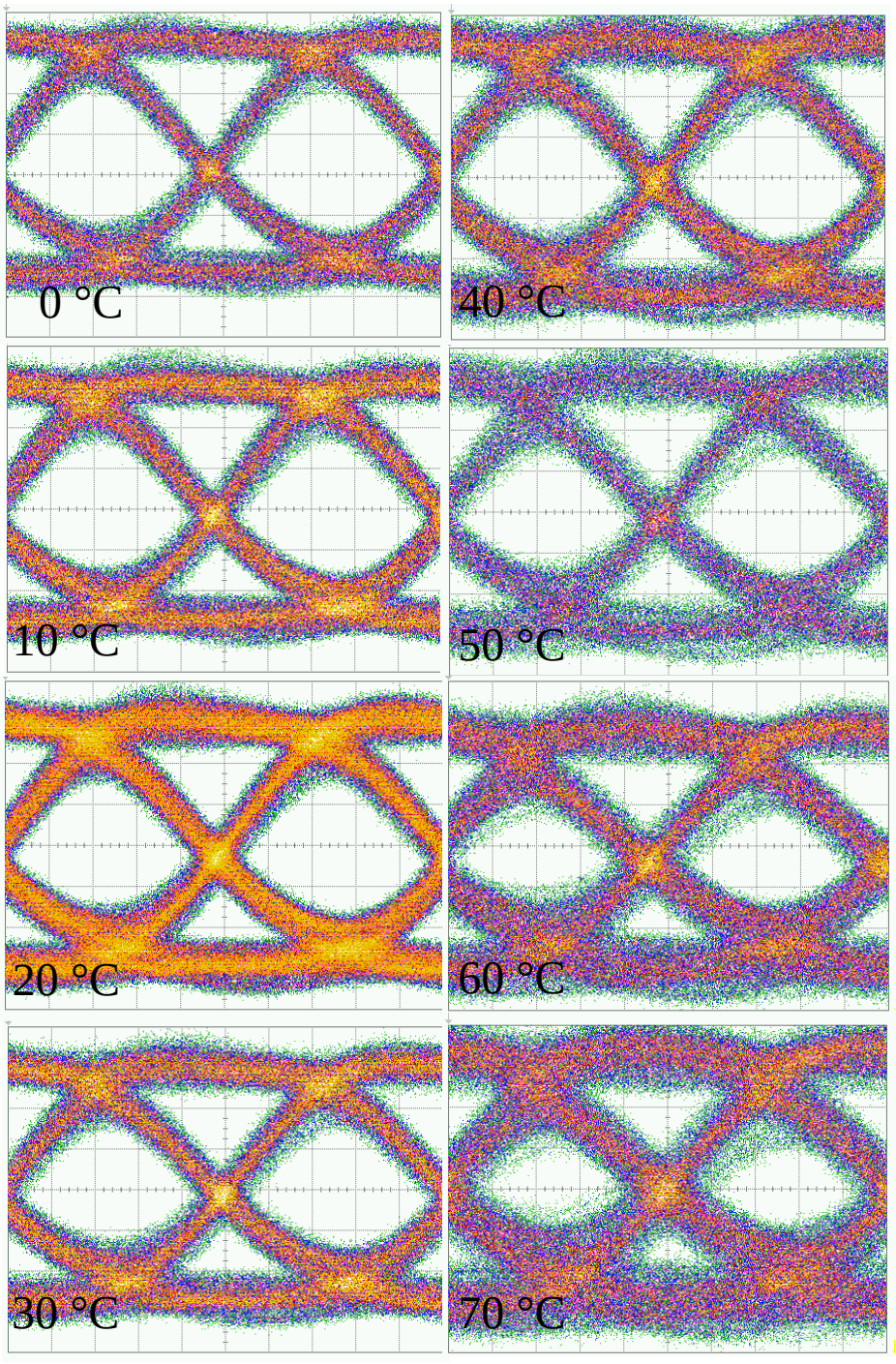

(a)

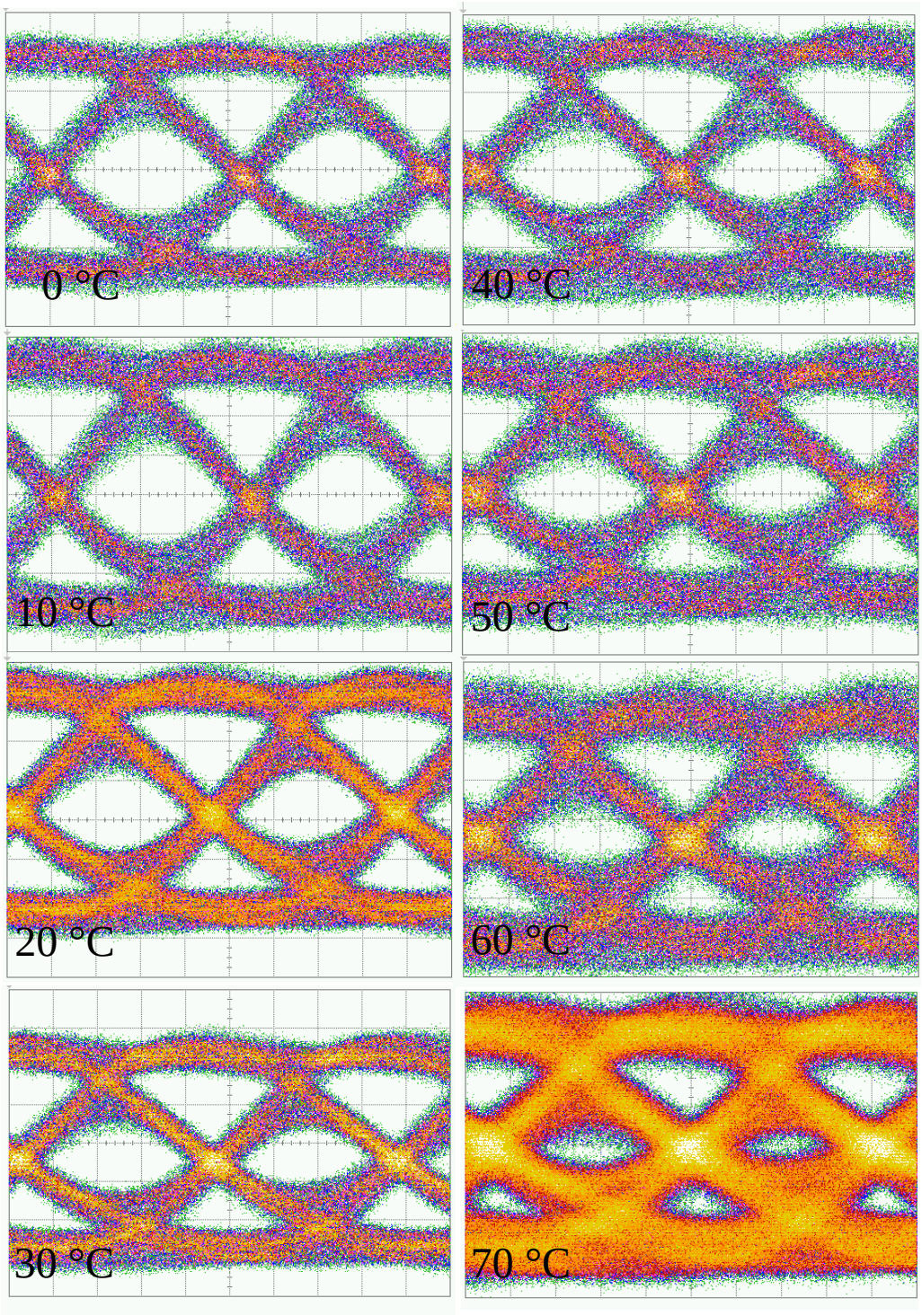

(b)

Fig. 2-25 Measured eye patterns for VCSEL with feedback, (a) 20 Gbps with an extinction ratio of < 5 dB, PRBS of 2^{31}-1 and bias current of 8 mA for the all cases, (b) 25 Gbps with an extinction ratio of < 5 dB and PRBS of 2^{31}-1 and bias current of 8 mA.

Fig. 2-26 show the measured eye pattern for VCSEL with lateral optical feedback of slow light waveguide at 25 Gbps with an extinction ratio of < 4 dB and PRBS of 2^{31}-1 while bias current varies from 4.5 mA to 10 mA with step of 0.5 mA.

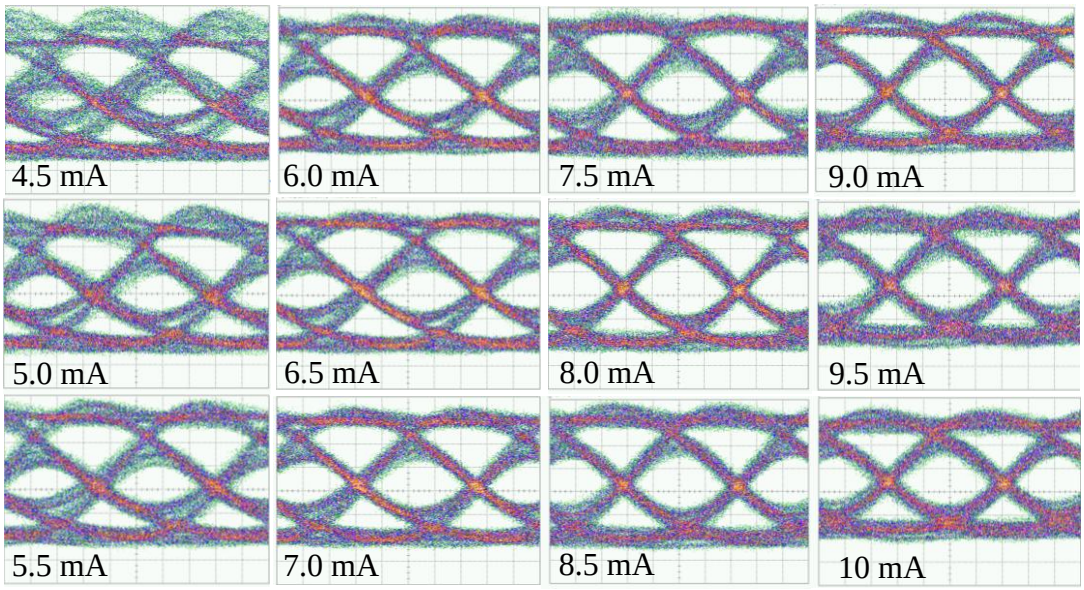

Fig. 2-26 Measured eye patterns for VCSEL with feedback, 25 Gbps with an extinction ratio of < 5 dB and PRBS of 2^{31}-1 and bias current of 4.5-10 mA.

2.13 Conclusion

In conclusion, a transverse-coupled-cavity VCSEL was proposed and demonstrated for the bandwidth enhancement. In multi-mode case, the 3-dB bandwidth was increased by a factor of 3 far beyond the relaxation oscillation frequency. The measured NFP showed strong optical coupling between the bow-tie shape coupled cavities, which could also be supported by the ripples in L-I characteristics. Clear 36 Gbps eye opening was attained with an extinction ratio of 4 dB. The result is comparable or even faster than the update highest speed VCSELs although the epi-structure and the coupled cavity structure have not been optimized yet..

In a quasi-single mode VCSEL a 3-dB bandwidth of 27 GHz was attained which is 3 times larger than our conventional VCSEL, while the epi-wafer structure and the coupled cavity have not been fully optimized yet. This is almost the record modulation bandwidth among high-speed single-mode VCSELs. Clear 36 Gbps eye opening of large signal modulations was attained with an extinction ratio of 4 dB. The modelling predicts larger enhancement in bandwidths by optimizing the TCC VCSEL structure. A concern could be the bias current/temperature dependences of the phase of the optical feedback light, which affect the bandwidth. It is practically important. We measured the bias and temperature dependence of large signal modulations. We have seen clear eye openings at bias currents of 4-10 mA and in temperature ranges of 0-60 ºC. Owing to the careful design of bow-tie shaped oxide apertures, the feedback phase could be stabilized to be in an out-of-phase condition, thus we are able to get the bandwidth enhancement in wide ranges of bias currents and temperatures. Further optimizations could offer ultra-high speed VCSELs beyond 50 Gbps for use in high-speed and energy-efficient datacentre photonics.

2.14 References

1) H. Dalir and F. Koyama, “Bandwidth enhancement of single-mode VCSEL with lateral optical feedback of slow light”, IEICE Electron. Express, Vol. 8, No. 13, pp.1075-1081, 2011.

2) G. Hirano, F. Koyama, K. Hasebe, T. Sakaguchi, N. Nishiyama, C. Caneau and Chung-En Zah,“Slow light modulator with Bragg reflector waveguide,” OFC, Post-deadline paper, PDP34, Anaheim, USA, 2007.

3) R. Lang and K. Kobayashi, “External optical feedback effects on semiconductor laser properties,” IEEE J. Quantum Electron, vol. QE-16, pp. 347–355, 1980.

4) H. Dalir, and F. Koyama, "Modulation bandwidth enhancement of VCSELs with lateral optical feedback of slow light", 2010 IEEE International Semiconductor Laser Conference (ISLC), Poster presentation.P10, Kyoto, Japan, Sep 2010.

5) R. Nagarajan, S. Levy, and J. E. Bowers, “Millimeter wave narrowband optical fiber links using external cavity semiconductor lasers,” J. Lightwave Technol., vol. 12, pp. 127–136, 1994.

6) H. R. Qing, T. C. Ping, Improved Rate Equations for External Cavity Semiconductor Lasers, IEEE J. Quantum Electron, vol. 25, no 6, 1989.

7) G. Morthier, R. Schard, O. Kjebon, IEEE Journal of Quantum Electronics, vol. 36, pp. 1468-1475, 2000.

8) M. Radziunas, A. Glitzky, U. Bandelow, M. Wolfrum, U. Troppenz, J. Kreissl, W. Rehbein, IEEE JOURNAL OF SELECTED TOPICS IN QUANTUM ELECTRONICS, vol. 13, no. 1, 2007.

3 Chapter: Resonant High Frequency Modulation for Radio over Fibre Application

Wireless coverage of the end-user domain has become an essential part of broadband communication networks. With the rapid growth of integrated broadband services, wireless systems are indispensable to have high data rates. The technical challenges involved in meeting this demand include utilizing higher carrier frequencies such as millimeter-waves for much faster wireless communication systems. Radio-over-fiber (ROF) links, which integrate fiber optics and wireless radio communication systems, have attracted considerable attention as suitable systems for broadband wireless services [1-5]. While millimeter-waves offer considerably large bandwidth for ultra-fast wireless communication, there remain key technical challenges in light sources. The simplest method for optically distributing RF signals is to directly modulate the intensity of lasers with the RF signal. In this regard, a primary challenge is to develop ultra-high speed lasers operating in the millimeter wave range. The modulation bandwidth of semiconductor lasers is restricted by the intrinsic limitation of relaxation oscillation frequencies. The bandwidth is practically limited to below 20 GHz. Most millimeter wave applications, however, require only a narrow bandwidth centered at a millimeter-wave frequency. An interesting approach for high-frequency modulations is to conduct resonantly enhanced modulation of semiconductor lasers with external cavities at millimeter wave frequencies [6].

In this chapter, we demonstrate a transverse-coupled-cavity (TCC) VCSEL with an integrated ultra-compact lateral feedback resonator with the aim of enhancing the modulation efficiency in the millimeter wave range. The device shows a large enhancement of over 30 dB in the modulation amplitude beyond 25 GHz.

3.1 Device Structure

Schematic Structure is exactly same as 2.4, while the oxidation formation is different. Fig. 3-1 shows the infrared image of the oxide aperture. Due to the large size of feedback cavity the device acts as a multi-mode operation. In addition, measurement set up is same as multi-mode case as described in the previous chapter.

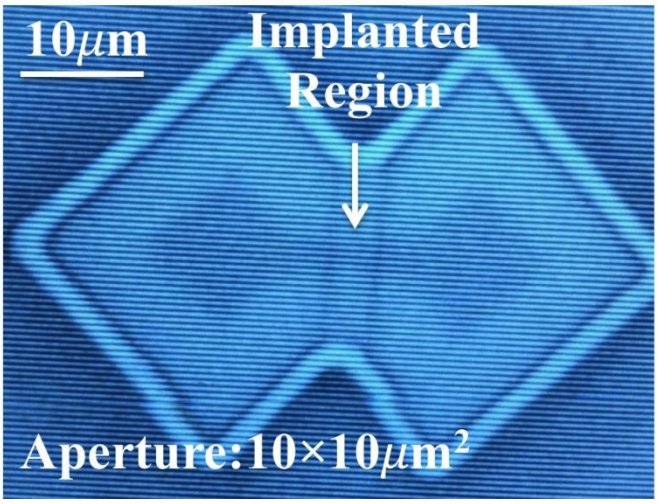

Fig. 3-1 Schematic structure of the TCC VCSEL.

3.2 Static Results

Figure 3-2 shows the measured light output/current (L/I) characteristics for different feedback currents while the laser current was varied from 0-10 mA. Threshold currents are below 1 mA. When the feedback cavity was pumped, it started lasing. The L/I characteristics were measured with screening the output from the feedback cavity by a needle. The intensity variation at zero VCSEL current was due to the lateral optical coupling from the lasing feedback cavity. Applying a reverse voltage of 1 V in the feedback cavity provides a smooth L/I curve (see Fig.3-2), showing that the ripple was due to the transverse optical feedback and that this was cancelled when the feedback effect was removed.

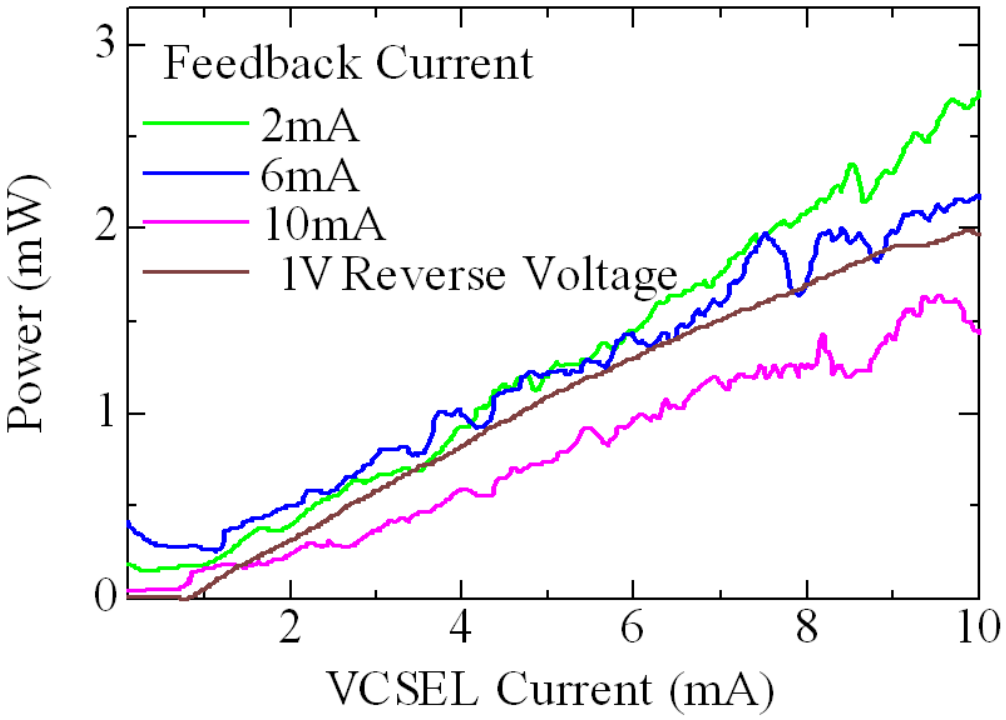

Fig. 3-2 Light output/current characteristics for different feedback currents. Applying a reverse-bias voltage yields result like for a conventional VCSEL.

The noise and signal distortion associated with optical feedback are important issues in RoF links. The relative intensity noise (RIN) and signal distortion are enhanced at the resonant frequency for edge emitting lasers with optical feedback [7, 8].

The device operates in multi transverse modes as shown in Fig. 3-3. The RIN of multi-mode VCSELs is larger than that of single-mode VCSELs. It is dominated by mode-partition noise in multi-mode fiber (MMF) links with mode-dependent loss [9]. These issues necessitate modeling and measurements of the enhanced nonlinear dynamics and noise of the present VCSEL at the coupled cavity resonance.

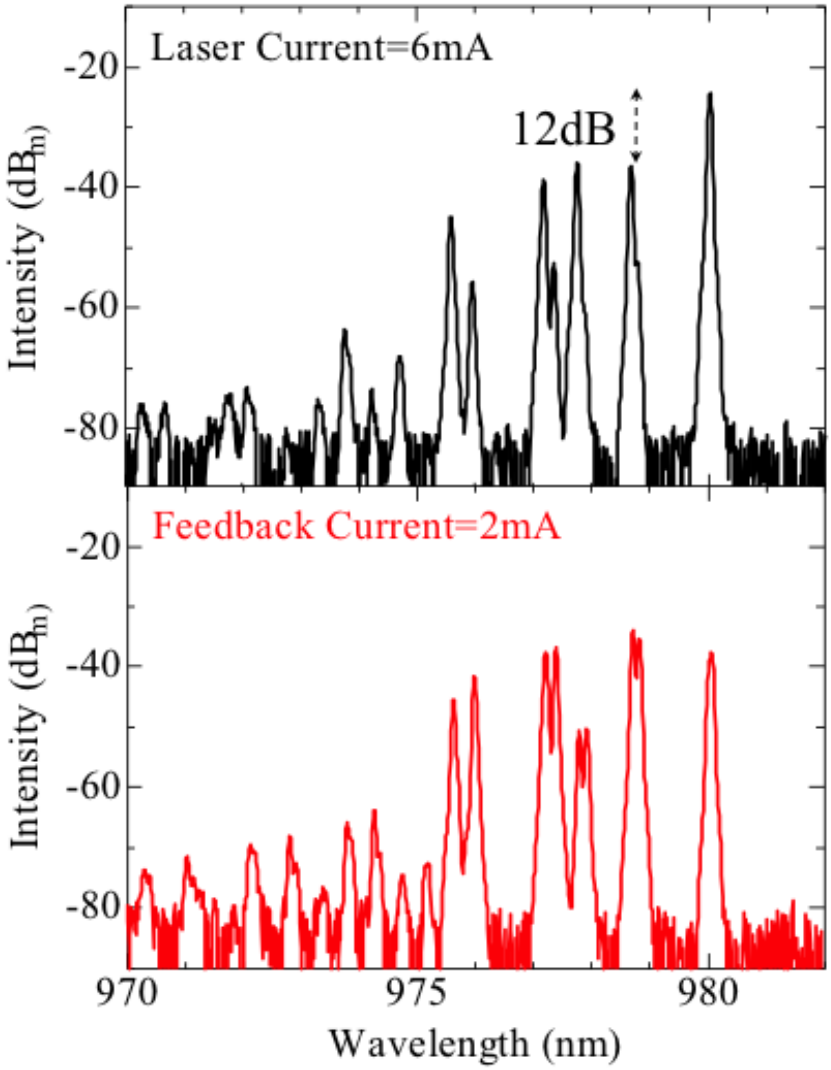

Fig. 3-3 Lasing spectra for the feedback cavity and the laser cavity for 2 mA and 6 mA currents of feedback and laser side, respectively.

3.3 Dynamic Results

Fig. 3-4 shows the measured small signal response for a TCC VCSEL with a fixed VCSEL current of 6 mA and different injection currents in the feedback cavity. By applying a reverse-bias voltage of 1 V in the feedback cavity, the feedback effect can be avoided. In this case the device shows a 3-dB modulation bandwidth of only 8 GHz. Resonant modulation enhancement larger than 30 dB can be seen beyond 25 GHz when the feedback cavity was under forward bias. Figure 3-4 shows that the resonance peak

frequency is sensitive to the feedback cavity current, which is of concern in practical applications.

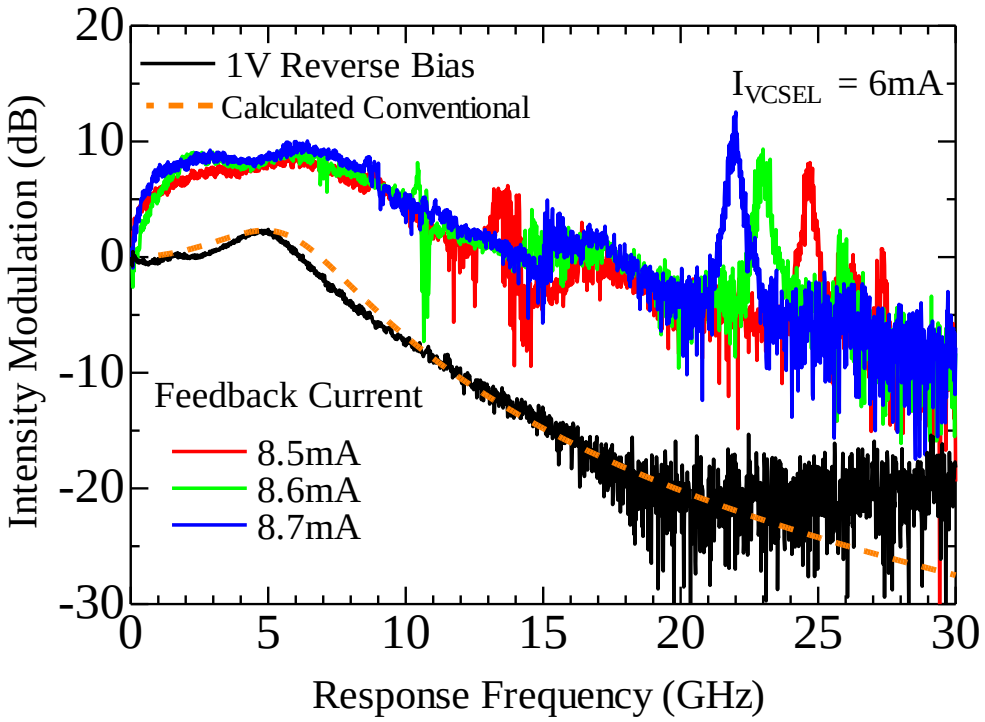

Fig. 3-4 Measured small-signal modulation response of 980 nm conventional VCSEL and TCC VCSEL.

We modeled the bandwidth enhancement using the Lang-Kobayashi rate equation [10]. In this modeling, the frequency chirping effect was ignored, and thus the phase θ is assumed to be time-independent.

Calculated small signal responses are shown in Fig. 3-5 for conventional VCSEL without feedback and TCC VCSEL, assuming the same material parameters as for conventional 980 nm VCSELs. The bias current was assumed to be 10 times the threshold. The important parameters are the coupling coefficient K_C and the phase of the lateral feedback light. The position of resonant modulation enhancement was strongly dependent on the delay time and the feedback phase θ. By adjusting the phase, we see large enhancement

in modulation amplitudes over 40 dB at a frequency beyond 25 GHz for both in-phase and out-of phase modulation.

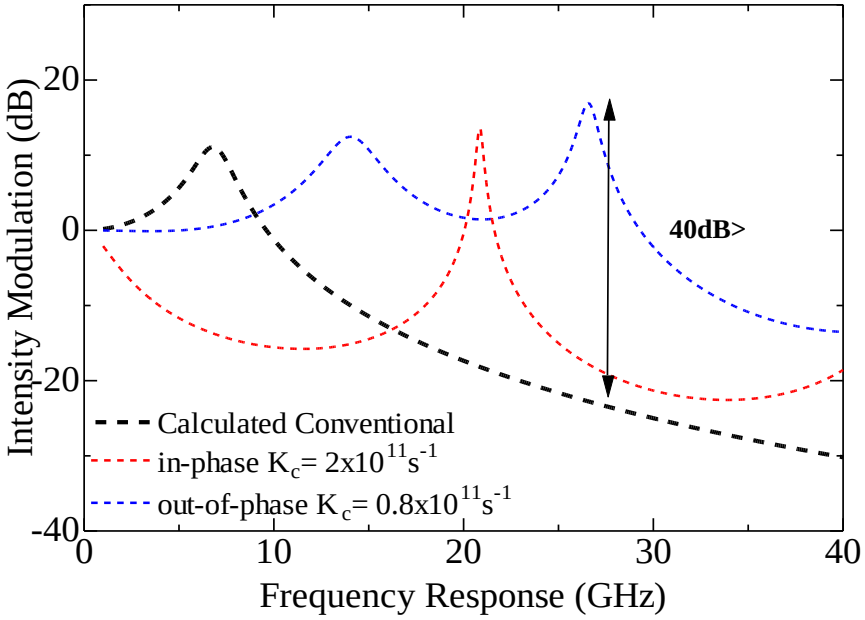

Fig. 3-5 Calculated small-signal modulation response of 980 nm conventional VCSEL and TCC VCSEL.

The modelling result shows reasonable agreement with the experimental result. Two cases of out-of-phase coupling ($\theta=\pi$) and in-phase coupling ($\theta=0$) are shown in Fig. 3-5. The modeling indicates the position of resonances is dependent on the phase. A resonance frequency of 27 GHz corresponds to inverse of delay time of 36 ps in the feedback. The delay time was in agreement with the theoretical prediction assuming a group index of 300 and round trip feedback cavity length of 35 μm (Fig. 3-1). Thanks to slowing light in the lateral direction, resonances at mm-wave frequencies can be obtained even for very small coupled cavities. By making coupled cavities smaller, we expect higher frequency resonances beyond 50 GHz.

3.4 Conclusion

In summary, we demonstrated the modulation enhancement of a TCC VCSEL for RoF applications. We have shown the PPR effect is not only good for the improving of the 3-dB bandwidth of 980 nm VCSEL, but also can enhance the modulation in RoF regim. An enhancement over 30 dB in modulation efficiency beyond 25 GHz was obtained. The theoretical modelling for the modulation response showed reasonable agreement with the experimental results. Resonantly enhanced modulation response was clearly shown at frequencies beyond the intrinsic modulation bandwidth of the laser without optical feedback. The proposed light source would be suitable for efficient narrow-band modulation in the millimetre wave range.

3.5 References

1) S. Kajiya, K. Ksukamoto, and S. Komaki, “Proposal of fiber-optic radio highway networks using CDMA method” IEICE Trans. on Electron., vol. E79-C, no. 1, pp. 496–500, 1996.

2) B.J. Koshy and P. M. Shankar, “Spread-Spectrum Techniques for Fiber-Fed Micro-cellular Networks”, IEEE Trans. on Veh. Technol., Vol. VT-48, No. 3, May 1999, pp. 847–857, 1999.

3) J. Wells, J., “Faster than fiber: the future of multi-Gb/s wireless,” IEEE Microwave Magn. New York, vol. 10, 104 –112, 2009.

4) Razavi, B., “Gadgets gab at 60 GHz,” IEEE Spectrum, vol. 45, no. 2, pp.46-58, 2008.

5) Park, C., and Rappaport, T. S., “Short-range wireless communications for Next-Generation Networks: UWB, 60GHz millimeter-wave WPAN, and ZigBee,” IEEE Wireless Communications, vol. 14, no.4, pp.70-78, 2007.

6) R. Nagarajan, S. Levy, A. Mar, and J. E. Bowers, "Resonantly enhanced semiconductor lasers for efficient transmission of millimeter wave modulated light ," IEEE Photon. Techn. Lett., vol.5, pp.4-6 ,1993.

7) T.D. Ni, X. Zhang, A.S. Daryoush, “Dynamic range of semiconductor laser in the presence of external cavity,” IEEE Microwave and Guided Wave Letters, vol. 4, no. 3, pp.68-70, 1994.

8) T.D. Ni, X. Zhang, A.S.. Daryoush, “Experimental study on close-in to microwave carrier phase noise of laser diode with external feedback,” IEEE Transactions on Microwave Theory and Techniques, vol.43, no.9, pp.2277- 2283, 1995.

9) A. Larsson, C. Carlsson, J. Gustavsson, A. Haglund, P. Modh and J. Bengtsson, “Direct high-frequency modulation of VCSELs and applications in fibre optic RF and microwave links,” New J. Physics, vol. 6, 176, 2004.

10) R. Lang and K. Kobayashi, “External optical feedback effects on semiconductor laser properties,” IEEE J. Quantum Electron, vol. QE-16, pp. 347–355, 1980.

4 Chapter: Push-Pull Modulation for Ultrahigh Speed Operations

With direct modulation of conventional VCSEL, any enhancement in optical output linked to increase of the gain to a value over transparency. The out-put light gains up to the increased stimulated recombination then unload the carriers and reduces the gain below transparency. The interaction between photon generation and carrier evacuation guides to the fundamental resonance with the modulated output reducing at 20 dB per decade after this resonance. By transverse push-pull modulation, the photonic energy within the cavities is kept constant and traveled back and afore along the transverse path with the output coming from one side cavity and the bit supplement from the other cavity. The ancient photon-carrier resonance is perfectly removed and substituted with the restriction on how fast the photonic energy may propagate back and forth in the structure. This limit is handled by the frequency breakaway between the dominant lasing mode and it closest side mode, the new oscillation frequency will be attained between the dominant lasing mode and it nearest side mode. By considering the out-of phase condition and injection of same current density each cavity side, we can keep the total current density constant with comparison to solitary laser. This results to keep the mean gain unchanged thus no blue shift will happen, while beating the transverse mode will offer higher bandwidth of operation, mainly limited by the parasitics and transverse coupling.

Here, two states have been considered; the first one is when one side cavity is lasing under certain injection current while the intensity of other side is suppressed. The second one is when both cavities are lasing via keeping the same total current as the first case. Even if the total photons in entire both cavities are unchanged, intensity modulation leads from spatially altering the transverse optical mode distribution via modification of injection currents in each VCSEL. In this situation an extremely ultra-fast direct modulation can

be expected free from relaxation oscillation frequencies determined by total photons as will be discussed in this chapter [1-3].

4.1 Measurement Set-up

Fig. 4-1 shows the measurement set up for push-pull modulation. A RF signal from the network analyser was equally divided to two paths. One of the divided signals was applied to one of the cavities with a bias current. The other one was applied, through an inserted RF mechanical phase shifter to make a π phase shift, to the other cavity side with the same bias current. The modulated signal through a multi-mode fiber (MMF) followed by a 25 GHz-bandwidth photo detector, while the light was collected from only one side of the cavities.

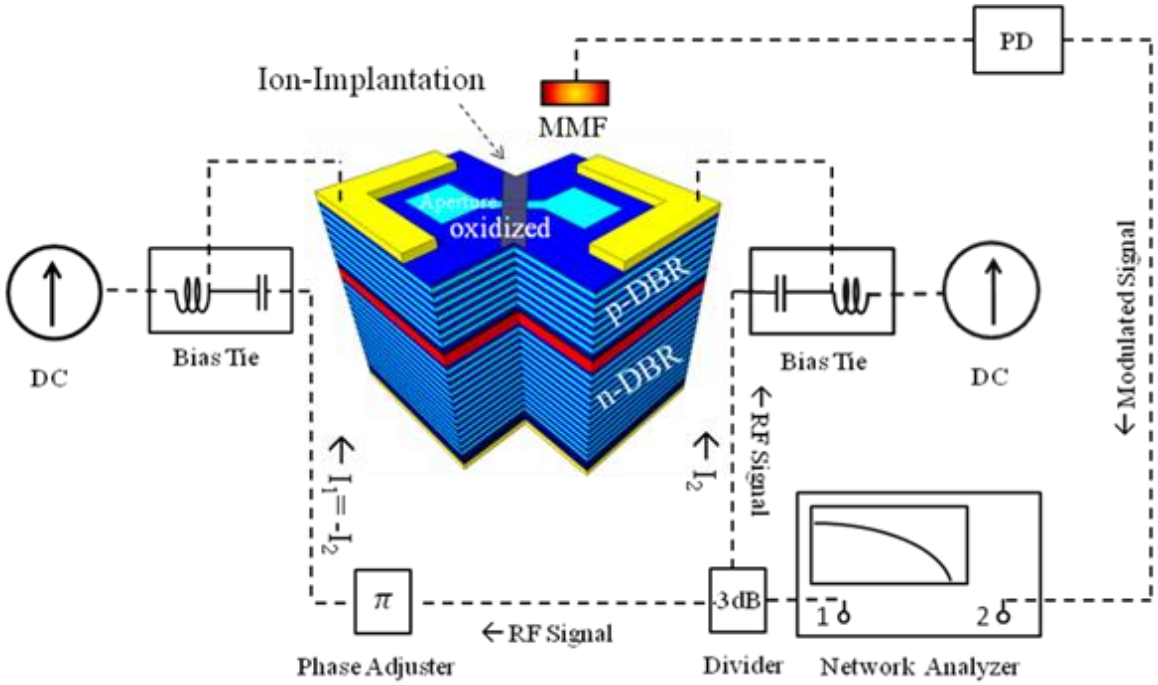

Fig. 4-1 Measurement setup for dynamic modulation characteristics of push-pull VCSEL.

4.2 Static characteristics

Near-field patterns (NFP) and far-field patterns (FFP) of fabricated bow-tie shape coupled cavity VCSELs. Figures 4-2(a) and (b) show the NFP of two states with different current distributions in the two cavities while the total injection current is fixed at 4 mA in the oxide defined two cavities. Only one cavity is pumped above the threshold in figure 4-2(a) while two cavities are equally pumped in figure 4-2(b). Figures 4-3(a) and 4-3(b) show the FFP while the total relative intensity of the NFP and FFP of the two states is almost unchanged. Figures 4-2(a) and 4-2(b) clearly show the localized field and the spreading field in the two cavities, respectively. Figure 4-3(a) shows a single-lobe far-field pattern, which is the same as a single-cavity VCSEL. On the other hand, the double-lobe far field pattern in figure 4-3(b) indicates the coherent coupling of two cavities with out-of-phase condition. The far-field patterns shown in figures 4-3(a) and 4-3(b) could be understood as the diffraction-limited images of figures 4-2(a) and 4-2(b), respectively.

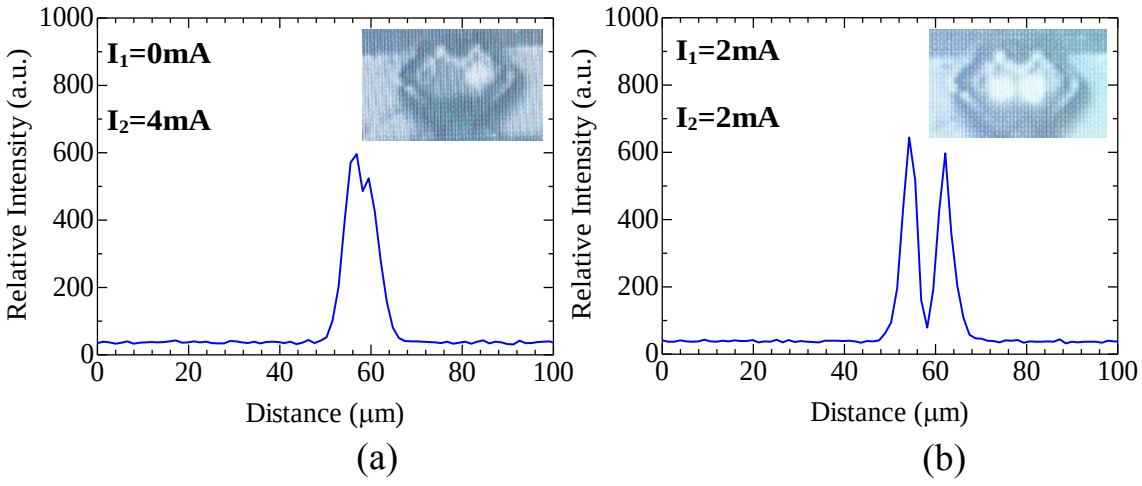

Fig. 4-2 Measured NFP of (a) non-coupled VCSELs and, (b) coupled VCSELs.

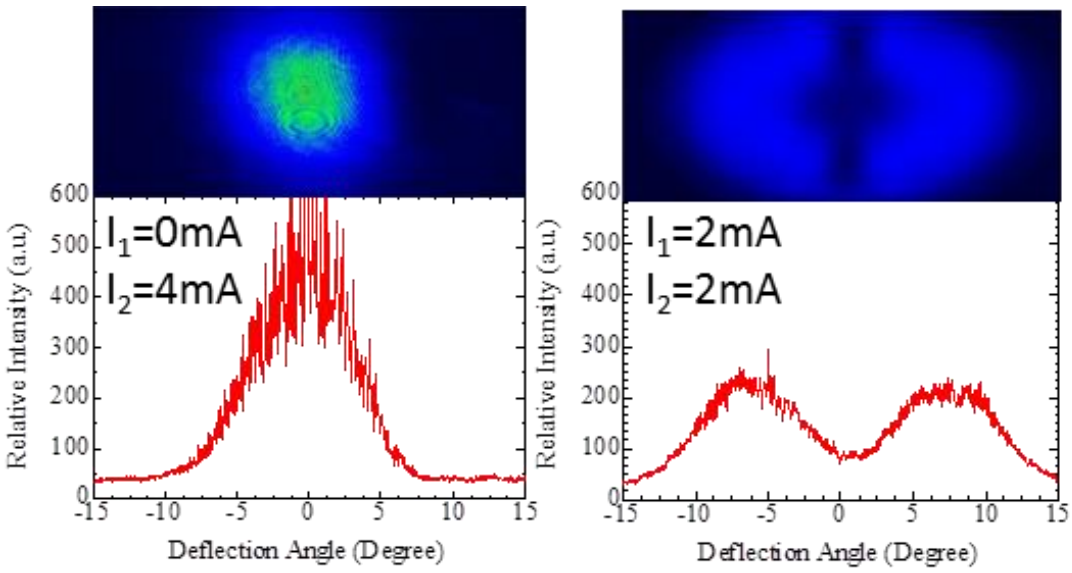

(a) (b)

Fig. 4-3 Measured FFP of (a) non-coupled VCSELs and, (b) coupled VCSELs with different current distributions.

We also measured the lasing spectrum of the case of figures 4-2(b) and 4-3(b). A multi-mode fibre (MMF) and optics were used so that the output from each cavity is collected independently. Fig. 4-4 indicates that two lasers (cavities) are coherently coupled and hence show the same lasing wavelength of dominant modes. A quasi-single mode with a side-mode suppression ration (SMSR) of 10 dB was obtained. According to these evidences we could claim that two-cavities are coherently coupled.

Figure 4-5 shows the results of L-I for two different states when a probe-needle screens one cavity and in this case a needle acts as a spatial filter. The two L/I indicate the output by pumping only each cavity. The two states are corresponding to push-pull intensity modulation of the two cavities in exactly out-of-phase. The field distribution variation makes the intensity modulation free from the relaxation oscillation frequency and only

would be dominated by the lateral coupling coefficient as discussed before. An extinction ratio of over 12 dB was obtained in the two states.

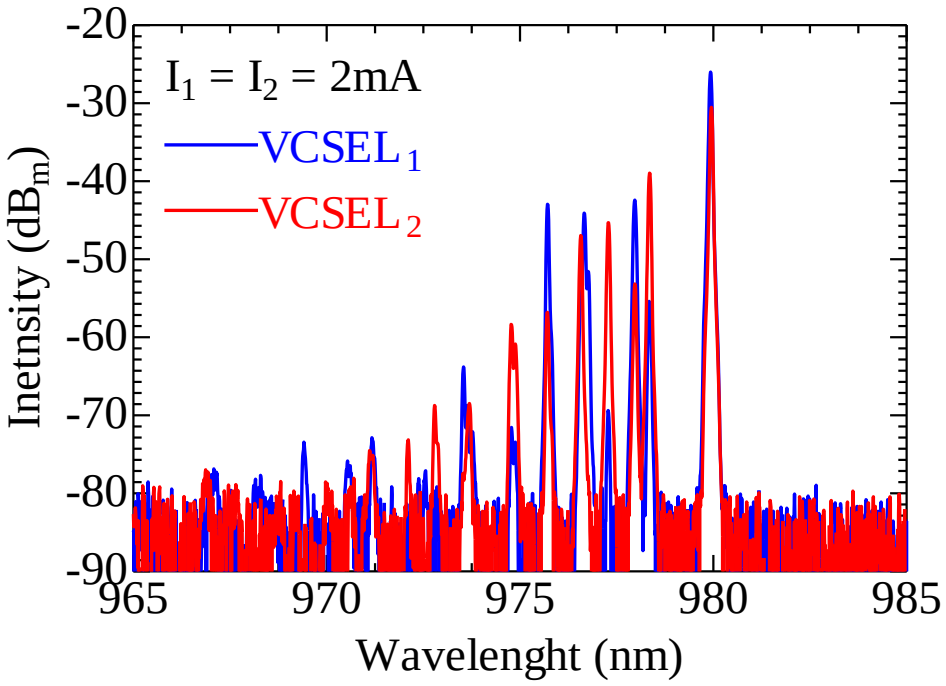

Fig. 4-4. Measured spectrum data of each VCSEL while both lasers are lasing with the same amount of current (2 mA).

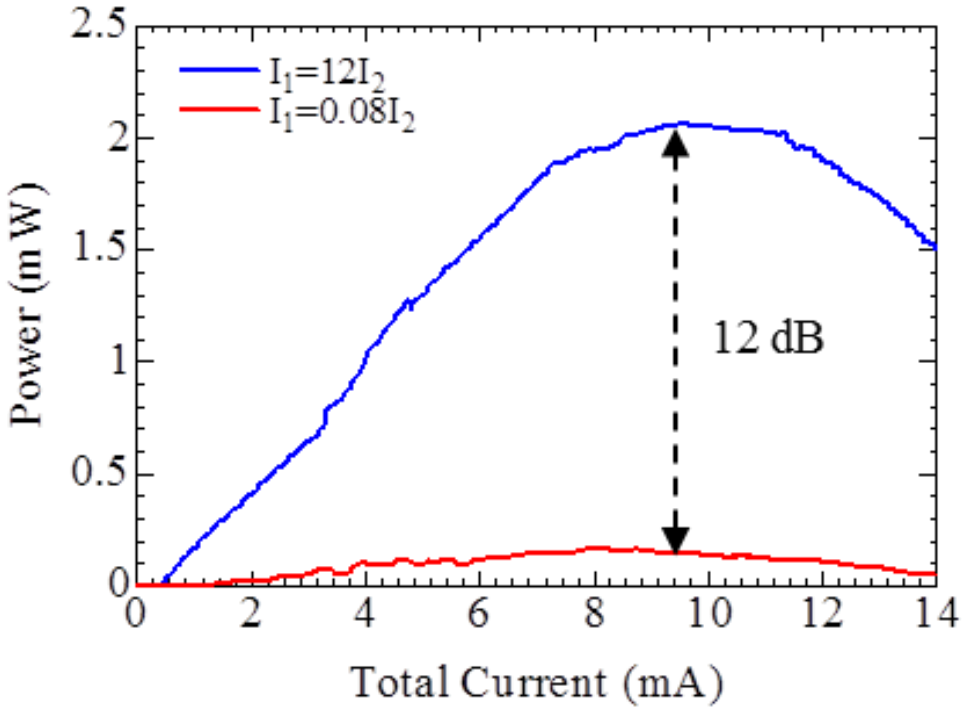

Fig.4-5. Measured L/I for reverse states, while the probe-needle acts as a spatial filter of one aperture and the total current inside the cavities are the same at each specific points.

4.3 Dynamic Results

The following rate equations for carrier and photon densities are defined while merely one longitudinal and transverse optical mode is lasing:

$$\frac{dN_k}{dt} = \frac{J_k}{qd} - \frac{N_k}{\tau_k} - X_k \nu g_k S \tag{4-1}$$

$$\frac{dS}{dt} = \sum_{k=1,2} \Gamma X_k \nu g_k S - \frac{S}{\tau_p} + \beta R_{sp} \tag{4-2}$$

For the cavities k=1,2 where N_k is the carrier density, J_k is the current density, d is the thickness of active region, X_k is the overlapping ratio of optical standing wave in the cavities, τ_k is the carrier life time, ν is the group velocity of the optical mode in the material, g_k is the material gain, Γ is the optical confinement factor, τ_p is the is the photon life time, S is the total photon density for both cavities, q is the electric charge, β is the spontaneous emission factor and R_{sp} is the spontaneous emission ratio per unit volume.

We carried out small signal rate equation analysis. We considered the injection current densities in the two cavities; $j_1(\omega)$ and $j_2(\omega)$ are given by

$$j_1(\omega) = Ae^{j\varphi} \times j_2(\omega) \tag{4-3}$$

where A and φ are amplitude and phase change between the injected current in the cavities. In order to make the equation easier we considered that both cavities have the same characteristics.

Fig. 4-6 shows the measured small signal modulation response of a conventional VCSEL with a single-cavity modulation and a push-pull modulation VCSEL with two RF current. Although the 3-dB modulation bandwidth of the conventional VCSEL is limited below 9 GHz, we see a clear resonant enhancement at a modulation frequency of 12.6 GHz by adjusting a delay time of 47 ps in the RF phase shifter, which is corresponding to 1.2 π. While the modelling tells us an optimal phase-difference to be π, the difference may come

from the fluctuation of delays in RF cables used in the experiment. In the measurement, a phase shifter gives us a fixed delay; eventually we could get the out-of-phase condition of RF signals only at a fixed frequency. As a result such a resonance enhancement can be seen. The dashed line and the red solid line show the calculated small signal response of a conventional VCSEL and an ideal push-pull modulation VCSEL using eqs. (4-1),(4-2), respectively. We are able to go beyond the limit of relaxation oscillation frequencies.

The measured result of large signal for push-pull modulation is shown in Fig.4-7 (a). In order to measure the push-pull we multiplexed four channels as shown in Fig. 2-11. RF signals are connected directly to the outputs of the multiplexer (inverting and non-inverting). In Fig. 4-7 (b), one side is open-circuited. From Fig.4-7 (a) and (b) we can clearly see that via using two contacts bandwidth can be boosted to higher bit rates. However, in the current measurement, low extinction ratio has been obtained due to lack of amplifier after the multiplexer.

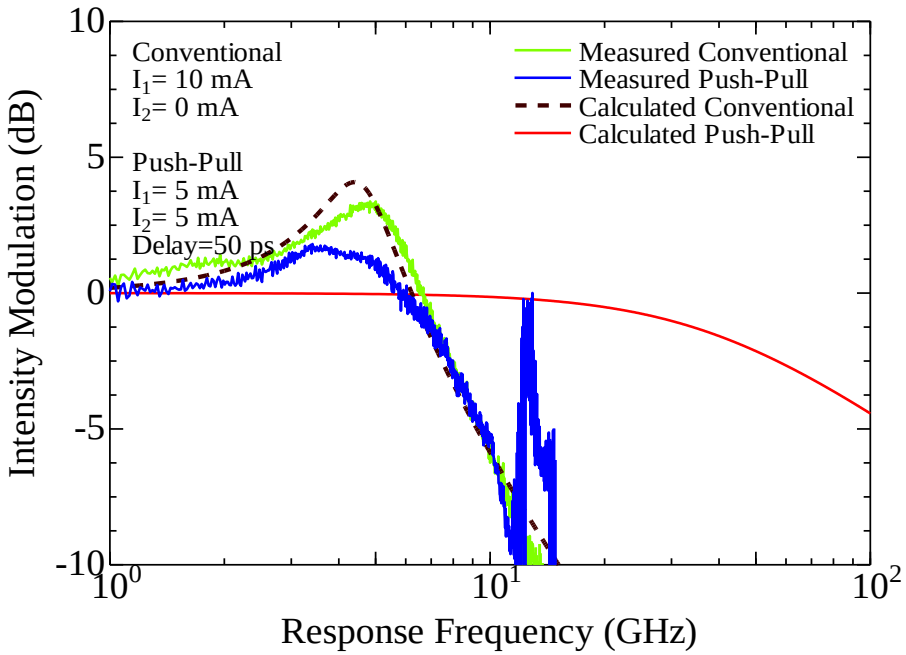

Fig. 4-6. Measured small signal modulation response of a conventional VCSEL with a single-cavity modulation and a push-pull modulation VCSEL with two RF current. The dashed black line

and the red solid line show the calculated small signal response of a conventional VCSEL and an ideal push-pull modulation VCSEL, respectively.

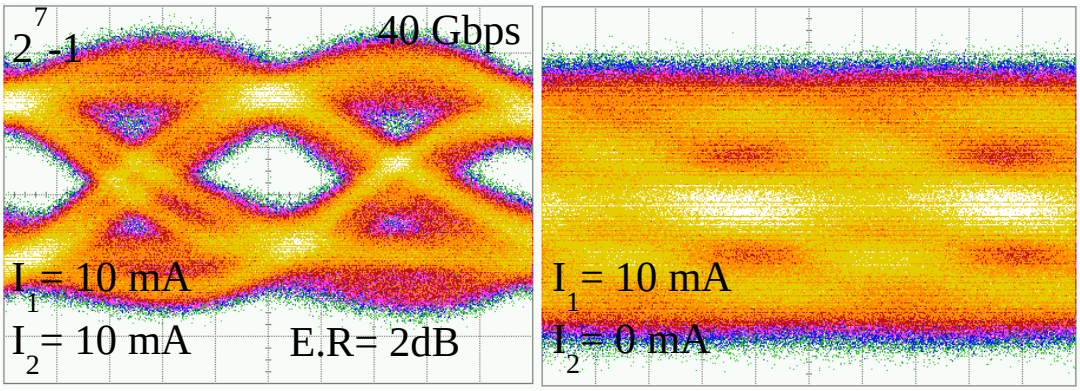

Fig. 4-7 Measured eye patterns for VCSEL with and without push-pull effect, (a) 40 Gbps with an extinction ratio of 2 dB, PRBS of 2^7-1 and bias current of 10 mA for the both sides, (b) 40Gbps with an extinction ratio of 2 dB and PRBS of 2^7-1 and bias current of 10 mA one side while the other side is open circuited.

4.4 Conclusion

In conclusion, we proposed a novel method to couple two closely integrated VCSELs, which offers a high coupling efficiency >90% with a negligibly small scattering loss between two cavities. The calculated scattering loss can be managed by optimizing the bow-tie shape. Transverse-mode switching offers a unique modulation concept that makes spatial intensity modulation while total photons inside the coupled cavities is unchanged under push-pull current modulation. We expect ultra-fast modulation free from relaxation oscillation frequencies for the out-of phase in two-RF signals applied into the coupled cavities. Our experimental data show that bandwidth can boost by push-pull modulation with the out-of phase condition. A 40 Gbps clear eye opening could be achieved with two contact case, while the single contact case could not track the speed. This simply implies that the push-pull modulation can be combined with PPR, while the bandwidth can be further enhanced. This proposed structure is useful for increasing the modulation speed of VCSELs.

4.5 References

1) C. Chen, K. L. Johnson, M. H. Brenner, and K. D. Choquette, “Push-Pull Modulation of a Composite-Resonator Vertical-Cavity Laser”, IEEE JOURNAL OF QUANTUM ELECTRONICS, vol. 46, no. 4, 2010.

2) J. Chen, R. Maciejko, and T. Makino, “Dynamic Properties of Push-Pull DFB Semiconductor Lasers”, IEEE JOURNAL OF QUANTUM ELECTRONICS, vol. 32, no. 12, 1996.

3) C. Y. Chuen, L.Y. Loy, N. Hiroshi, “Directly modulated laser diode with chirp control”, US patent, no. WO2003079507 A2, application no. PCT/GB2003/001185, 2003.

5 Chapter: Ultra-Compact Electro-Absorption Modulator Integrated with VCSEL

Electro absorption (EA) modulator is a semiconductor device with the same structure as the VCSEL. In VCSELs, we inject large amount of current density to achieve stimulated emission. While in EA modulator, we apply electric field (reverse bias) to modify the absorption spectrum. At zero bias, absorption is week, under strong reverse biased, absorption is large. No carriers are injected into the active region. However, carriers are generated due to absorption of light. Mechanisms of EA devices are Franz-Keldysh effect and quantum-confined stark effect (QCSE) for conventional bulk semiconductor and quantum well structure. Both of these electro absorption effects are prominent near the band gap of semiconductor laser. In the previous chapters we have devoted our effort to enhance the modulation bandwidth by apply PPR effect. Although, we could boost the modulation speed of VCSEL from 18 Gbps to 36 Gbps, but still the modulation speed was limited below 40 Gbps. In the previous chapter, we have tried to combine another effect which is called “Push-Pull” to the PPR. Indeed we could see clear eye opening for 40 Gbps in case of applying both effect, even with-out fully optimizing of the mesa shape or oxidation shape, but the clear point was in order to achieve over 40 Gbps, current density will be increased. In this chapter a compact electro absorption based on TCC VCSEL will be considered, to solve the current density problem.

5.1 Franz-Keldysh Effect

Electro-absorption modulators in bulk materials can be obtained by exploiting of Franz-Keldysh effect [1]. The Franz–Keldysh effect is a mutation in optical absorption by a semiconductor when an electric field is utilized. The Franz–Keldysh effect is the outcome of wave functions “infiltrating “into the band gap. When an electric field is connected, the electron and hole wave functions become spacy operates rather than plane waves. The spacy function includes a "tail" which outstretches into the forbidden band gap. Regarding to Fermi's Golden Rule, the more overlap there is between the wave functions of a free electron and a hole, the stronger the optical absorption will be. The spacy tails slightly overlap even if the electron and hole are at different potentials. The absorption spectrum now includes a tail at energies below the band gap and some oscillations above it. This explanation does, however, omit the effects of excitons, which may surmount optical properties near the band gap. Fig. 5-1 illustrates the simple scheme of the Franz–Keldysh effect.

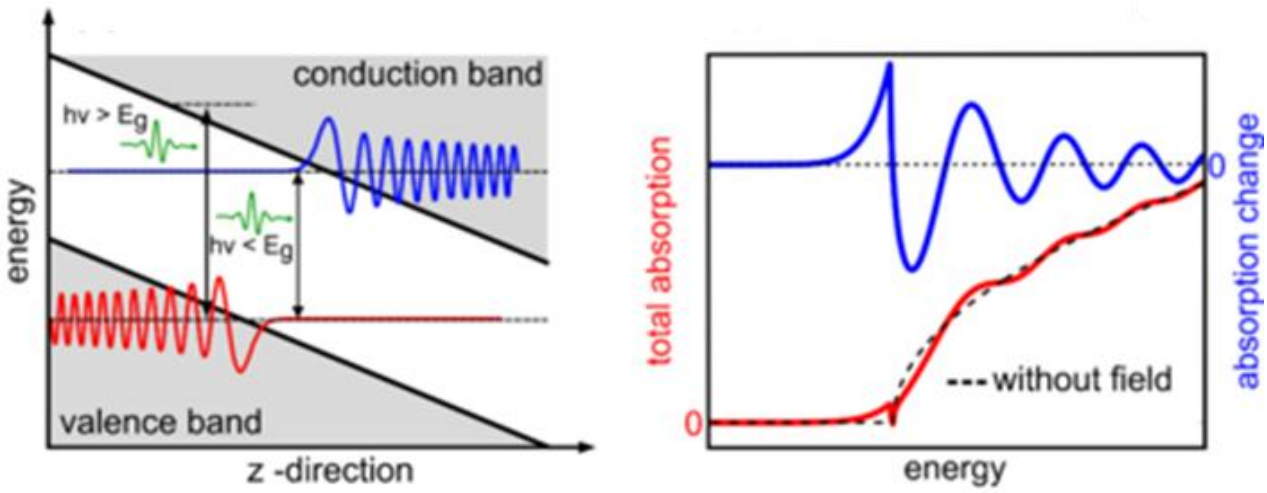

Fig. 5-1 (left) Schematic depiction of the Franz-Keldysh effect. The solutions of Schrödinger’s equation with additional electric potential are spacy functions, which decay exponentially into the forbidden gap region. This fact results in increased absorption of photons with less energy than the gap energy (see also right). The absorption change of photons with higher energy than the gap energy shows an oscillatory behaviour due to interferences of airy functions in the conduction band.

5.2 Quantum-confined Stark Effect

In an active quantum well, the basic phenomena of absorption change is the quantum confined stark effect (QCSE), [2-5]. In Fig. 5-2 a schematic view of QCSE in a semi-classical case can be seen. This illustration shows electron and hole in the valence and conductance area. The energy $\hbar\omega_1$ which is required to lift the lower particle to the location of upper case is directly proportional to their height gap. This is the least photon energy that can help to have an absorption process. By applying reverse voltage as a bias, linear potential of a constant electric field will across the boxes and resulting to tilt the both energy level. The particles are still separated but move closer to each other in terms of energy difference. Now the photon with less energy $\hbar\omega_2 < \hbar\omega_1$ are enough to overcome the gap between hole and electron.

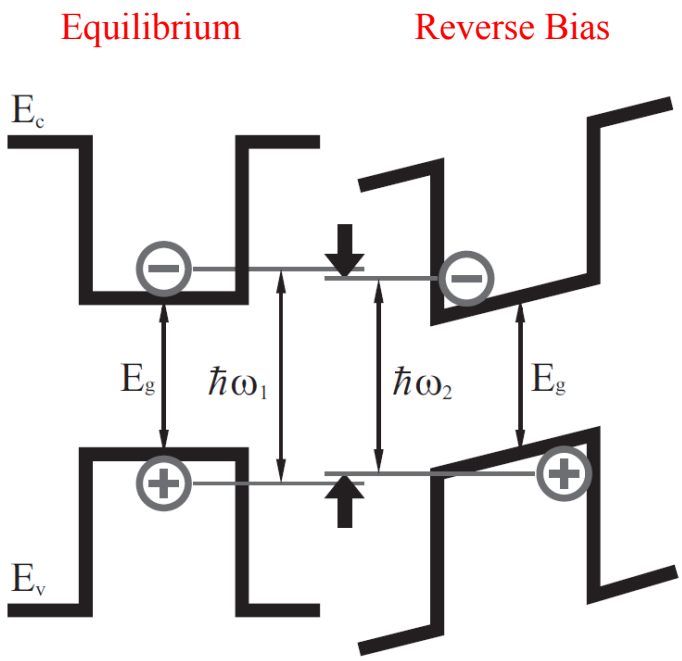

Fig. 5-2 Schematic picture of the quantum confined Stark effect in semi-classical view.

As the energy difference between the electrons and holes reduces, amplitude absorption is also reduced, this cause a sharp peak in the vicinity of absorption.

5.3 Integration concepts of VCSEL and modulator

In order to realize the compact modulator, a modulator transversely integrated to the 980 nm VCSEL. Figures 5-3 indicates oxide aperture of the fabricated transverse coupled cavity (TCC) VCSEL. The vertical structure is the same as conventional 980nm InGaAs/GaAs VCSEL. The bottom distributed bragg reflector (DBR) mirror includes 41.5-period Si-doped $Al_{0.92}GaAs$/ $Al_{0.16}GaAs$ DBR on a 500 nm thick silicon-doped GaAs buffer layer. The active region has three $In_{0.2}GaAs$/GaAs quantum wells implanted in one-λ thick $Al_{0.3}Ga_{0.7}As$ separate confinement hetero-structure layer. 30 nm thick $Al_{0.98}GaAs$ is placed in order to form transverse oxide confinement. The top DBR mirror includes a 21-period carbon-doped $Al_{0.92}GaAs$/ $Al_{0.16}GaAs$ DBR, followed by a highly doped p-contact layer. Proton implantation with six various voltages steps from 60kV to 350kV at the centre of joint connection of the coupled cavities were implanted with doses of $10^{15}cm^{-2}$. The measured SIMS profile figured out that the proton penetrated into the entire top-DBR. So that electrical isolation of over 1 MΩ was obtained. Oxidation formation includes double square apertures of 3μm×3μm are connected to form bow-tie shaped oxide apertures while the joint region is less than few microns. The modulator length is only 8 μm.

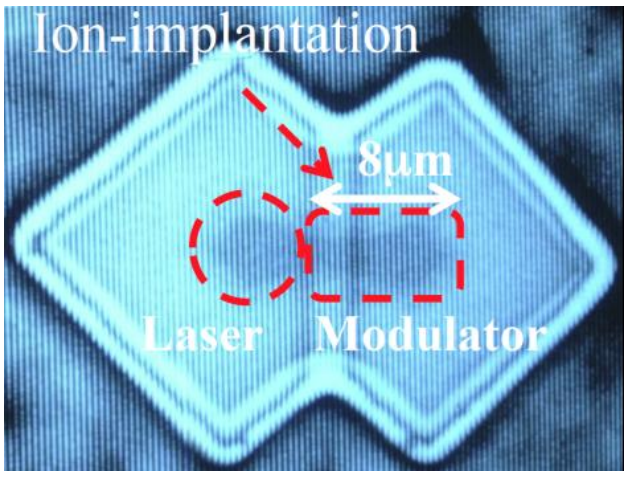

Fig. 5-3.Top view of the slow-light modulator laterally integrated with VCSEL.

5.4 Mechanism of QCSE in the TCC VCSEL

By applying reverse-bias voltage in our ultra-compact modulator side (8μ m), strong electro-absorption occurs. While by increasing the absorption coefficient in the modulator, the lateral penetration of the light is reduced and hence the total radiation power decreases. This electro absorption happens due to the QSC effect in our device. Figure 5-4(a) and (b) show the two states OFF and ON which is related to the O.C and reverse bias voltage, respectively.

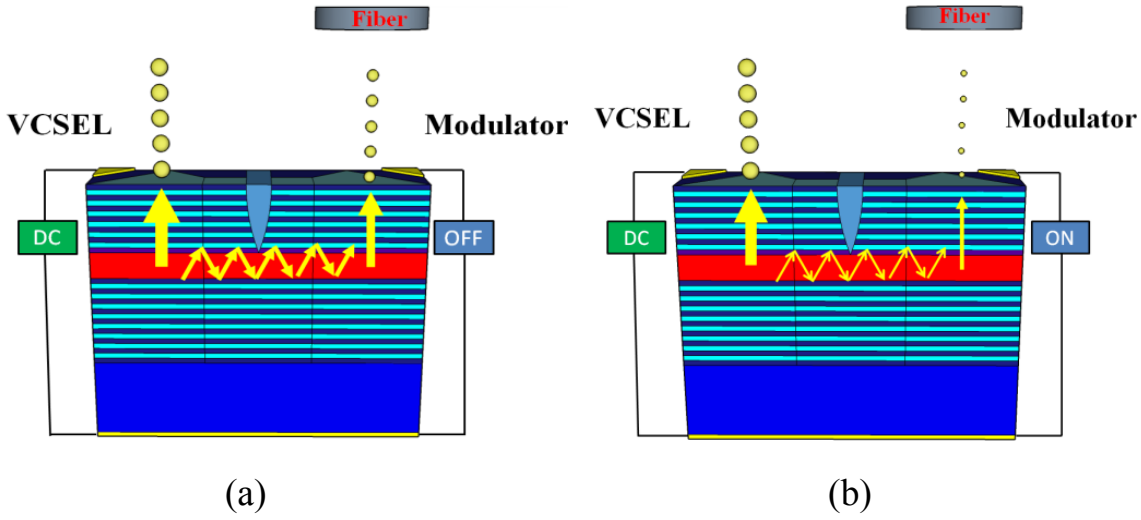

Fig. 5-4. Two states operation while (a) modulator side is open circuit (b) reverse bias voltage is operated.

5.5 Static Results

Fig. 5-5. Shows the near field pattern (NFP) data for un-modulated and modulated states while the 6 mA DC current, was injected to the laser side and the modulator side was operated with reverse bias voltage of 0V and 1V, respectively. The figure clearly indicates the intensity of the modulator section disappears by applying a reverse bias in the modulator.

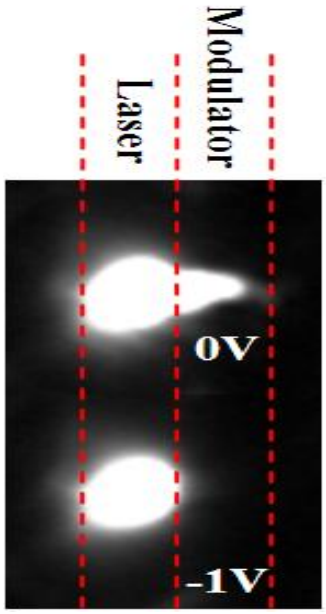

Fig. 5-5. NFP data for un-modulated and modulated states while 6 mA DC current is set in the laser side and modulator side is biased with 0V and -1V respectively.

We measured the spatially-resolved intensity as a function of modulator voltages as shown in Fig. 5-6. The output from the VCSEL and the modulator is separately measured by collecting each power through a multi-mode fiber. We are able to realize a static extinction ratio of 6dB for a reverse-bias voltage of 200 mV. Such an ultra-low voltage could be obtained even for a compact (8 μm) modulator thanks to a large group index of 150 in the Bragg reflector waveguide and the lateral optical resonance in the modulator. Also, it is noted that the intensity of the VCSEL side is almost unchanged ever for applying a modulator voltage. The threshold current is 1 mA, which is also unchanged for different modulator voltages. The result shows the intensity modulation dominantly takes place in the modulator. A fiber coupled power from the modulator is 0 dBm at a VCSEL bias current of 8 mA, which could be improved by inhibiting the vertical emission from the VCSEL by covering the surface of the VCSEL with a metal.

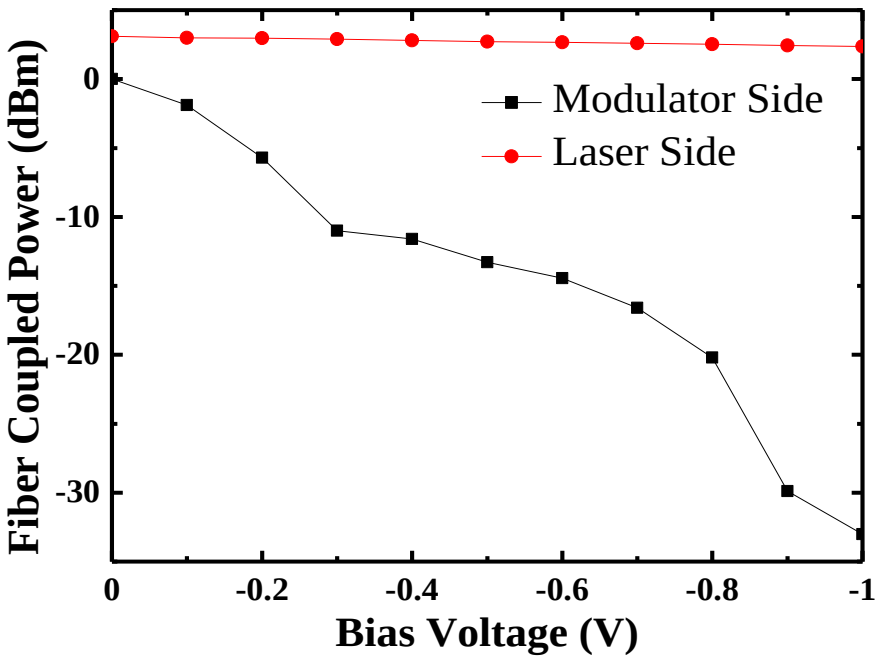

Fig. 5-6 Spatially-resolved intensity from VCSEL and the modulator as a function of modulator voltages.

5.6 Dynamic Results

We carried out the measurement of small signal modulation. The output from the modulator is modulated by superimposing a RF signal at a reverse-bias voltage of 0.2V while the VCSEL is pumped by DC current. Output light is captured by a photo-detector (PD) with a bandwidth of 25 GHz through a multi-mode fibre. The small signal modulation response was measured by using a network analyser with a bandwidth of 40 GHz as shown in Fig. 5-7. We see two resonance peaks which come from the carrier-photon resonance of the VCSEL and the photon-photon resonance observed in our transverse coupled cavity VCSELs [3]. The optical feedback from the modulator affects the modulation response and the details are under study. The 3-dB bandwidth is almost 30 GHz although the modulation bandwidth is below 10 GHz for a conventional VCSEL fabricated from the same epi-wafer. We could see a noticeable bandwidth enhancement by using the modulator integration.

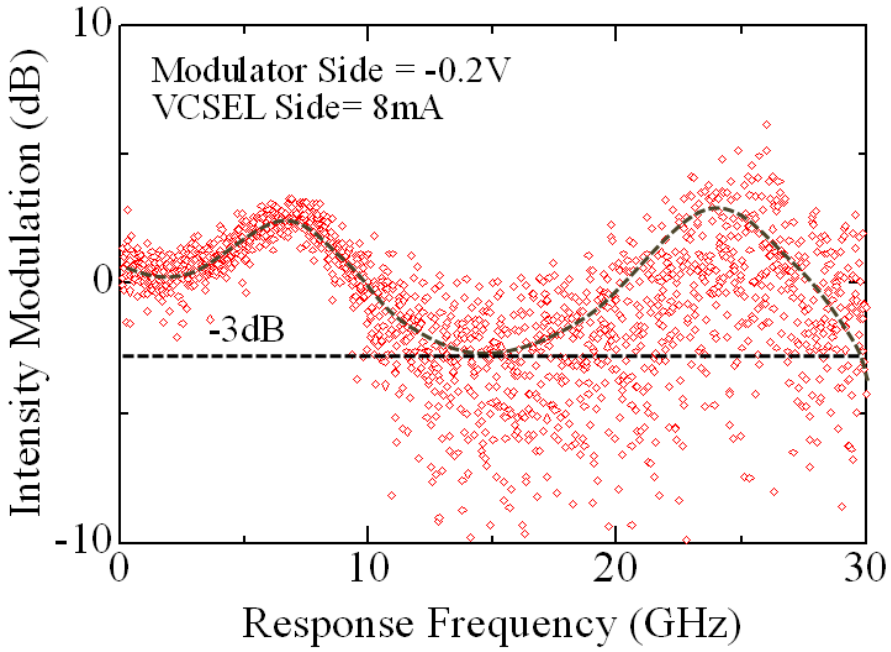

Fig. 5-7. Measured small-signal modulation response of the modulator integrated VCSEL with bias voltage of 0.2V and VCSEL bias current of 8 mA.

We carried out NRZ large signal modulations with a pseudo random bit sequence of 2^7-1 as shown in Fig. 5-7. The modulation voltage swing from a 40 Gbps multiplexer is below 400 mV_{pp}. Although it is the first trial for large-signal modulation of the modulator-integrated VCSEL, we see eye opening up to 25 Gbps with an extinction ratio of 6 dB. Some other device shows eye opening even for higher bit rates of 32 Gbps while the modulation bias voltage is higher. The device structure and the operating conditions have not been fully optimized yet; we could expect better modulation performances.

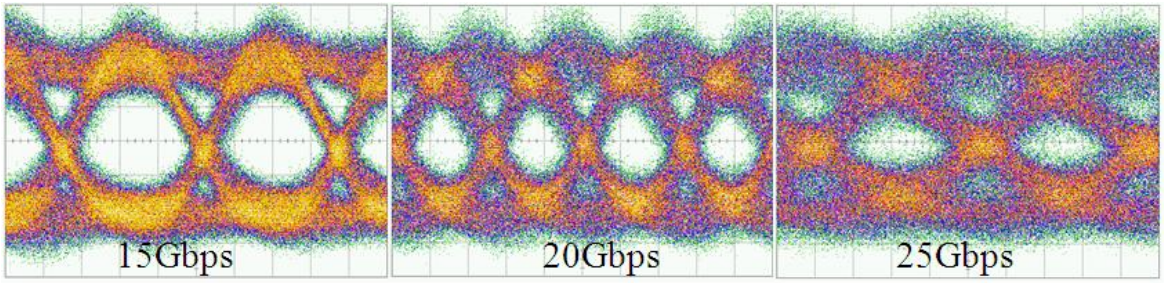

Fig. 5-8. Measured eye patterns for modulator-integrated VCSEL, (left) 15Gbps, (centre) 20Gbps and (right) 25Gbps with an extinction ratio of 6 dB, PRBS word length of 2^7-1 and VCSEL bias current of 8 mA.

5.7 Conclusion

In this chapter, we demonstrated a compact (8μm long) electro-absorption modulator laterally integrated with a 980nm InGaAs VCSEL incorporating a bow-tie-shape oxide aperture. We obtained a low driving voltage below 400mV_{pp} for 6 dB extinction ratio. A large signal modulation up to 25 Gbps and small signal modulation up to 30 GHz were demonstrated. Our spectrum show that this modulator is working based on QSCE. Our ultra-compact modulator integrated VCSEL can boost the modulation speed far beyond the direct modulation bandwidth with low-power consumption for use in next-generation computing and communication networks.

5.8 References

1) W. Franz, "Einfluß eines elektrischen Feldes auf eine optische Absorptionskante", Z. Naturforschung, vol. 13a, pp.484–489, 1958.

2) L. F. Zagonel, "Nanometer Scale Spectral Imaging of Quantum Emitters in Nanowires and Its Correlation to Their Atomically Resolved Structure", Nano Letters, vol.11, pp.568–573, 2011.

3) D. A. B. Miller, D.S. Chemland and T. C. Damen, "Band-Edge Electroabsorption in Quantum Well Structures: The Quantum-Confined Stark Effect", Physical Review Letter, vol. 53, no.22, 1984.

4) D. A. B. Miller, D.S. Chemland and T. C. Damen, "Electric field dependence of optical absorption near the band-gap of the quantum-well strcutures", Physical Review B, vol. 32, no.2, 1985.

5) D. A. B. Miller, D.S. Chemland and T. C. Damen, "Electroabsorption by stark effect on room-temperature excitons in GaAs/GaAlAs multiple quantum well structures", Appl. Phys. Lett., vol. 42, no.10, 1983.

6 Taper Hollow Waveguide for VCSEL Integration

In this chapter in the first part a spatial-mode multiplexer/demultiplexer using a Bragg reflector tapered hollow waveguide is proposed. Depending on each spatial mode, vertical radiation takes place at a cut-off condition while the radiation position is dependent on the order of each spatial mode. Modelling of our structure is carried out by using a film mode-matching method. The result shows low wavelength dependence and no noticeable polarization dependence while a low insertion loss is expected. Clear vertical radiation could be observed, depending on the order of spatial modes. In the second part, we proposed a high-efficient out-of-plane optical coupler based on a tapered hollow waveguide. Modelling shows low polarization dependence and low wavelength dependence in a 35 nm wavelength window (C-band). The relative lateral displacement per spot-size of vertical output for the entire C-band is less than 0.13 and 0.38 for TE and TM input-mode, respectively. At the same time, polarization dependent insertion loss is below 1.35 dB for both TE and TM input-modes.

Our proposed devices enable us to integrate surface-normal optical devices such as photo-detectors and VCSELs. The devices will be useful for ultra-high capacity optical interconnects using spatial mode multiplexing.

6.1 Spatial-mode Multiplexer/Demultiplexer

6.1.1 Device Structure

Fig. 6-1 shows the schematic structure of our proposed spatial-mode multiplexer/demultiplexer. Bragg reflectors (3pairs Si/SiO_2) enable us to confine different spatial modes in an air core. In addition, tapering the air core results in the vertical radiation at a cut-off condition for each spatial mode [1]. The radiation position is dependent on the order of each spatial mode. Thus, this waveguide device functions as a spatial mode

multiplexer/demultiplexer. Also, the vertical coupling enables us to integrate surface-normal optical devices such as photo-detectors and VCSELs. A unique behaviour in a narrow core tapered hollow waveguide shown in Fig. 6-1 was previously found [2]. We calculated the intensity field distribution for the hollow waveguide with tapering a core thickness. We figured out that light is radiated in a vertical direction at a cut-off condition that the core thickness is:

$$D = \frac{(n+1)}{2}\lambda \tag{6-1}$$

with the spatial mode number of n [2]. Thus, the radiation point is dependent on the order of spatial modes for tapered hollow waveguides.

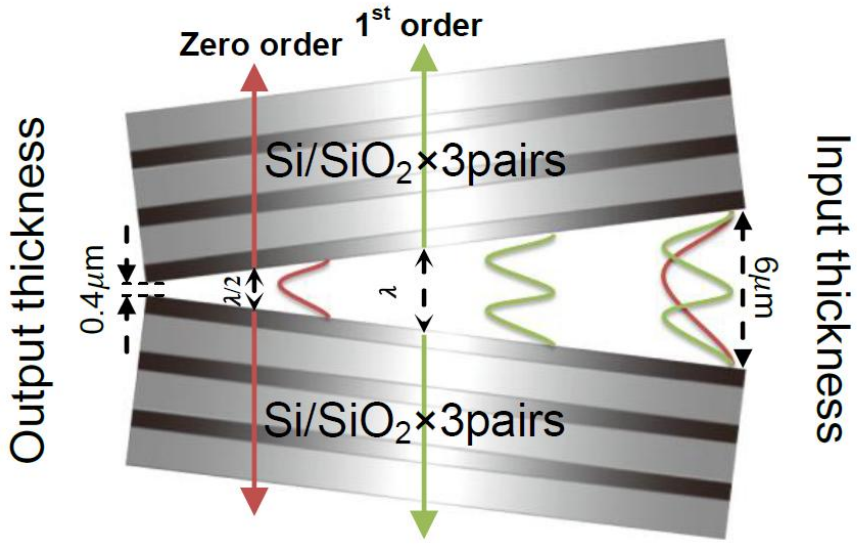

Fig. 6-1 Schematic structure of the spatial mode multiplexer /demultiplexer based on the tapered hollow waveguide.

6.1.2 Modelling and Results

The modelling of the proposed structure is carried out by using a mode-matching method (FIMMWAVE, Photon Design). Since the structure is symmetric in the vertical direction, we could calculate a half of the symmetric structure.

The calculated intensity distribution for a fundamental mode and the higher order modes is shown in Fig. 6-2 for a hollow waveguide with tapering a core thickness from 6μ m to 0.4μ m while the length of the device is 1mm. Different spatial modes are excited from an air core of 6μ m.

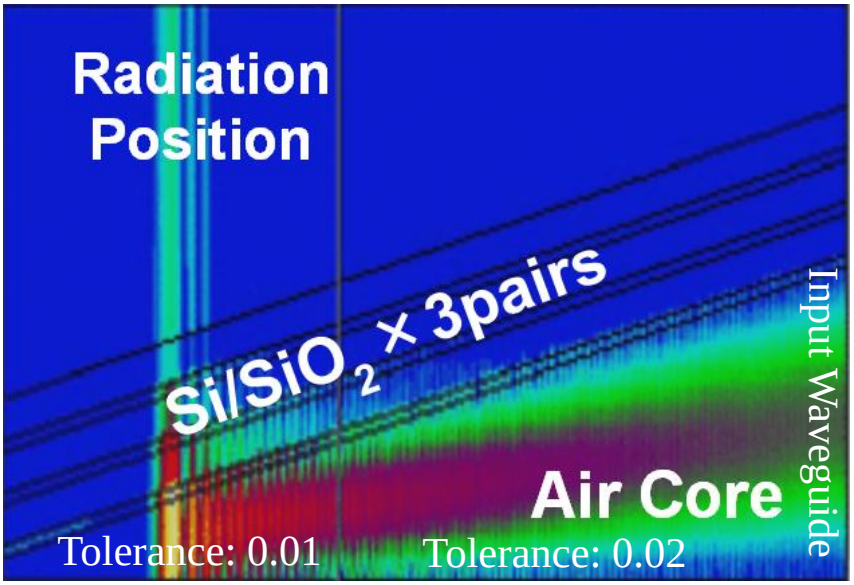

Fig. 6-2 Calculated field distribution of vertical radiation, of fundamental mode.

In order to calculate, integration order zero of the taper algorithm was utilized. While the order one is most suitable for near-adiabatic structures, which does not necessarily apply here. The order zero is likely require a smaller value of "min step-size fraction" to converge. Value of "tolerance" was set of 0.02 to 0.01. I splitted the taper into two parts as most of the computational effort should be concentrated on the end of the taper, where the

light exits the structure. This was done using the "RANGE" function in the interpolation function as shown in Fig. 6-2.

Fig. 6-3 shows the calculated intensity profile of the vertical radiation for fundamental and higher order modes with different wavelengths. The results exhibit clear spatial mode demultiplexing. . In addition, its demultiplexing characteristics are less dependent on wavelength; the calculation is done for the wavelength of 1550 and 1600 nm. This device showed that the radiated position is slightly dependent on the wavelength. The position shift is about 8.92 μm,17.58 μm,26.78 μm,35.71 μm,44.64 μm,53.57 μm and 62.5 μm per a wavelength shift of 50 nm for the fundamental , first, second, third, fourth, fifth and sixth order mode respectively. Indeed angle of tapered hollow waveguide is acting as a major role to determine this dependency, thus in order to reduce the wavelength dependency more, we can increase the angle of tapered hollow waveguide. Even for this wavelength band, a cross-talk of below -15 dB between different channels is expected. In addition, we can see the low wavelength dependence of its demultiplexing characteristics in the figure.

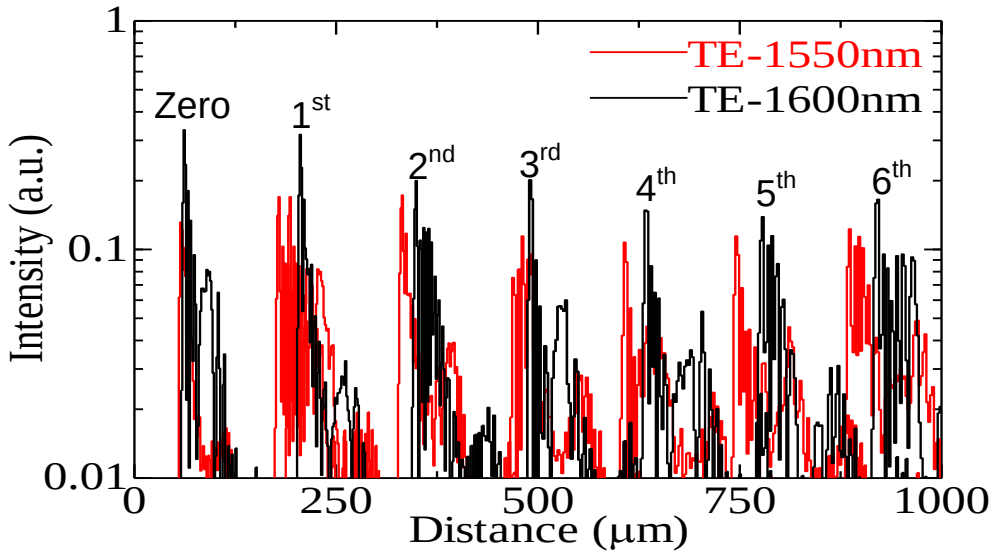

Fig. 6-3 Calculated wavelength dependence of spatial mode demultiplexing. (Intensity profile of vertically radiated light for different spatial modes with wavelengths of 1550 nm and 1600 nm)

Fig.6-4 also depicts the polarization dependence of spatial mode demultiplexing. From this graph a cross-talk of below -15 dB between different channels is expected for orthogonal polarization states. Thus, no noticeable polarization dependency at the same time is obtained. The shift of the radiation point is in the range of 1 μm to 4 μm for different polarization states. These are practically very important for the large wavelength tolerance of VCSELs and for avoiding the polarization control of VCSELs. We calculated the coupling efficiency, namely the insertion loss for our device. By increasing the length of the proposed device with a fixed input thickness, the angle of the taper hollow waveguide decreases. On the other hand, power efficiency which is strongly dependent on the taper angle is reducing. However, by well optimization we can keep the insertion loss as low as <1.5 dB. The detail will be discussed later.

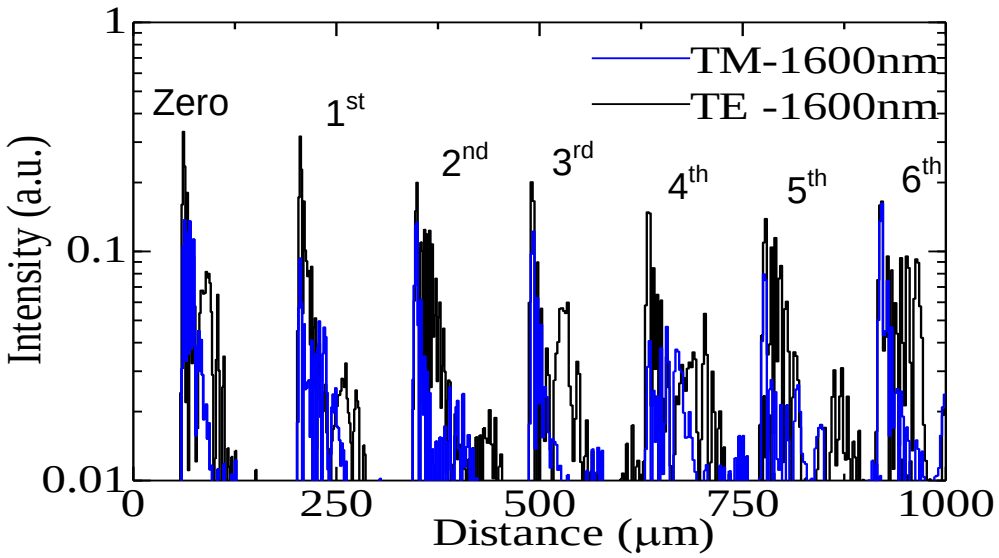

Fig.6-4 Calculated polarization dependence of spatial mode demultiplexing. (Intensity profile of vertically radiated light for different spatial modes with TE and TM mode input)

6.2 Vertical to In-plane Coupler

6.2.1 Device Structure

Fig.6-5 shows the schematic structure of our proposed in-plane to vertical coupler. Highly reflective distributed Bragg reflectors (3-pairs Si/SiO_2) enable us to confine light in an air core. In addition, tapering the air core results in the vertical radiation at a cut-off condition depending on wavelength, while the radiation position for longer wavelength ambulate to the location of thicker core. We found that the radiation position is less dependent on wavelength in the entire C band. Thus, this waveguide device functions as a wavelength-insensitive in-plane to vertical coupler.

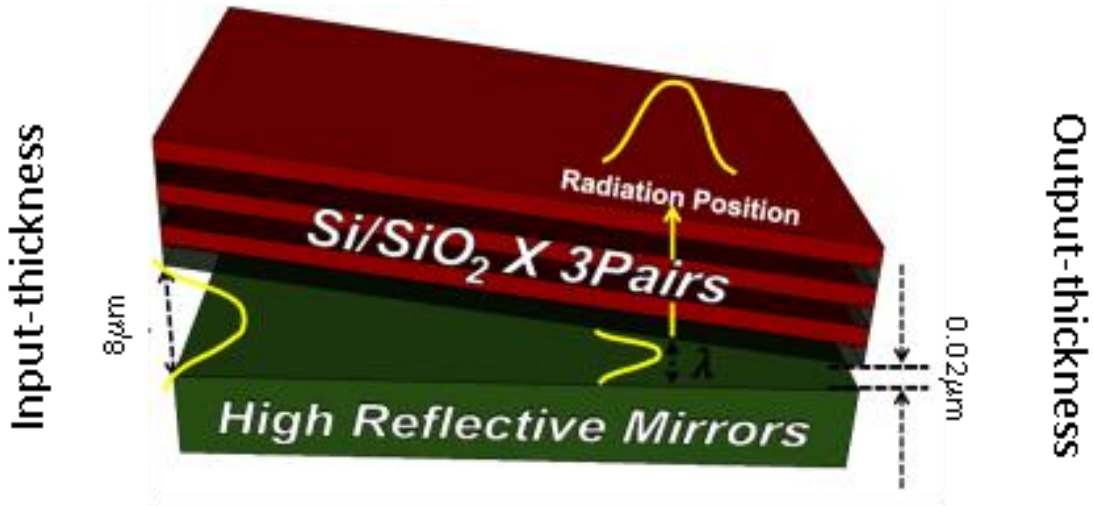

Fig. 6-5. Schematic structure of in-plane to vertical coupler based on tapered hollow waveguide.

We calculated the intensity field distribution for the hollow waveguide with tapering a core thickness. We assumed a perfect mirror as a bottom mirror, which can be replaced by Si/SiO_2 distributed Bragg reflector for real devices. The intensity distribution is calculated same as shown in Fig.6-2, while here core thickness changes from 8 to 0.02 μm and the length of the device varies from 100 μm to 1.5 mm. In this calculation, we assumed a TE-mode Gaussian beam with a wavelength range of C-band as input.

6.2.2 Modelling Results

The calculated intensity profile of vertical radiation is shown in Fig. 6-6. The calculation was carried out for the wavelength range from 1530 to 1565 nm (C-band) with a TE-mode. This figure illustrates that the radiated position is almost overlapped in the entire wavelength region. The position-shift is small enough to make low-wavelength dependence in the entire of C-band.

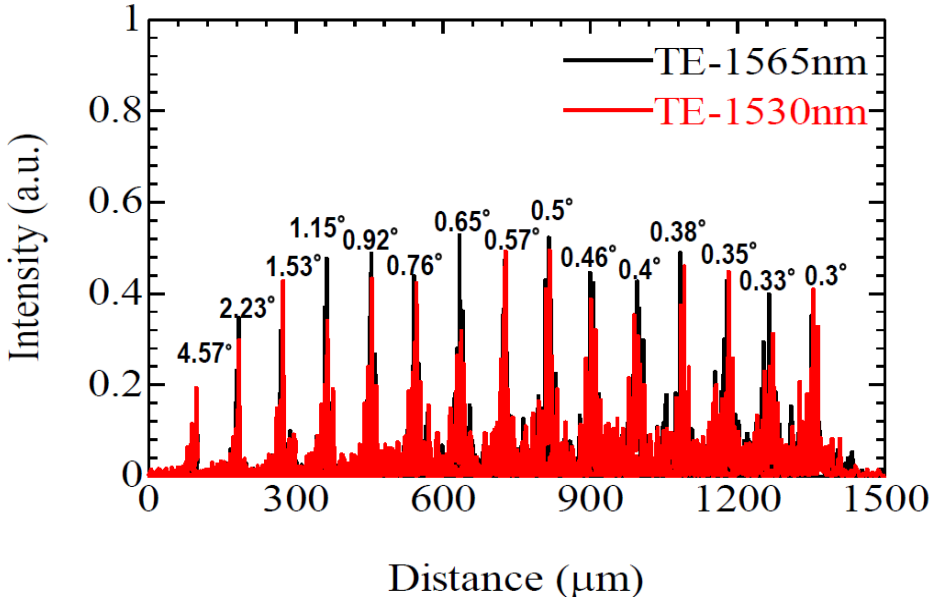

Fig. 6-6 Calculated wavelength dependence of 90° bend device with different taper angles. (Intensity profile of vertically radiated light for different taper-angle with wavelengths of 1530 nm and 1565 nm)

Figure 6-7 also shows the polarization dependence of TM and TE mode at 1550 nm, which also shows no noticeable polarization dependence. The position displacement of TE, TM mode is in a range of 0.1-0.8 nm in the entire C-band. Due to the larger in-put thickness of the taper hollow waveguide the displacement is much smaller than the results which obtained in Fig. 6-4. On the other hand the spot-size is in range of 1-23 nm, therefore this allows displacement over spot-size to be negligible.

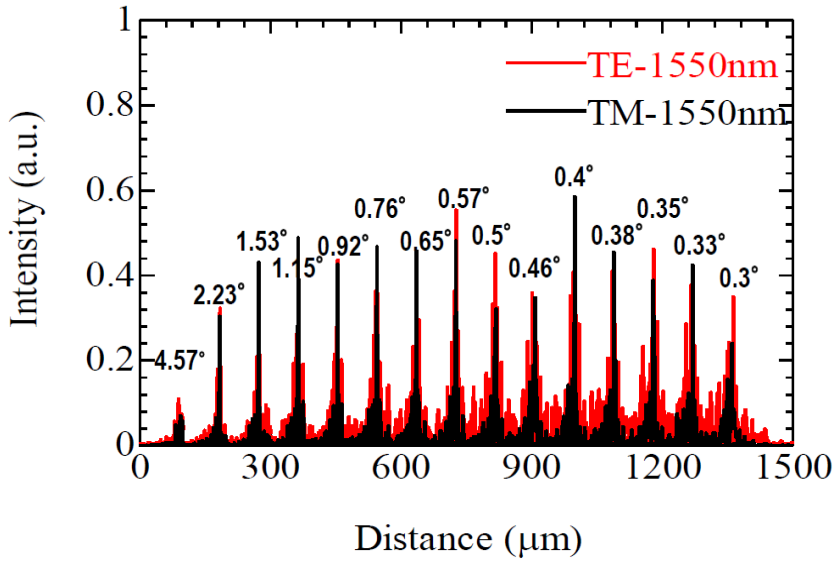

Fig. 6-7 Calculated polarization dependence of 90° bend device with different taper angles. (Intensity profile of vertically radiated light for different taper-angle with wavelengths of 1565nm and TE, TM mode input).

A conventional in-plane to vertical coupler needs to use a spot-size converter, which usually needs a noticeable size. In contrast, our device functions as a spot-size converter. Since our proposed coupler easily adjusts the spot-size via taper-angle modification.

Figure 6-8 shows the calculated output spot-size (full width at a half of maximum) as a function of a taper angle from 4.57° to nearly 0°. This figure clearly shows a possibility of enabling a wide range of spot-size from a few μ m to over 23 μ m.

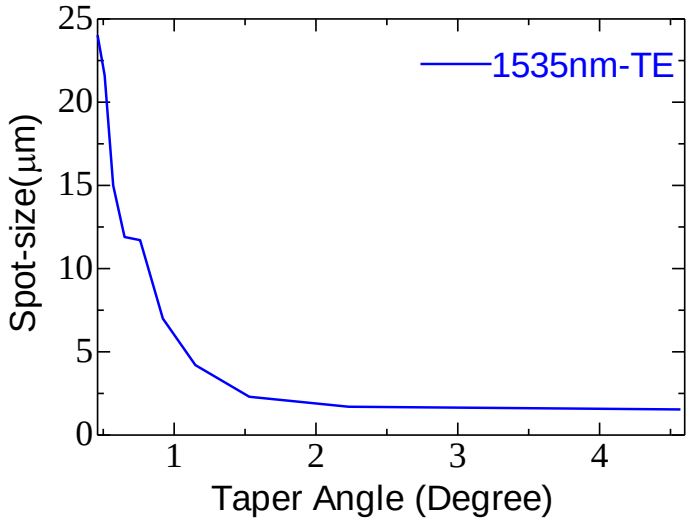

Fig. 6-8 Calculated spot-size (FWHM) of 90° bend device with different taper angle with 1535 nm input.

Figure 6-9 shows the calculated insertion loss for both TM and TE modes of input with different angles while the taper angle is increased from 2.3° to 0.3°. It can be seen that by reducing the taper angle insertion loss will change from 0.4 dB - 0.5 dB to 1.35 dB - 1.25 dB for input of TE and TM mode, respectively.

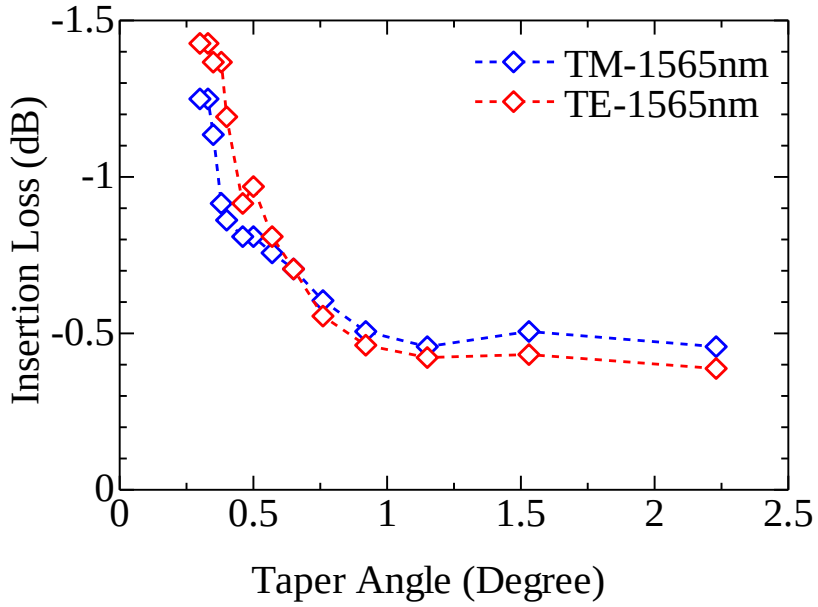

Fig. 6-9 Calculated insertion loss of 90° bend device with different taper angles with wavelengths of 1565 nm for TE and TM mode input.

6.3 Conclusion

In conclusion, based on a tapered hollow waveguide we proposed a spatial multiplexer/demultiplexer and high-efficient in-plane to vertical optical coupler. In the case of multiplexer/demultiplexer, clear demultiplexing for different spatial modes was presented. Low wavelength sensitivity and polarization independence was expected. Also, high efficiency of vertical radiation could be expected.

On the other hand, in case of high-efficient in-plane to vertical optical coupler, our results show no-noticeable polarization dependence and low wavelength dependence in the entire C-band (1530 nm-1565 nm). The lateral position-shift per spot-size for the entire C-band is less than 0.13 and 0.38 for the TE and TM modes of input, respectively. The calcu-

lations show that the wavelength window is wide enough with an optical bandwidth of 35 nm. At the same time we obtained low polarization dependent insertion loss below 1.35 dB and 1.25 dB for the TE and TM modes of input, respectively. This device functions as a spot-size converter, which can be managed from few μm to 23 μm for TE input-mode via taper-angle modification. Finally, these proposed devices can be utilized for a variety of applications such as in-plane coupling of VCSELs and detectors for use in high-density optical interconnects.

6.4 References

1) Y. Sakurai and F. Koyama, "Control of group delay and chromatic dispersion in tunable hollow waveguide with highly reflective mirrors," Japan. J. Appl. Phys., vol. 43, no. 8B, pp. 5828–5831, 2004.

2) T. Miura, Y. Yokota and F. Koyama, "Proposal of tunable demultiplexer based on tapered hollow waveguide with highly refractive multilayer mirrors, LEOS, Sydney Australia, TUL3, pp.272-273, Nov. 2005.

7 Other Applications and Future Prospects of Lateral Integration of VCSEL

7.1 Other Application

7.1.1 In-plane Integration of VCSEL with Photo-detector

Another potential application which could be laterally integrated with VCSEL would be a concept to form photo-detector integrated VCSELs. In this configuration one cavity must be suppressed by the reverse bias voltage at 1volt (in case of modulator we have already shown that 1 V reverse bias can suppress the top emission in the modulator), while the other cavity can be used as a laser. Here some preliminary data would be discussed. In Fig. 7-1, we can see the equivalent circuit for TCC VCSEL, while top emission in one cavity side is dominantly suppressed by appropriate reverse bias voltage. The amount of bias voltage is directly proportional to the resistance of each cavity side.

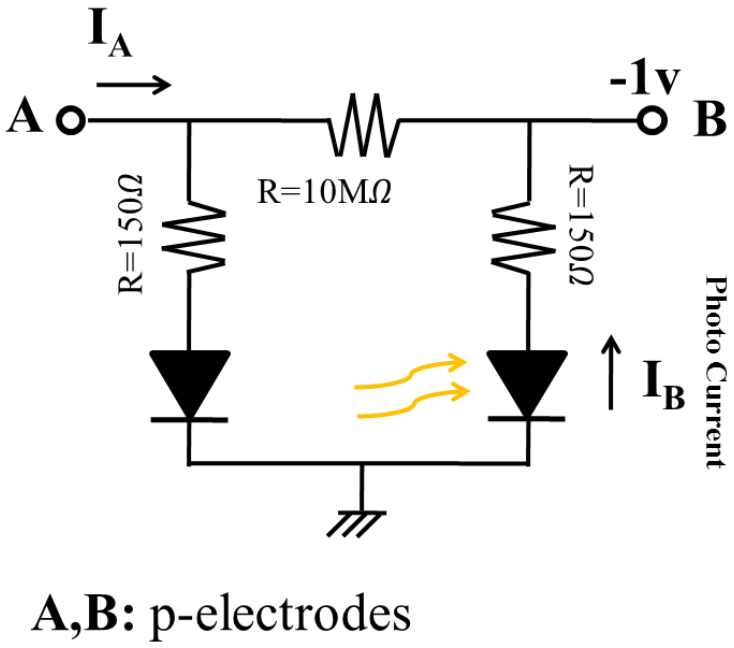

Fig. 7-1 Equivalent circuit of TCC VCSEL, while the top emission of the right cavity side is suppressed by reverse bias 1V.

This time, the proton implantation with six-step different acceleration voltages from 60 to 350 kV doses of 10^{15} cm^{-2} was performed at the centre of the joint connection of the coupled cavities. According to the measured depth profile (see Fig. 7-2), the protons penetrated almost the entire top DBR, the total thickness of which was 4 μm. An electrical isolation over 10 MΩ corresponding to a leakage below 1 μA was attained under forward bias conditions of the one cavity and reverse bias of the other cavity (-1V).

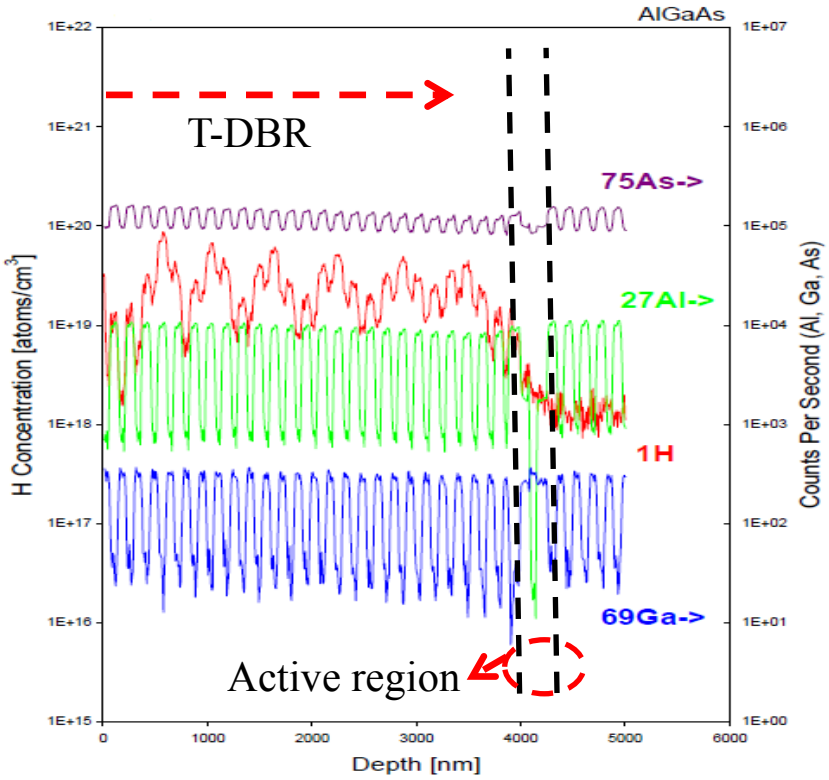

Fig. 7-2 Measured secondary ion mass spectrometry in a proton implanted epitaxial wafer.

Infrared image of oxide aperture of the device we uses for the photo-detector purpose is shown in Fig. 7-3.

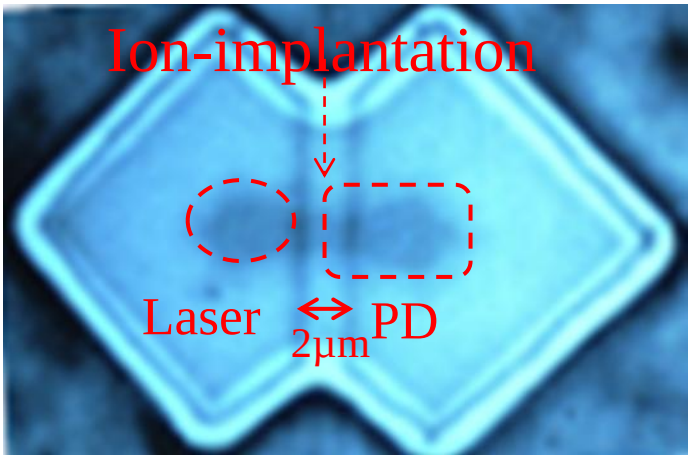

Fig. 7-3 Measured secondary ion mass spectrometry in a proton implanted epitaxial wafer.

In order to measure the photo current data, DC supplier each side of the TCC VCSEL independently. One side acts as laser with forward bias and the other side act as a photo-detector with reverse bias 1V as shown in Fig. 7-1. We changed the forward current from threshold point to the saturation point of laser side consistently with a step of 0.1 mA-0.5 mA, photo-current data of the other side was recorded from the other DC supplier which was connected to the photo-detector, the results of the photo-current data as a function of laser current is shown in Fig. 7-4.

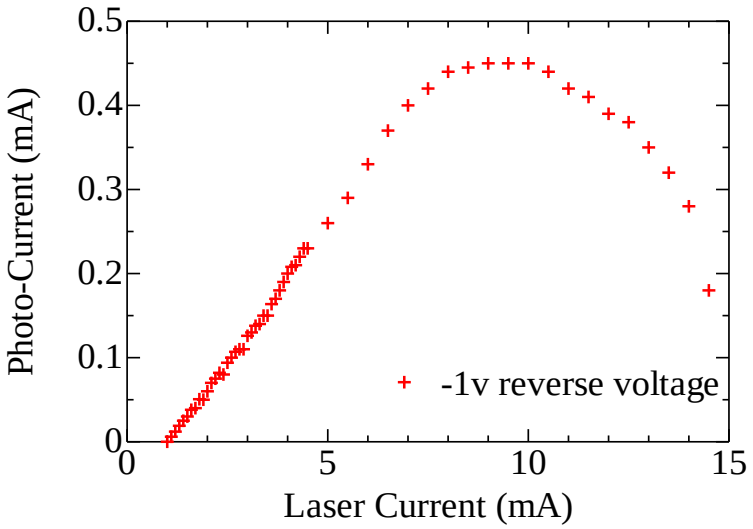

Fig. 7-4 Measured photo-current data of the TCC VCSEL.

Fig. 7-5 Shows L-I curve of the top emission of VCSEL side, while the other cavity is completely suppressed by reverse voltage bias 1V. This result is quite in good agreement with the photo-current data we obtained, while the threshold current is about 0.9 mA we could see a photo current data started from 1 mA. In other hand the VCSEL out-put power was saturated at around 9 mA, in the same condition the photo-current data was saturated in the same point as laser side. This is another evidence of strong electrical isolation between the cavities, while the optical coupling could be easily occurred.

Fig. 7-6 shows the lateral coupled power as a function of laser current, from this fig the coupling efficiency of over 20% is expected.

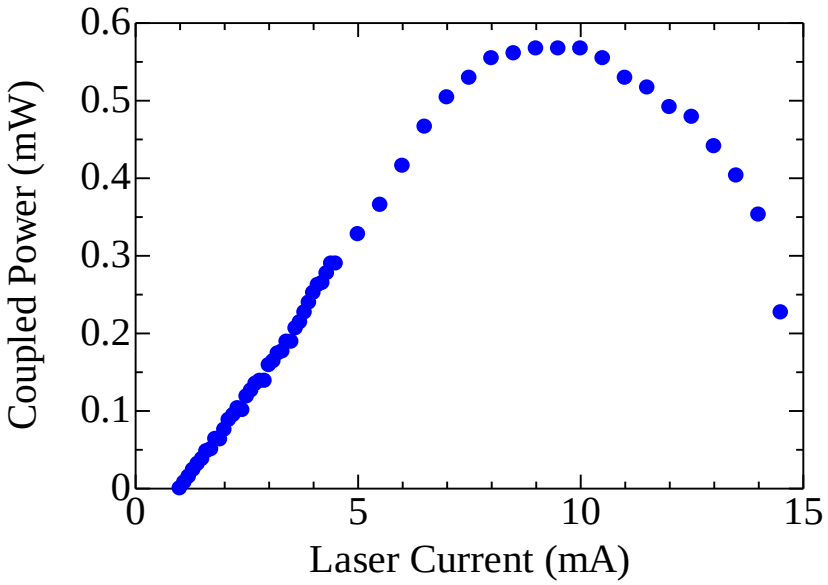

Fig. 7-6 Measured lateral coupling of the TCC VCSEL.

7.2 Future Prospect of the Lateral integration of VCSEL

7.2.1 Lateral Coupling

In order to further develop the lateral integration in VCSEL, we need to make some structure to increase the yield in lateral coupling, so far bow-tie shape showed quiet promising path for connection of dual VCSEL, this shape of connection is necessary for the push-pull scheme, but for other application we can change the structure shape to increase the yield of coupling. For instance in case of electro-absorption integrated with modulator we can simply increase the waveguide width in the modulator side, by engineering the size of oxide aperture, we are able to enhance the yield of lateral coupling. Fig 7-6 shows the top view of the fabricated device. Inset top and bottom in Fig.7.6. Illustrate oxide aperture shape and lasing condition, respectively. By this structure almost entire VCSELs on the epi-wafer structure showed lateral coupling evidence. Here the epi-wafer structure is almost same as chapter two while the number of top DBR pairs is 26pairs.

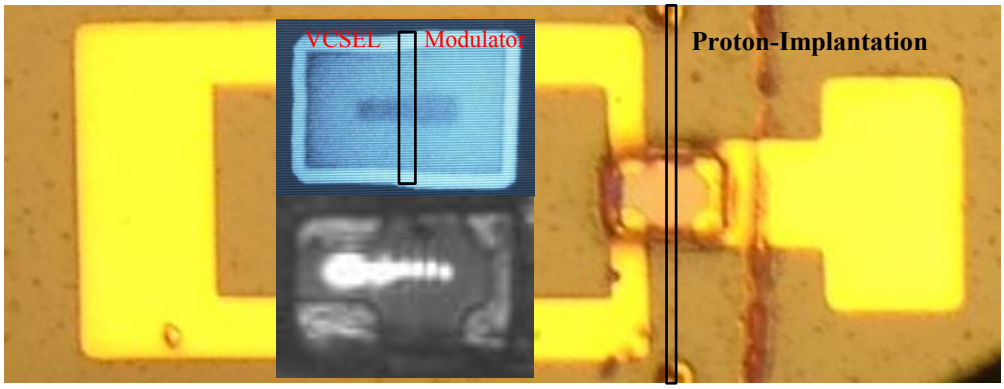

Fig. 7-6 Measured photo-current data of the TCC VCSEL.

The reason of making wider waveguide from VCSEL to modulator is shown in Fig. 7-7.

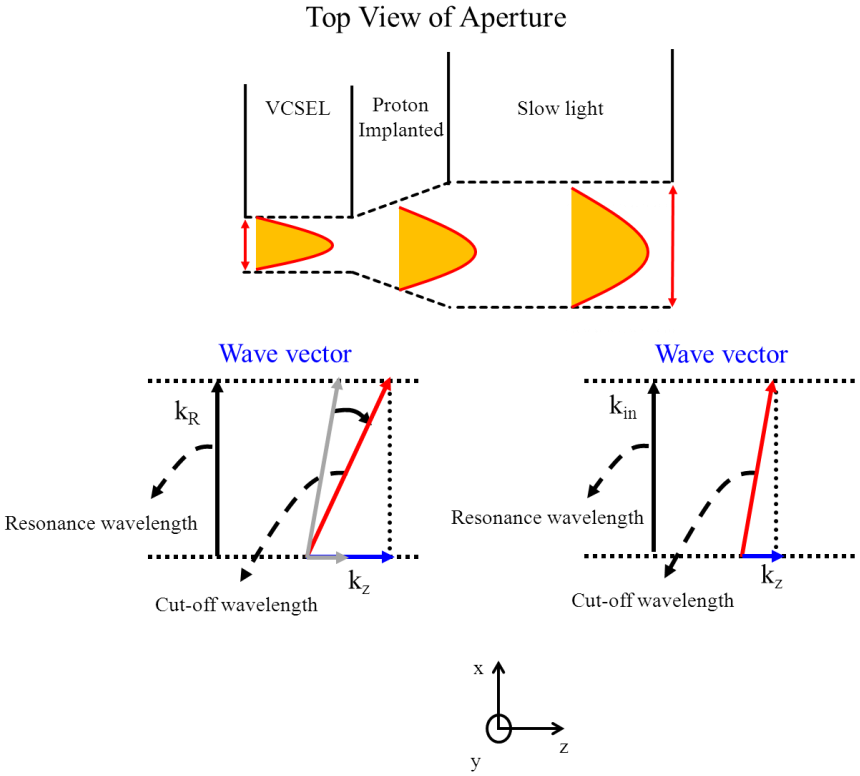

Fig. 7-7 (top) Proposal of oxide aperture, and (bottom) cut off waveguide for different waveguide width.

From Fig. 7-7 , we can easily say that from shorter waveguide to wider waveguides cut off moves from far from cut off wavelength to near cut off this condition will increase the coupling, like Fig .7-7 (bottom) left to right, of course reverse situation makes lower coupling. Fig. 7-8 show the coupling from the wider waveguide to shorter waveguide.

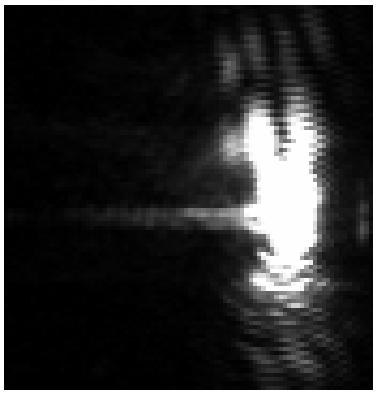

Fig. 7-8 Lateral propagation of light from longer width of waveguide to shorter width of waveguide

However, in order to further improve the lateral coupling we need to suppress the top emission from the laser side. To this end, we can simply increase the number of pairs of top DBR to for example 40 pairs, then by reducing the number of pairs in the modulator side (using ICP RIE or wet etching process), we are able to suppress the top emission of laser side. This provides eventually higher out-put power in the modulator section. In the current fabricated device we are able to couple about 1 mW to the modulator side, while with the proposed way we can improve to beyond 1 mW.

Also another alternative solution would be coating of dielectric mirror on the top of VCSEL side.

7.2.2 Bandwidth Enhancement

Based on the Lang- Kobayashi single-mode rate equation we defined the bandwidth enhancement 60% and 3 times larger to the comparison with conventional VCSEL, when the photon life time of conventional VCSEL was relatively high and small, respectively.

The bandwidth enhancement in the calculation was mainly due to the increase of the modal gain and reduction of photon life time. At that calculation we simply ignored the detuning effect on the bandwidth enhancement. However, in the mathematics aspect we can simply show the potentially bandwidth can be boosted over 100 GHz. In the experiment, we need to precisely control the phase of the feedback, this part would be a drawback for the practical application, but if we can handle the phase of the feedback by oxidation formation, then the phase would be automatically fixed at the appropriate phase we need. So far in chapter two, I have shown that experimentally phase can be locked in pie. If in the same way we can control the phase near enough to pie, not exactly pie, then bandwidth can be much more improved.

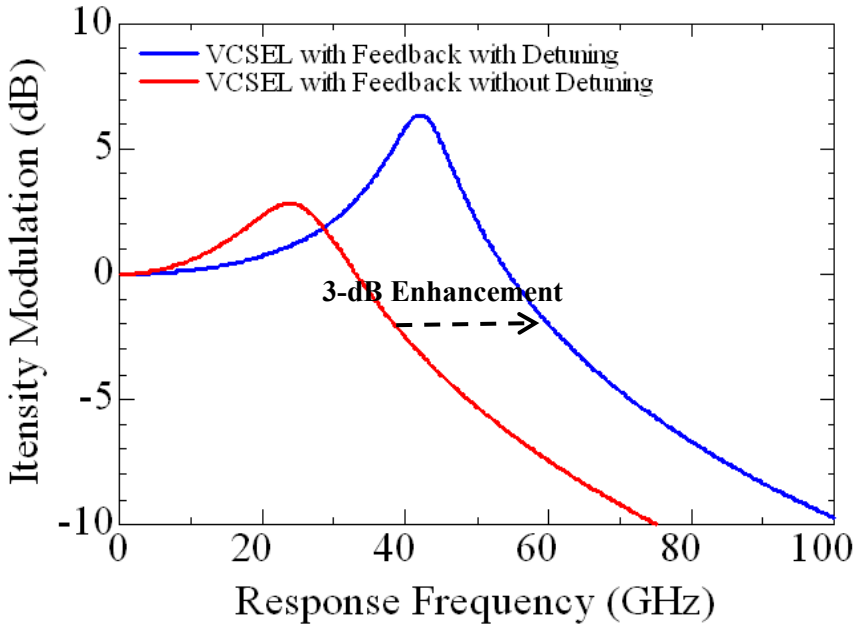

Fig. 7-9 Calculated small signal for VCSEL with lateral feedback, with and with-out detuning range.

In Fig. 7-9, the parameter which is used is same as chapter 2, while the bandwidth of conventional VCSEL is limited to 11 GHz, we can reach 40 GHz, which is basically based on modal gain enrichment and photon life time reduction. In blue line the bandwidth could go beyond 60 GHz, this difference comes from detuning of the main and the sub modes in the transverse modes. This part can be easily understandable from the mutual injection locking case.

8 Conclusion

In conclusion, we have devoted our effort on the lateral integration of VCSEL in order to boost the modulation bandwidth of the conventional VCSEL. To this end, we studied coupled cavity VCSEL case which two cavities are transversely coupled. The author showed a possibility of bandwidth enrichment of conventional VCSEL by exploiting the photon-photon resonance effect. While this phenomenon was well established in DFB lasers, but for the first time experimentally author proved the potential of integration with VCSEL. The world's fastest 980 nm VCSEL was achieved by exploiting the PPR effect. Although, the modulation speed was preliminary limited by the photo-detector limitation. In spite of the fact that, the 3-dB cut off frequency of over 29 GHz for the multi-mode TCC VCSEL could be observed. We also showed that by well designing of the shape of oxidation in TCC VCSEL, we can control the phase to be always in out-of-phase regime. As a result we could see 25 Gbps clear eye opening even at elevated temperature (0-60 ° C). By reducing the size of aperture of TCC VCSEL, some of the higher order modes could be suppressed. Thus we could get quasi-single mode operation with SMSR of 23 dB. Draw back was that the bandwidth slightly reduced to 27 GHz. At the same time, a 36 Gbps clear eye opening with extinction ratio of 4 dB was attained. In order to realize a 40 Gbps modulation speed, we endeavoured to combine this upshot with others possible effects. For this matter, we synthesized this phenomenon with push-pull effect. We experimentally obtained 40 Gbps eye opening with mixed effects, while using only PPR effect eye was completely closed at this speed. Low extinction ratio in this measurement was mostly due to the lack of electrical amplifier to increase the modulation swing, while the total injected current was 20 mA for the combined cases, we could only apply voltage swing of 300 mV. Although, this problem can be easily solved by increase of voltage swing to 1 volt, but the current density

for realizing the speed beyond 40 Gbps would be too large. For this reason, we tried to combine the PPR effect with QCSE in electro-absorption modulator. Preliminary we reached at 25 Gbps eye opening with high extinction ratio, while the voltage swing was the lowest ever reported (<400 mV_{pp}) and the size of device was also the smallest ever made (8 μm long).At the same time, we obtained 30 GHz small signal response for the composed phenomena (PPR and QCS effects), while some un-known noises raised up after 12 GHz, we could not reach higher bit rates at this experiment. In order to obtain the small signal noise free, further optimization of PPR effect is required. Finally we showed a possibility of spatial mode multiplexer/demultiplexer based on tapering of the hollow waveguide. The modelling results indicate that the cross talk between channels should be small enough to be used in practical application. At last in order to realize green optical interconnect going beyond 1 Tbps, we propose a composition of taper hollow waveguide with the TCC VCSELs as shown in Fig. 7-10.

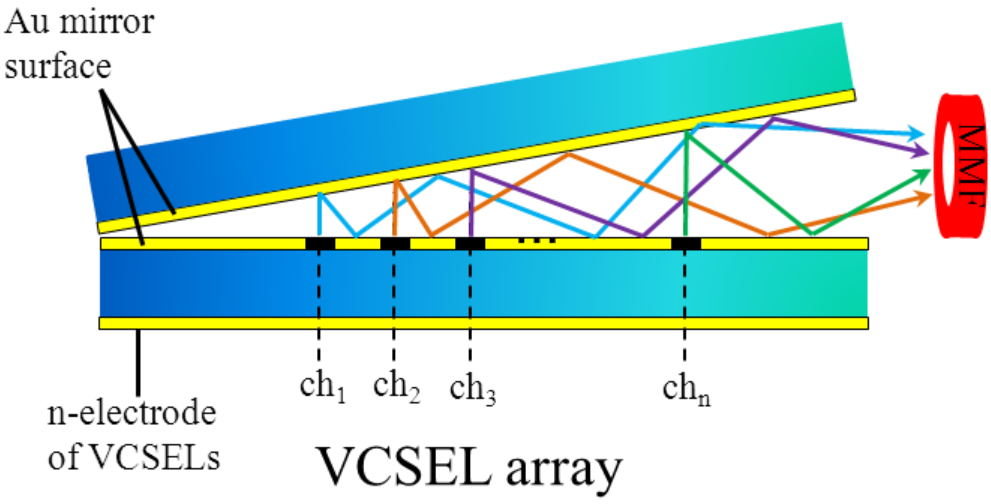

Fig. 7-10 Proposal of VCSEL integration of TCC VCSEL with taper hollow waveguide.

Publications

Journals

[1] **Hamed Dalir**, Yasushi Yokota and Fumio Koyama, "Spatial Mode Multiplexer/Demultiplexer Based on Tapered Hollow Waveguide", *IEICE Electron. Express*, Vol. 8, No. 9, pp.684-688, 2011.

[2] **Hamed Dalir** and Fumio Koyama, "Bandwidth Enhancement of Single-mode VCSEL with Lateral Optical Feedback of Slow Light", *IEICE Electron. Express*, Vol. 8, No. 13, pp.1075-1081, 2011.

[3] **Hamed Dalir**, Fumio Koyama "29GHz directly modulated 980nm vertical-cavity sur-face emitting lasers with bow-tie shape transverse coupled cavity", *Appl. Phys. Lett.*, 103, pp. 091109-1-4, 2013.

[4] **Hamed Dalir** and Fumio Koyama, "High Frequency Modulation of Transverse-Coupled-Cavity VCSELs for Radio over Fiber Applications", *IEEE Photonics Technology Letters*, Vol. 26, No. 3, pp. 281 - 284, 2013.

[5] **Hamed Dalir** and Fumio Koyama, "High-Speed Operations of Bow-tie-shape Oxide Aperture VCSELs with Photon-Photon Resonance", Appl. Phys. Express, *Appl. Phys. Express*, Vol. 7, No. 2, pp. 022102, 2014.

[6] **Hamed Dalir**, Yuta Takahashi, Fumio Koyama "Compact low driving voltage (<400mVpp) electro-absorption modulator laterally integrated with VCSEL", *Electronics Letters*, Vol. 50, No. 2, pp. 101-103, 2014.

[7] **Hamed Dalir** and Fumio Koyama, "Proposal of High Efficient Vertical to In-plane Coupler based on Tapered Hollow Waveguide", *Japanese Journal of Applied Physics*, accepted, Feb., 2014.

[8] **Hamed Dalir** and Fumio Koyama, "Push-Pull Modulation of Spatial Intensity Distribution of Transverse Coupled Cavity VCSEL", *Japanese Journal of Applied Physics*, submitted.

[9] **Hamed Dalir** and Fumio Koyama, "Highly-temperature Stable High-speed Transverse Coupled Cavity VCSEL", *Electronics Letters*, submitted.

International Conference:

[1] **Hamed Dalir**, Fumio Koyama "Ultrafast Direct Modulation of Transverse-mode Coupled Cavity VCSELs far Beyond the Relaxation Oscillation Frequency", Photonics West, Oral Presentation, 9001-5, San Francisco, USA, 2014.

[2] **Hamed Dalir**, Fumio Koyama "In-plane integration of VCSEL with photo detector by using laterally coupled cavities", Photonics West, Oral Presentation, 9001-7, San Francisco, USA, 2014.

[3] **Hamed Dalir**, Yuta Takahashi, Fumio Koyama, "Low Driving Voltage (< 400mVpp) Electro-absorption Modulator Laterally Integrated with VCSEL", OFC, accepted, San Francisco, USA, 2014.

[4] **Hamed Dalir**, Akihiro Matsutani, Fumio Koyama," Push-pull modulation of lateral coupling of dual VCSEL cavities using a bow-tie shape, Vertical-Cavity Surface-Emitting Lasers XVII, SPIE Photonics West 2013, pp. 8639-31, San Francisco, USA, 2013.

[5] **Hamed Dalir**, Fumio Koyama "Modulation Response Enhancement of Transverse-coupled Cavity VCSELs for Radio over Fiber Applications", MOC, Oral Presentation, C4, Tokyo, Japan, 2013.

[6] **Hamed Dalir**, Fumio Koyama "Modulation Bandwidth Enhancement of Quasi-single-mode Transverse Coupled Cavity VCSEL", IPC-PD, PD3, Seattle, USA, 2013.

[7] **Hamed Dalir**, Fumio Koyama "Beyond 28.6GHz Directly Modulated 980nm VCSEL with Transverse Optical Feedback of Slow Light, iNOW 2013, Corsica, France, 2013.

[8] **Hamed Dalir**, Akihiro Matsutani, Fumio Koyama "Modulation of Spatial Intensity Distribution of Laterally Coupled Twin VCSELs", 2013 Conference on Lasers and Electro-Optics Pacific Rim, CLEO-PR, ThK3-2, Kyoto, Japan, 2013.

[9] **Hamed Dalir**, Fumio Koyama "Laterally Coupled Cavity VCSELs for Push-Pull High Speed Modulation", IEEE Summer Topicals, MA4.3 Hawaii, USA, 2011

[10] **Hamed Dalir**, Fumio Koyama "High-speed Direct Modulation Beyond 29GHz of 980nm Transverse Coupled Cavity VCSEL", 2013 Conference on Lasers and Electro-Optics Pacific Rim, CLEO-PR, PD5, Kyoto, Japan, 2013.

[11] **Hamed Dalir** and Fumio Koyama, "Proposal of In-plane to Vertical Coupler Based on Tapered Hollow Waveguide", OSA's 96th Annual Meeting, FW5E.4, Rochester, USA, 2012.

[12] **Hamed Dalir** and Fumio Koyama, "Electrical Transverse-Mode Switching of Laterally Coupled Cavity VCSELs", iNOW, Poster Presentation, San Francisco, USA, 2012.

[13] **Hamed Dalir**, Yasushi Yokota, and Fumio Koyama, "Spatial mode multiplexer/demultiplexer based on tapered hollow waveguide", 16th Opto-Electronics and Communication Conference (OECC), Oral Presentation, 7E2-2, Kaohsiung, Taiwan, 2011.

[14] **Hamed Dalir** and Fumio Koyama, "Enhanced modulation bandwidth of VCSELs with lateral optical feedback beyond the frequency of relaxation oscillations", iNOW, Poster Presentation, July-August, St. Petersburg, Russia and Wurzburg, Germany, 2011.

[15] **Hamed Dalir** and Fumio Koyama, "High speed modulation and multiplexing technology of VCSEL", Workshop Taiwan-Japan "Nano Devices", Poster Presentation, Yokohama, Japan, 2011.

[16] **Hamed Dalir** and Fumio Koyama, "Large signal modulation analysis of lateral-optical-feedback VCSELs", 16th International Conference on Micro-Optics (MOC), Oral Presentation, MD1, Hsinchu, Taiwan, 2010.

[17] **Hamed Dalir** and Fumio Koyama, "Modulation bandwidth enhancement of VCSELs with lateral optical feedback of slow light", 22nd IEEE International Semiconductor Laser Conference (ISLC), Poster Presentation, P10, Kyoto, Japan, 2010.

[18] **Hamed Dalir** and Fumio Koyama, "Proposal of 90 Degree Bend Tapered Hollow Waveguide", The International Global COE Symposium -VCSELs and Nano-photonics Innovation for Green ICT, Dec. Tokyo, Japan, 2011.

[19] **Hamed Dalir** and Fumio Koyama, "High speed modulation and multiplexing technology of VCSEL", Workshop Taiwan-Japan "Nano Devices", Poster Presentation, 1 -3 March, Yokohama, Japan, 2011.

Domestic Conferences:

[1] **Hamed Dalir** and Fumio Koyama, "27 GHz Directly Modulated Transverse Coupled Cavity VCSEL by Utilizing the Photon-Photon Resonance", 61th Spring Meeting of Japan Society of Applied Physics Conference (JSAP), submitted, Tokyo, Japan, 2014.

[2] **Hamed Dalir**, Yuta Takahashi, Toshikazu Shimada and Fumio Koyama, "Strong Lateral Coupling from VCSEL to Slow Light Waveguide by Width Modification", 61th Spring Meeting of Japan Society of Applied Physics Conference (JSAP), submitted, Tokyo, Japan, 2014.

[3] **Hamed Dalir** and Fumio Koyama, "Modulation Bandwidth Enhancement of Laterally-coupled Cavity VCSELs for Radio over Fiber Applications", 74th Autumn Meeting of Japan Society of Applied Physics Conference (JSAP), Oral Presentation,16p-A8-6, Kyoto, Japan, 2013.

[4] **Hamed Dalir** and Fumio Koyama, "Beyond 25GHz Directly Modulated 980nm VCSEL with Lateral Optical Feedback", JSAP-OSA Joint Symposia, Oral Presentation, Kyoto, Japan, 2013.
[5] **Hamed Dalir** and Fumio Koyama, "Transverse Coupled Cavity VCSELs for Push-Pull Modulation", JSAP-OSA Joint Symposia, Oral Presentation, 16p-D4-8, Kyoto, Japan, 2013.
[6] **Hamed Dalir**, Fumio Koyama, "Electrical Transverse-Mode Switching of Laterally Coupled Cavity VCSELs", IEICE General Conference, C-4-9, 2013.
[7] **Hamed Dalir** and Fumio Koyama, "90° Bend Device Based on Tapered Hollow Waveguide", 59th Spring Meeting of Japan Society of Applied Physics Conference (JSAP), Oral Presentation, 18a-GP4-14, Tokyo, Japan, 2012.
[8] **Hamed Dalir** and Fumio Koyama, "Taper Structure for Lateral Coupling from VCSEL To Slow Light Waveguide", 59th Spring Meeting of Japan Society of Applied Physics Conference (JSAP), Oral Presentation, 17p-GP12-3, Tokyo, Japan, 2012.
[9] **Hamed Dalir**, and Fumio Koyama, "Proposal of Spatial Mode Multiplexer/Demultiplexer Based on Tapered Hollow Waveguide", 72th Autumn Meeting of Japan Society of Applied Physics Conference (JSAP), Oral Presentation, 24p-KA-13, March, Tokyo, Japan, 2011.
[10] **Hamed Dalir** and Fumio Koyama, "Proposal of laterally coupled VCSELs for modulation-bandwidth enhancement", 71th Autumn Meeting of Japan Society of Applied Physics Conference (JSAP), Oral Presentation, 16p-H-5, September, Nagasaki, Japan, 2010.

Patents

1) 特願 2010-187242　面発光型半導体レーザおよび光伝送装置（Fumio Koyama，**Hamed Dalir**，Toshikazu Shimada）
2) 特願 2013-217167　面発光型半導体レーザ、面発光型半導体レーザ装置および光伝送装置（Fumio Koyama，**Hamed Dalir**）

Acknowledgement

It is with immense gratitude that I acknowledge to my Professor, Fumio Koyama, whose encouragement, supervision and support from the preliminary to the concluding level enabled me to develop an understanding of the subject. I sincerely appreciate Professor Kohroh Kobayashi, Professor Masayuki Izutsu, Associate Professor Tomoyuki Miyamoto and Professor Hiroyuki Uenohara, of Tokyo Institute of Technology, for their general guidance, I also grateful to Assistant Professor Takahiro Sakaguchi and Dr. Akihiro Matsutani for their technical supports.

I'd like to say big thanks to Professor Emeritus Yasuharu Suematsu, Professor Emeritus Kenichi Iga for their inspiration of this research. The author wishes to thank professors of related field in Tokyo Institute of Technology for their worthwhile discussions in various instances, principally to Professor Masahiro Asada, Professor Shigehisa Arai, and Professor Kotaro Kajikawa.

I would like thank lab secretaries Ms. Setsuko Itou, Ms. Hiromi Yoshida, Ms. Hiroko Kokeguchi and Ms. Tomie Chiba for their sincere help and support in laboratory. I cannot find words to express my gratitude to my parents and my wife for their understanding, support and love. I consider it an honour to work with, Mr. Xiaodong Gu, Mr. Masanori Nakahama and Mr. Yuta Takahashi.

Lastly, I am indebted to my many colleagues who supported me in any respect during the completion of the project.

The author has financially supported by Japanese Society for the Promotion and Science Fellowship (JSPS) and partly by Yoshida Scholarship Foundation (YSF). This study was mainly supported by a Grant-in-Aid for Scientific Research (Grant Number: S22226008) from the Ministry of Education, Culture, Sports, Science and Technology of Japan.